

**Development and Characterization of Extracellular Matrix Based
Vascular Graft Biomaterials**

By

Kathryn Alyce McKenna

A DISSERTATION

Presented to the Department of Biomedical Engineering
of the Oregon Health & Science University
School of Medicine
in partial fulfillment of
the requirements for the degree of

Doctor of Philosophy
in Biomedical Engineering

August 2011

Department of Biomedical Engineering
School of Medicine
Oregon Health & Science University

CERTIFICATE OF APPROVAL

This is to certify that the Ph.D. dissertation of
Kathryn Alyce McKenna
has been approved

Monica T. Hinds, Ph.D.
Assistant Professor, Thesis Advisor

Stephen R. Hanson, Ph.D.
Professor, Thesis Committee Member

Kenton W. Gregory, M.D.
Associate Professor, Thesis Committee Member

András Gruber, M.D.
Associate Professor, Thesis Committee Member

John C. Mitchell, Ph.D.
Associate Professor, Thesis Committee Member

Wassana Yantasee, Ph.D.
Assistant Professor, Thesis Committee Member

I dedicate this work to my family: my wonderful baby girls, Sierra and Kaia,; my husband, Sean; my parents, Lynn and Ellen; my sisters, Wendy, Jenny and their sweet babies; and as always to Da Boyz, Aero, Rosco and little Riley.

Table of Contents

Table of Contents	i
List of Figures.....	vii
List of Tables and Equations	xvii
List of Abbreviations.....	xviii
Acknowledgements.....	xxiv
Abstract	xxvi
Chapter 1: Introduction.....	1
1.1 Cardiovascular Disease.....	1
1.2 The Extracellular Matrix of the Arterial Wall.....	3
1.2.1 Elastin.....	5
1.2.2 Collagen.....	12
1.2.3 Fibronectin	14
1.3 Vascular Graft Biomaterials.....	15
1.3.1 Electrospinning of Extracellular Matrix Proteins.....	16
1.3.2 Modifications of Vascular Graft Biomaterials.....	17
1.4 Endothelial Cells	19
1.4.1 Endothelial Outgrowth Cells	21
1.4.2 Endothelial Cell Adhesion.....	22
1.4.3 Endothelial Cells as Force Transducers.....	25
1.4.4 The Role of Endothelial Cells in Thrombosis and Coagulation.....	26
1.5 Dissertation Overview	29

Chapter 2: Structural and Cellular Characterization of Electrospun Recombinant

Human Tropoelastin Biomaterials	30
2.1 Abstract.....	30
2.2 Chapter Overview.....	31
2.3 Introduction.....	31
2.4 Materials and Methods	35
2.4.1 Materials	35
2.4.2 Electrospinning of rTE.....	35
2.4.3 Cross-linking of electrospun rTE	36
2.4.4 Electrospun rTE fiber characterization.....	36
2.4.5 Smooth muscle cell adhesion to adsorbed rTE.....	37
2.4.6 Smooth muscle cell growth on electrospun prTE	38
2.4.7 Statistical analyses.....	40
2.5 Results.....	41
2.5.1 Morphology and substructure of rTE and prTE fibers	41
2.5.2 Smooth muscle cell adhesion to adsorbed rTE.....	45
2.5.3 Smooth muscle cell morphology and proliferation on electrospun prTE	46
2.6 Discussion	49
2.7 Conclusion	55

Chapter 3: Mechanical Property Characterization of Electrospun Recombinant

Human Tropoelastin for Vascular Graft Biomaterials.....	56
3.1 Abstract.....	56
3.2 Chapter Overview.....	57

3.3	Introduction.....	57
3.4	Materials and Methods	61
3.4.1	Materials	61
3.4.2	Electrospinning of rTE.....	63
3.4.3	Cross-linking of Electrospun rTE.....	64
3.4.4	Electrospun rTE Fiber Characterization	65
3.4.5	Mechanical Properties of prTE.....	65
3.4.6	Burst Pressure of prTE Scaffolds	67
3.4.7	Endothelial Cell Growth on prTE Scaffolds.....	67
3.4.8	Statistical analyses.....	68
3.5	Results and Discussion	68
3.5.1	Morphology and Substructure of prTE Fibers	69
3.5.2	Mechanical Properties of prTE.....	71
3.5.3	Burst Pressure of prTE Scaffolds	77
3.5.4	Endothelial Cell Growth on prTE Scaffolds.....	78
3.6	Conclusions	80
 Chapter 4: Burst Pressure Based Analysis Method for Tissue Engineered Vascular Constructs: A Constitutive Model Development.....		81
4.1	Abstract.....	81
4.2	Chapter Overview.....	82
4.3	Introduction.....	82
4.4	Methods	86
4.4.1	Model Development.....	87

4.4.2	Model Verification	90
4.5	Results.....	93
4.6	Discussion	95
4.7	Conclusion	98
Chapter 5: Comparison of effect of protein surface on thrombotic and inflammatory responses with comparative <i>in vitro</i>, acute <i>ex vivo</i> shunt, and chronic <i>in vivo</i> studies		
.....		99
5.1	Abstract.....	99
5.2	Chapter Overview.....	100
5.3	Introduction.....	101
5.4	Methods	105
5.4.1	Endothelial Outgrowth Cell Isolation	105
5.4.2	Graft Construction	106
5.4.3	Graft Coating.....	107
5.4.4	EOC Flat Plate Culture.....	108
5.4.5	EOC Seeding on Protein Modified ePTFE Conduits	108
5.4.6	Platelet Aggregation	109
5.4.7	Gene Expression	109
5.4.8	APC Functional Assay.....	110
5.4.9	Factor Xa Functional Assay	110
5.4.10	Total DNA	110
5.4.11	Baboon Arteriovenous (AV) ex vivo Shunt Model.....	111
5.4.12	Baboon Arteriovenous (AV) ex vivo Shunt Durability Model	113

5.4.13	Baboon Aorto-iliac in vivo Bypass Model	114
5.4.14	Correlation of in vitro Hemostasis and ex vivo and in vivo Thrombosis.....	116
5.4.15	Statistical analyses.....	117
5.5	Results.....	117
5.5.1	Endothelial Outgrowth Cell Isolation	117
5.5.2	Flat plate studies	118
5.5.3	Gene Expression on Protein Coated Flat Plates	120
5.5.4	Functional Responses on Protein Coated Flat Plates	123
5.5.5	Platelet Aggregation	125
5.5.6	Ex vivo shunt Graft Studies	126
5.5.7	Cell Retention on EOC-seeded ePTFE grafts	127
5.5.8	Platelet Response on EOC-seeded ePTFE grafts	129
5.5.9	Gene Expression for EOC-seeded ePTFE grafts.....	130
5.5.10	Functional Activity Assays for EOC-seeded ePTFE grafts	132
5.5.11	In vivo shunt Graft Studies	135
5.5.12	Tissue Ingrowth	137
5.6	Discussion	141
5.7	Conclusions	147
Chapter 6: Conclusions and Future Directions.....		149
6.1	Characterization of Protein Structure	149
6.2	Strengthening the Electrospun Tropoelastin Biomaterial	152
6.3	Strain energy density function of electrospun tropoelastin.....	154
6.4	<i>In vivo</i> implant with paired controls.....	155

6.5	Flow Conditioning of EOC-seeded Collagen Modified ePTFE Grafts.....	156
6.6	Scientific Impact.....	156
	References.....	159
	Appendix A.....	179
	Appendix B.....	182
	Appendix C.....	186
	Biographical Sketch	187

List of Figures

Chapter 1: Introduction	1
Figure 1.1. Common Plaque formation sites in the vascular tree [2].....	2
Figure 1.2. Cross-sectional schematic of the structure of the arterial wall. The three major vessel layers from the lumen outward are the: intima, media, and adventitia. The internal and external elastic lamina matrix layers are also represented. [8].....	4
Figure 1.3. Structure of Elastin: The structure and assembly of the elastic fibers are responsible for the elastic nature of the protein. Elastin molecules stretch and align under loading and relax and bundle up after the load is removed. [27].....	7
Figure 1.4. Structure of Tropoelastin: The structure of the full-length tropoelastin monomer is shown with the N-terminus leading to the coil region, which is responsible for the elasticity in the molecule, to the lower hinge region in the spur, and a bridge to the cell binding C-terminus. [28].....	8
Figure 1.5. Time series (hh:mm:ss) of frames from a confocal movie showing the dynamic process of rTE coacervation at 50 mg/ml and 37°C. The 00:00:00 panel shows the initial solid sphere structure and the 00:06:32 panel shows the final hollow sphere-pocket structure. Tropoelastin was stained with Oregon Green for visualization. Tropoelastin is shown in green and the solvent PBS is shown in black. (Scale bar = 50 μm). Dr. Robert Glanville, Rebecca Sarao, and Rose Merten at the Oregon Medical Laser Center Bioimaging Facilities obtained these images.....	12
Figure 1.6. Collagen Structure. Collagen fibrils assemble to form a collagen triple helix structure. [27]	13
Figure 1.7. Normal versus abnormal function for key cell types [8]	20
Figure 1.8. Blood flow-mediated mechanical stresses acting on the arterial wall. Hoop stress (σ) and wall shear stress (τ_w) are defined and illustrated above. [82].....	21

Figure 1.9. Model of endothelial mechanotransduction by mechanical shear stress. Signal can be transduced at the luminal surface (A) between cell junctions (B) directly to adhesion sites on the ECM matrix (C), and to the nucleus (D). [106]	26
Figure 1.10. Three phases of the coagulation cascade in thrombosis. (A) The initiation phase is started with the release of TF leading to thrombin generation. (B) The propagation phase amplifies the response to form cross-linked fibrin clots. (C) The termination phase inactivates coagulation factor through the action of APC.....	28
Chapter 2: Structural and Cellular Characterization of Electrospun Recombinant Human Tropoelastin Biomaterials	30
Figure 2.1. Comparison of electrospun rTE fibers from 9, 15, and 20 wt% solutions. The rTE fibers were randomly oriented. Fiber diameters were directly proportional to the concentration of the rTE solution. The electrospun rTE fibers from 9 and 15 wt% solutions had only round cross-sections, while isolated electrospun rTE fibers from 20 wt% solutions had flat cross-sections. SEM micrographs at magnifications of 1000X, 5000X, and 10000X.	42
Figure 2.2. SEM micrograph of extracted native elastin from a porcine carotid artery. Scale bars indicate 10 μ m.....	43
Figure 2.3. TEM micrograph of substructure of 15 wt% electrospun rTE fibers. Voids are visualized within the fibers. Scale bar indicate 500nm. Dr. Jack McCarthy assisted with the TEM imaging of this material.	44
Figure 2.4. SEM micrograph of uncross-linked electrospun rTE (left) and cross-linked electrospun prTE (right) fibers produced from a 15 wt% rTE solution. No change in fiber structure was seen using the DSS cross-linker.	45
Figure 2.5. Characterization of the adhesion of SMCs to adsorbed rTE. SMCs were allowed to adhere to rTE, fibronectin (Fn), collagen type I (Col), or tissue culture treated plastic (TCP) in either adhesion media or adhesion media with a blocking reagent: EDTA, Pertussis toxin, or lactose. EDTA significantly reduced SMC adhesion	

to the rTE and Fn coated wells. *p<0.05, compared to the same coating with adhesion media, ANOVA with a Tukey post-hoc test..... 46

Figure 2.6. Morphology of SMCs seeded onto electrospun 15 wt% prTE for (A) 24 and (B) 48 hours. Confocal images of prTE fibers (green) with actin cytoskeleton-phalloidin (red) and nuclei (blue) of SMCs. SMC pseudopodia made attachments to individual prTE fibers (arrows in A), SMC concentrations increased between 24 and 48 hours, and SMCs formed actin stress fibers (arrows in B). Scale bar indicates 20 μ m. 47

Figure 2.7. SMC proliferation on electrospun prTE, coated prTE, Poly-D-Lysine (Lysine D glass), and tissue culture plastic (TCP) over a 7 day time course. Note: Cell metabolic activity was quantified using alamarBlue assay and the data normalized to the fluorescence reading at day 1. Data are the average of 3 lots of rTE solutions. 48

Chapter 3: Mechanical Property Characterization of Electrospun Recombinant

Human Tropoelastin for Vascular Graft Biomaterials..... 56

Figure 3.1. Stained electrophoresis gel showing purified human tropoelastin from 7 different batches (lanes 1-3 and 5-8) illustrating the purity of the product and reproducibility of the purification process. Lane 4 is a molecular weight standard. This gel was provided by Dr. Robert Glanville at the Oregon Medical Laser Center..... 62

Figure 3.2. Diagrammatic representation of human tropoelastin protein domains. The number of the corresponding exons and the sizes of the domains are shown. The exon numbering system is based upon the bovine elastin gene sequence. The human gene has no exons 34 and 35 , while exon 26A is rarely expressed in human tropoelastin. Cross-linking domains are shaded black and hydrophobic domains are white. This structure was identified and produced by Dr. Cheryl Maslen, Dr. Robert Glanville, Darcie Babcock and the Oregon Medical Laser Center research team..... 63

Figure 3.3. Electrospun tubular prTE vascular scaffold. (A) The vascular scaffold was 7 cm in length, 4 mm internal diameter, and consisted of pure prTE fibers. (B) The

prTE fibers were randomly oriented with average fiber diameters of 580 ± 94 nm. The scale bar indicates 5 μ m. 70

Figure 3.4. MATLAB image analysis of fiber orientation. (A) Image of electrospun prTE fibers (B) Normalized probability distribution function plotted as probability of the feature orientation versus angle. Fibers were randomly oriented in these samples. Dr. Sean Kirkpaterick wrote the original MATLAB code that was modified for this analysis. 71

Figure 3.5. Average stress-strain curves for electrospun prTE fibers from a 15 wt% solution for both circumferential and longitudinal orientations (average with 95% confidence interval). The only significant difference in mechanical properties was in the elastic modulus of the tested orientations. Mechanical data was obtained with the excellent technical assistance of Ping Cheng Wu at the Oregon Medical Laser Center. 72

Figure 3.6. Mechanical properties of the electrospun prTE scaffolds. (Top) Representative stress-strain curves of electrospun prTE, extracted porcine elastin, and native porcine carotid arteries. (Bottom) Table of mechanical properties including ultimate tensile strength (UTS), percent elongation at failure, and elastic moduli of electrospun prTE compared to extracted porcine elastin and native porcine carotid arteries. The UTS and elastic moduli of electrospun prTE were not significantly different from the extracted elastin in the longitudinal direction. Note: ^aindicates no significant difference (ANOVA, Tukey post hoc, $p > 0.05$), compared to electrospun prTE in the same orientation, *indicates a significant difference (ANOVA, Tukey post hoc, $p < 0.05$) for comparisons to electrospun prTE in the same orientation, and **indicates $p < 0.01$, t-test. Mechanical data was conducted with the excellent technical assistance of Ping Cheng Wu at the Oregon Medical Laser Center. 74

Figure 3.7. (A) BMEOCs stained for vWF (red) with a DAPI (blue) nuclear stain. (B) Control for vWF stain with the DAPI nuclear stain. (C) Endothelial cell monolayer on 15 wt% prTE after 48 hours in culture. Nuclei are stained with DAPI and the

cytoskeleton (f-actin) is stained with rhodamine phalloidin (red). BMEOCs attached and spread on the prTE scaffold. 79

Chapter 4: Burst Pressure Based Analysis Method for Tissue Engineered Vascular Constructs: A Constitutive Model Development..... 81

Figure 4.1. Graphical representation of the coordinate system used for this model. A cylindrical coordinate system was used. r is the radius, z is the axial or longitudinal displacement along the length, t is the wall thickness, and θ is the circumferential orientation of the cylinder..... 86

Figure 4.2. Biaxial testing device. A linear force transducer is coupled to the fixed end of the vessel (left hand side of this figure). The displacement is controlled with a motor and a linear slide on a custom built testing platform (right hand side of this figure). 91

Figure 4.3. Schematic of testing apparatus..... 92

Figure 4.4. Stress strain plot for an extracted elastin graft for the circumferential and longitudinal orientations..... 94

Figure 4.5. Polynomial curve fit for the strain energy density function..... 95

Chapter 5: Comparison of effect of protein surface on thrombotic and inflammatory responses with comparative *in vitro*, acute *ex vivo* shunt, and chronic *in vivo* studies 99

Figure 5.1. Arteriovenous Shunt model system (A). A dialysis type permanent shunt was placed between the femoral artery and vein. The shunt utilized the animal's blood flow as the driving force with a distal clamp to maintain a flow rate of 100 mL/min. All blood was recirculated back into the animal to minimize blood loss. (B) Typical image obtained from the gamma camera during the study. The image ranges from blue to red for low to high platelet numbers respectively with temporal and spatial resolution. (C) Flow loop positioned on the gamma camera with a flow probe and

distal tubing clamp. Images A and B were obtained from Dr. Stephen Hanson who developed the shunt model system..... 112

Figure 5.2. Illustration of the aorto-iliac bilateral bypass graft model. Grafts are implanted between the aorta and iliac vessels with an end to side anastomosis and the bypassed vessel ligated to direct flow through the shunts. This image was obtained from Dr. Stephen Hanson who developed this model..... 114

Figure 5.3. Sectioning diagram for *in vivo* anastomosis evaluation. Sections were cut throughout the anastomosis to evaluate tissue ingrowth. 115

Figure 5.4. Sectioning of the *in vitro* controls for each section of the graft used for RNA isolation, functional assays and imaging. 117

Figure 5.5. EOCs outgrowth cells at passage 0 on fibronectin coated wells. Image shows typical EOC cobblestone morphology. Deirdre Anderson acquired and provided this image..... 118

Figure 5.6. EOCs on each ECM surface after 48 hrs in culture. Dishes were coated with 5 $\mu\text{g}/\text{cm}^2$ for 1 hour at room temperature. Cells (3×10^5) were plated on each surface, and maintained in 10% EGM-2 media for 24 hours and Hyskon flow media for 24 hours. Scale bar = 20 μm 119

Figure 5.7. DNA/well of EOCs after 48 hrs in culture on each ECM coating. Collagen type I and fibronectin had significantly greater DNA content, and thus more cells, than collagen type IV and α -elastin (ANOVA - Tukey post hoc, $*p < 0.05$). Deirdre Anderson ran the pico green assays. 120

Figure 5.8. EPCR gene expression: There was a significant difference between type I collagen and α -elastin (ANOVA-Tukey post hoc, $*p < 0.05$). 121

Figure 5.9. CD39 gene expression: There were significant differences between type I and IV collagens and α -elastin (ANOVA-Tukey post hoc, $*p < 0.05$). 121

Figure 5.10. (A) TM gene expression (B) VCAM gene expression (C) TFPI gene expression. There were no significant differences between substrates (ANOVA)..... 123

Figure 5.11. APC activity assay: Type 1 collagen and fibronectin had significantly greater activity than type IV collagen and α -elastin (ANOVA-Tukey post hoc, * $p < 0.05$). Deirdre Anderson assisted with the functional activity assay for this study. ... 124

Figure 5.12. TFPI activity assay: The amount of factor Xa ($\mu\text{g/mL}$) produced in samples with and without blocking TFPI. Samples without TFPI inhibition had no detectable Xa. There were no significant differences between substrates (ANOVA). Deirdre Anderson assisted with the functional activity assay for this study. 124

Figure 5.13. Platelet aggregation time and percent clearance for Chronolog type I fibrillar collagen and MP type I collagen. MP collagen at 40 $\mu\text{g/mL}$ had a more variable response and significantly longer clearance time than Chronolog collagen at 20 $\mu\text{g/mL}$. The % clearance or magnitude of the response was not significantly different between collagens. (ANOVA-Tukey post hoc, * $p < 0.05$). Ulla Marzec assisted with the platelet aggregation studies. 126

Figure 5.14. EOCs on type I collagen coated ePTFE graft surface after 48 hours. Nuclei stained with DAPI are shown in blue and the cytoskeleton (f-actin) is stained with rhodamine phalloidin shown in red. EOCs attached and spread on the ePTFE modified surface..... 127

Figure 5.15. Durability of $^{111}\text{Indium}$ labeled EOCs on protein coated ePTFE at 100 mL/min flow rate tested in the baboon shunt system. There was an initial drop (from static to first 5 min frame) in cell numbers with the initiation of flow, but cells remained stable on the graft through 60 min at standard flow rates used in the *ex vivo* shunt studies. Ulla Marzec and Jennifer Greisel assisted with the *ex vivo* shunt studies. 128

Figure 5.16. Durability of $^{111}\text{Indium}$ labeled EOCs on protein coated ePTFE with a flow rate increase from 100 mL/min to 250 mL/min tested in the baboon shunt model system between 60 and 90 min after the initiation of flow. There is no significant

difference in cell coverage (ttest). Ulla Marzec and Jennifer Greisel assisted with the ex vivo shunt studies. 129

Figure 5.17. Cumulative platelet deposition on the EOC ePTFE graft surface over the first 40 min of the flow period. Fibronectin modified samples are shown in red, and type I collagen impregnated samples are shown in blue. Ulla Marzec and Jennifer Greisel assisted with the ex vivo shunt studies. 130

Figure 5.18. TFPI gene expression for *in vitro* controls for the shunt studies. There was a significant difference in expression between type I collagen and fibronectin when paired to the study day (paired ttest, *p < 0.05). 131

Figure 5.19. VCAM gene expression for *in vitro* controls for the shunt studies. There was a significant difference in expression between type I collagen and fibronectin when paired to the study day (paired ttest, *p < 0.05). 131

Figure 5.20. APC activity assay on the *in vitro* controls for type I collagen and fibronectin modified shunts. There were no significant differences in activity between protein coatings. APC data were paired for the study day (paired ttest). Deirdre Anderson assisted with the functional activity assay for this study. 132

Figure 5.21. Factor Xa activity assay on the *in vitro* controls for type I collagen and fibronectin modified shunts. There were no significant differences in activity between protein coatings. Factor Xa data were paired for the study day (paired ttest). Deirdre Anderson assisted with the functional activity assay for this study. 133

Figure 5.22. Correlation of platelet accumulation on the graft surface and FXa production in the presence of TFPI blocking antibody on both type I collagen and fibronectin coated ePTFE grafts. Deirdre Anderson assisted with the functional activity assay for this study. 134

Figure 5.23. Fibrin accumulation on 2cm length of the type I collagen and fibronectin modified ePTFE shunt grafts. There were no significant difference in the amount of fibrin deposited on the surface of the graft between protein coatings (paired ttest) data

were paired to the study day. Ulla Marzec and Jennifer Greisel assisted with the fibrin quantification for the ex vivo shunt studies. 135

Figure 5.24. Implant of type I collagen coated EOC-seeded ePTFE graft in a baboon aorto-iliac bypass model. Dr. Howard Song implanted grafts with the assistance of the ONPRC surgical staff. 136

Figure 5.25. Explant after 1 month of a type I collagen coated EOC-seeded ePTFE graft in a baboon aorto-iliac bypass model. All grafts were patent at 1 month. 136

Figure 5.26. Representative histology sections of 1 month explants of type I collagen coated EOC-seeded ePTFE grafts in a baboon aorto-iliac bypass model. All implant grafts were patent at 1 month, but there was variable pannus ingrowth between samples with (A) showing little ingrowth and (B) showing significantly more tissue ingrowth. The TF expression for the matched *in vitro* control was higher in the B sample than the A. Deirdre Anderson assisted with the tissue ingrowth evaluations for this study. 137

Figure 5.27. Tissue ingrowth for untreated ePTFE controls and collagen coated EOC-seeded ePTFE grafts one month after implant. Further implants will be conducted to determine significant differences between the control and the EOC-seeded grafts. These are average values for proximal and distal anastomoses for two grafts per animal and two animals per group for a total of four grafts per treatment group. Deirdre Anderson assisted with the tissue ingrowth evaluations for this study. 138

Figure 5.28. Tissue ingrowth for untreated ePTFE controls and collagen coated EOC-seeded ePTFE grafts one month after implant. There were no significant differences between the control and the EOC-seeded grafts. These are averaged numbers for proximal and distal anastomoses averaged between two grafts per animal and two animals per group for a total of four grafts per treatment group. Deirdre Anderson assisted with the tissue ingrowth evaluations for this study. 139

Figure 5.29. Tissue ingrowth for collagen coated EOC-seeded ePTFE grafts one month after implant. There were differences between animals. These are averaged

numbers combining the proximal and distal anastomoses with two grafts per animal for a total of 4 anastomoses per animal analyzed. Deirdre Anderson assisted with the tissue ingrowth evaluations for this study.	140
Figure 5.30. Endothelial cell layer on ePTFE control grafts (left) and EOC-seeded type I collagen modified grafts (right). A distinct cell layer can be seen on both luminal surfaces. Deirdre Anderson assisted with the tissue ingrowth evaluations for this study.	141
Chapter 6: Conclusions and Future Directions.....	149
Figure 6.1. TEM of a tropoelastin coacervate. Banding can be seen along self assembled fibrils. TEM imaging was done with the assistance of Dr. Jack McCarthy.	150
Figure 6.2. Distribution of fiber for co-electrospinning of collagen and tropoelastin. There was a larger spread of protein for tropoelastin than collagen. Collagen is shown on the left hand side and tropoelastin is shown on the right hand side.	153
Figure 6.3. Coelectrospun tropoelastin and collagen fibers. Distinct fiber morphologies are seen within the biomaterial.	154

List of Tables and Equations

Tables

Table 2.1: Fiber diameter and pore size for electrospun rTE and extracted porcine elastin	43
--	----

Equations

Equation 4.1: Deformation vector	84
Equation 4.2: Stretch Ratio for an incompressible material	84
Equation 4.3: Longitudinal Stretch Ratio	87
Equation 4.4: Circumferential Stretch Ratio	87
Equation 4.5: Longitudinal Green's Strain	88
Equation 4.6: Circumferential Green's Strain.....	88
Equation 4.7: Longitudinal Strain Energy Density Function.....	88
Equation 4.8: Exponential Strain Energy Density Function.....	88
Equation 4.9: Material Function.....	89
Equation 4.10: Circumferential Kirchhoff Stress.....	89
Equation 4.11: Longitudinal Kirchhoff Stress	89
Equation 4.12: Circumferential Kirchhoff to Cauchy Stress Conversion.....	89
Equation 4.13: Longitudinal Kirchhoff to Cauchy Stress Conversion	90
Equation 4.14: Circumferential Cauchy Stress	90
Equation 4.15: Longitudinal Cauchy Stress.....	90

List of Abbreviations

Ab	antibody
ADP	adenosine diphosphate
ACD	acid citrate dextrose
AHA	American Heart Association
ANOVA	analysis of variance
APC	activated protein C
AV	Arteriovenous
BMEOC	bone marrow derived endothelial outgrowth cell
BS3	<i>bis</i> (sulfosuccinimidyl) suberate
BSA	bovine serum albumin
C	celsius
C	circumferential
CD133	Cluster of differentiation marker 133 –stem sell marker
CD31	Cluster of differentiation marker 31 = PECAM
CD39	Cluster of differentiation marker 39
Col	collagen
CPM	counts per minute
CVD	cardiovascular disease
DAPI	4',6-diamidino-2-phenylindole

DI	deionized water
DMEM	Dulbecco's Modified Eagle Medium
DNA	deoxyribonucleic acid
DSS	disuccinimidyl suberate
EBM	endothelial basal medium
EBP	elastin binding protein
EC	endothelial cell
ECM	extracellular matrix
EDTA	ethylenediamine tetraacetic acid
EGF	endothelial growth factor
EGM	endothelial cell growth media
E_{ij}	Green's Strain
eNOS	endothelial nitric oxide synthase
EOC	endothelial outgrowth cell
EPC	endothelial progenitor cell
EPCR	endothelial protein C receptor
EPCR	endothelial protein C receptor
ePTFE	expanded polytetrafluoroethylene-Goretex®
F	axial force
FAK	focal adhesion kinase
FBS	fetal bovine serum
FN	fibronectin

FVII(a)	(activated) coagulation factor VII
FX(a)	(activated) coagulation factor X
GAPDH	glyceraldehyde 3-phosphate dehydrogenase
GPCR	G-protein-coupled receptor
H&E	hematoxylin and eosin
HBSS	Hank's balance salt solution
HEPM	human embryonic palatal mesenchymal cell
HFP	1,1,1,3,3,3-hexafluoro-2-propanol
ICAM	intercellular Adhesion Molecule
II	prothrombin
IIa	thrombin
IL-6	interleukin 6
IL-8	interleukin 8
IX	coagulation factor IX
L	longitudinal
L-glut	L-glutamine
LDL	low-density lipoprotein
λ_i	stretch ratios
L_z	longitudinal length
mAb	monoclonal antibody
MAGP-1	chaperon protein
MAP kinases	Mitogen-activated protein kinases

MCP-1	monocyte chemotactic protein-1
MEM	minimum essential media
MNC	mononuclear cell
NO	nitric oxide
P	pressure
Pa	pascal
PBS	phosphate buffered saline
PCL	poly ϵ -caprolactone
PDO	polydioxanone
PECAM	platelet endothelial cell adhesion molecule = CD31
PEO	poly(ethylene oxide)
PET	poly(ethylene terephthalate)-Dacron®
PGA	poly glycolic acid
PLA	poly lactic acid
PLGA	poly lactide-co-glycolide
PLGA	poly(lactic-co-glycolic acid)
prTE	poly recombinant tropoelastin
PSF	Penicillin streptomycin fungizone
r_i	inner radius
RNA	ribonucleic acid
$r_o W$	strain energy density function
rTE	recombinant tropoelastin

SEM	scanning electron microscopy
Si	silicon
S_{ij}	Kirchhoff stress
σ_{ij}	Cauchy stress
SMC	smooth muscle cells
σ_{θ}	Hoop Stress
TCP	tissue-culture treated plastic
TEM	transmission electron microscopy
TF	tissue factor
TFPI	tissue factor pathway inhibitor
TM	thrombomodulin
TNF α	tumor necrosis factor alpha
τ_w	wall shear stress
UTS	ultimate tensile strength
V	coagulation factor V
Va	coagulation factor Va
VCAM	vascular cell adhesion molecule
VDA	video dimension analyzer
VEGF-R2	vascular endothelial growth factor receptor-2
VII	coagulation factor VII
VIIa	activated coagulation factor VII
VvG	Verhoeff van Giesen

vWF	von Willebrand factor
w/v	weight/volume
wt%	weight percent
X	coagulation factor X
Xa	activated coagulation factor X
XIII	coagulation factor XIII

Acknowledgements

First, I would like to thank my primary advisor Dr. Monica Hinds. She has always been there to listen to my ideas and provide feedback and direction on these projects. She has been an excellent mentor throughout this process. I would also like to thank Dr. Stephen Hanson who brought his excellent expertise to OHSU introducing the primate model thus allowing us to conduct relevant graft analysis. He has provided valuable insight into thrombosis biology throughout the process to maintain critical perspective. I would also like to thank Dr. Kenton Gregory who has been an excellent mentor to me over the past ten years both with my thesis work as well as at OMLC. He has provided me with the unique opportunity to study tropoelastin based biomaterials which could not have happened without him. I would also like to thank my thesis committee members Dr. András Gruber, Dr. John Mitchell, and Dr. Wassana Yantasee who have provided their excellent review of this work, each contributing their unique perspective. I would also like to thank Rebecca Sarao for her scientific input and excellent review skills—watch out for those capital Ws, as well as, each of my other coauthors for their valuable scientific input. I would like to thank Dr. Jack M. McCarthy for his assistance with SEM and TEM imaging. He always took the time to help and discuss my projects. He was a true inspiration at OHSU and will be greatly missed! I would also like to thank Dr. Brian Kim for his assistance with cross-linking modalities, and Dr. Sean Kirkpatrick for his assistance in evaluating fiber orientation. I would also like to thank Dr. Michael Rutten for isolation of the bone marrow mononuclear cells. Tropoelastin was produced with the excellent technical assistance of Amy Jay, Cher Hawkey, and Rose Merten. I would like

to say a special thank you to Ulla Marzec who is an amazing wealth of knowledge on everything “platelet” and keeps the ONPRC lab running with efficiency and Jennifer Greisel for the expert management of the animals and data analysis. Deirdre Anderson was a great teammate on the ePTFE graft project and the functional assay expert. Finally, I would like to thank all my labmates at both OMLC and OHSU. Science is truly a collaborative process without all of your input these projects would not have been possible.

This work was funded in part by the NIH R01-HL095474, NIH R01-HL103728, and the Department of the Army, Grant Nos. W81XWH-04-1-0841 and W81XWH-05-1-0586.

This work does not necessarily reflect the policy of the government and no official endorsement should be inferred.

On a personal note, I would like to thank my family. They have endured along with me making sacrifices to help promote my success. Sean, you are my love and my rock; Sierra and Kaia, my inspiration; and Mom and Dad my foundation.

Abstract

Development and Characterization of Extracellular Matrix Based Vascular Graft Biomaterials

Kathryn Alyce McKenna

Department of Biomedical Engineering
School of Medicine
Oregon Health & Science University

August 2011

Thesis Advisor: Monica T. Hinds, Ph.D.

There is a significant need for viable small diameter vascular graft biomaterials.

Treatment options for bypass grafts are limited to either autologous vessels, which are often not available and can be affected by pre-existing disease, or synthetic grafts, which are limited to vessels larger than 6 mm in diameter. Small diameter vascular grafts have been under development for more than 50 years with limited clinical success. Vascular grafts often fail due to thrombosis, intimal hyperplasia, and aneurysm formation. This dissertation centers on the influence of the extracellular matrix (ECM) on vascular functional responses. The ECM is the primary support for the vascular endothelium and can influence apoptosis, proliferation, cell shape and contractility. Novel human recombinant tropoelastin vascular graft biomaterials and ECM modified clinically relevant synthetic ePTFE vascular grafts were developed and evaluated.

Vascular biomaterials are needed that support cell growth, are non-thrombogenic, minimize intimal hyperplasia, match the structural and mechanical properties of native

vessels, and allow for regeneration of arterial tissue. Novel electrospun human recombinant tropoelastin vascular graft biomaterials were developed that demonstrated comparable structural and mechanical properties to native elastin. These three-dimensional tubular biomaterials demonstrated good vascular cell biocompatibility and growth characteristics.

There is a need to provide a means by which researchers can acquire and meaningfully compare properties of vascular construct designs. A biaxial constitutive model and testing methods were developed using a modified burst pressure testing system to measure and derive strain energy density functions for tissue-engineered vascular constructs.

Endothelial outgrowth cells (EOCs) are a promising source of autologous endothelial cells that can be readily isolated and expanded *in vitro*. EOC functional responses to extracellular matrix proteins have not been well characterized. The thrombogenic and inflammatory potential of these cells was evaluated on protein modified clinically relevant ePTFE small diameter grafts. Platelet accumulation in *ex vivo* shunt testing was independent of surface coating, but showed a distinct correlation to factor Xa generation for paired *in vitro* controls.

Collectively, this dissertation provides new insights into the connections between extracellular matrix proteins, vascular cells, and vascular functional responses.

Chapter 1: Introduction

1.1 Cardiovascular Disease

Cardiovascular disease remains the number one cause of morbidity and mortality in the Western world. In 2006, nearly 81 million people were affected by cardiovascular disease in the United States [1]. This has a significant effect on the United States health care system with total direct and indirect treatment costs totaling 503.2 billion dollars for 2010 [1]. Atherosclerosis is a significant cardiovascular disease of muscular arteries, in which, the inner layer becomes thickened by fatty deposits and fibrous tissue leading to vessel narrowing, which reduces and ultimately blocks blood flow. Early atherosclerotic lesions localize preferentially at branches and bifurcations in the vascular tree where arterial geometries are complex and flow fields disturbed (Figure 1.1). The highly localized topography of early lesions is particularly interesting in view of similar exposure levels, within these lesion prone sites, to oxidized LDL and other toxins as lesion resistant sections of arteries. Focal disease patterns indicate that unique conditions exist at these sites, such as localized mechanical factors, predisposing these regions to disease initiation and propagation.

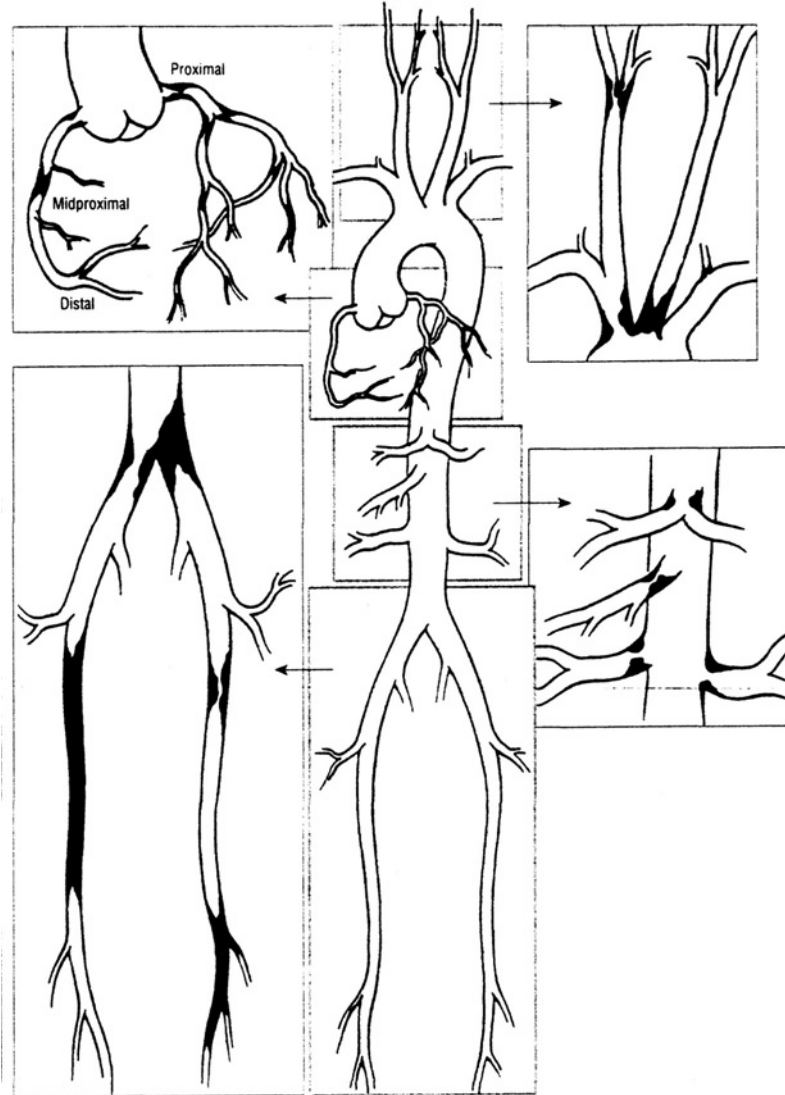


Figure 1.1. Common Plaque formation sites in the vascular tree [2]

As the disease progress, surgical intervention becomes necessary to restore blood flow to vital tissues. One treatment option is to bypass the diseased arterial segment, thus restoring blood flow to downstream tissues by shunting blood around the occluded section. Dr. Vasilli Kolesov performed the first coronary artery bypass surgery using the internal mammary artery in 1964 [3]. Treatments using vascular grafts have not significantly changed in 30 years, with mammary artery and saphenous vein autografts

remaining the gold standard treatment options for bypass surgery. Synthetic materials, such as expanded poly(tetrafluoroethylene) (ePTFE) and poly(ethylene terephthalate) (PET or Dacron[®]), were introduced to the market in 1975 by Impra[®] Inc. and W.L. Gore[®] and have been successfully used for large diameter vessels, but are not appropriate for vessels under 6 millimeters in diameter [4-6]. Vascular grafts often fail due to thrombosis, intimal hyperplasia, and aneurysm formation [7]. The goal of this work is to improve vascular graft biomaterials by incorporating extracellular matrix (ECM) proteins into vascular graft biomaterials and mimic the native environment's mechanical and cell signaling properties.

1.2 The Extracellular Matrix of the Arterial Wall

The arterial wall is composed of three distinct layers defined by organized layers of cellular and ECM components. The structure is designed to withstand and respond to the vasculature's complex mechanical environment throughout the cardiac cycle including fluid mechanical tangential shear forces, longitudinal and circumferential stress and strains, as well as its response to vasoactive substances. The intima is the innermost layer. This thin layer contains a monolayer of endothelial cells (ECs) as well as the subendothelial space occupied by ECM proteins, commonly referred to as the basement membrane. The middle layer is the media, which is the thickest layer consisting primarily of smooth muscle cells in an ECM of collagen, elastic fibers, and proteoglycans. The media helps propel blood through the arteries by stretching during systole and recoiling during diastole. The outer layer is the adventitia that contains smooth muscle cells, fibroblasts, collagens, nutrient vessels (vasa vasora), nerves, and

lymphatics that service the artery. The intima and media are separated by the internal elastic lamina, while the external elastic lamina separates the media from the adventitia.

Normal arterial structure is depicted in Figure 1.2.

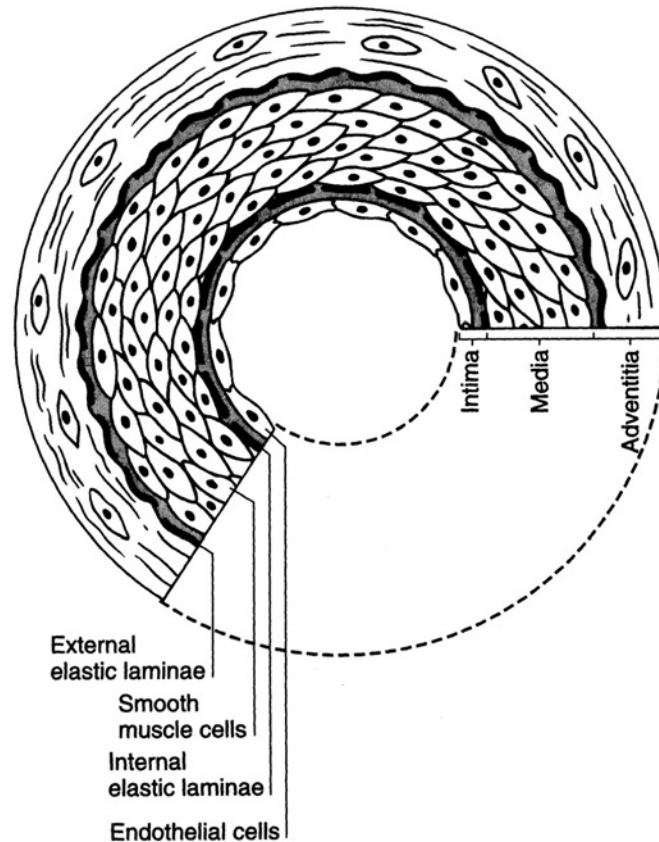


Figure 1.2. Cross-sectional schematic of the structure of the arterial wall. The three major vessel layers from the lumen outward are the: intima, media, and adventitia. The internal and external elastic lamina matrix layers are also represented. [8]

The importance of the ECM has been recognized for providing mechanical support, adding strength and resilience to the arterial wall, as well as, its role in regulating cellular functions. The ECM is the primary support for the vascular endothelium [9], which organizes and maintains a stable functional monolayer of cells [10]. The functions of ECs influenced by the ECM are complex and are regulated through multiple signaling

pathways controlling apoptosis proliferation, cell shape and contractility [9]. The basement membrane is 20 to 200 nm thick, anchors the ECs within the intima, and primarily consists of type IV collagen and laminin ECM proteins [11]. The basement membrane ECM is spatially and temporally regulated during angiogenesis *in vivo*, and influences cell attachment and proliferation *in vitro*. A stable basement membrane provides anti-proliferative cues to the cells, but under disease conditions provisional ECM proteins (collagen and fibronectin) are laid down, which signal cell proliferation and the formation of new blood vessels [9]. Understanding the interplay between the ECM's mechanics and functional cellular responses is critical to develop and implement new treatments for cardiovascular disease as well as to elucidate the ECM's role in vascular biology.

1.2.1 *Elastin*

The elastic fibers of the arterial wall contain two morphologically distinct components: crosslinked elastin molecules and microfibrils, which link elastin molecules into a fiber structure (Figure 1.3). Elastic fibers are found within many connective tissues of body. This protein's primary mechanical function is to allow for elastic recoil in connective tissues such as blood vessels, tendons, ligaments and skin [12]. Additionally, elastin has an important cell signaling role modulating cell proliferation, contractility and migration. Elastin comprises 30% of the dry weight of the aorta, 75% of elastic ligaments such as the ligamentum nuchae, 5% of skin and 4% of tendon [13, 14]. Elastin is thermally stable to 140°C and is relatively biologically and chemically inert, as compared to other matrix proteins such as collagen, and is one of the most hydrophobic proteins known

[12]. The elastin gene is well conserved with greater than 70% similarity across vertebrate species, resulting in low cross species antigenicity [14]. Elastin is rich in nonpolar amino acids. The hydrophobic domains, specifically the proline and glycine residues, make up 42% of the elastin monomer (tropoelastin), and have been proposed to be responsible for the elastic properties of elastic fibers [15-18]. Glycine is the most abundant amino acid in elastin, comprising more than 30% of the protein. Valine, leucine, isoleucine, and alanine compose most of the balance of elastin components. The microfibrils are rich in acidic glycoproteins and are organized into 8-16 nm fibrils with a beaded appearance. These fibrils contain two forms of 350 kDa glycoprotein fibrillin and two micro-fibril-associated glycoproteins MAGP-1 and MAPG-2 [14]. The dynamic interaction of the elastin molecules and the microfibrils within the elastic fiber are responsible for the elastic recoil property of elastic tissues. The pathologic loss of elastin, or deficiency in elastin expression, is associated with end stage aneurysm disease and supraaortic stenosis [19-26].

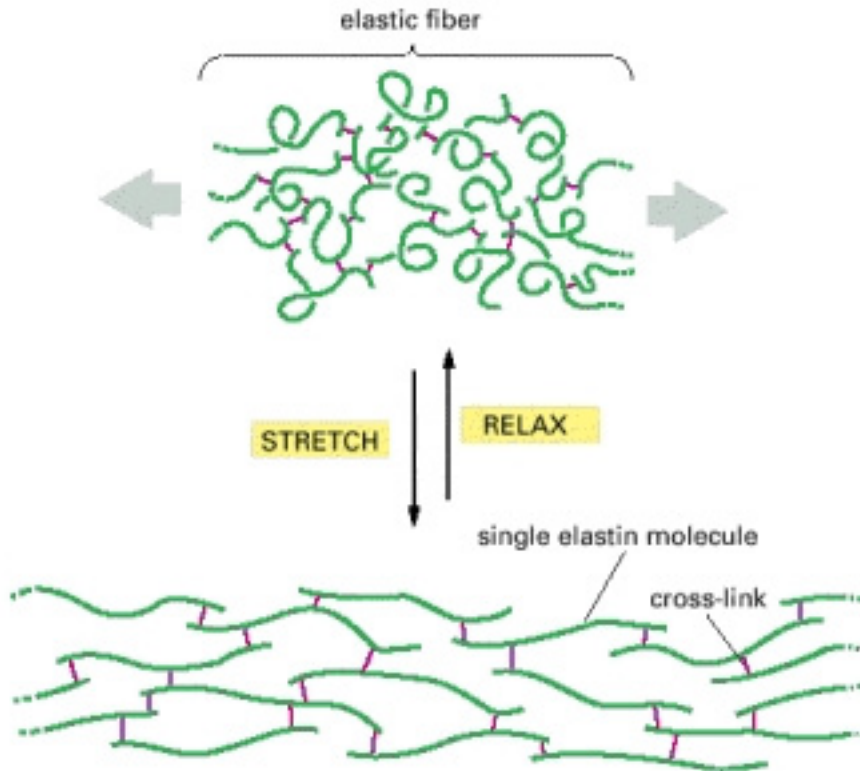


Figure 1.3. Structure of Elastin: The structure and assembly of the elastic fibers are responsible for the elastic nature of the protein. Elastin molecules stretch and align under loading and relax and bundle up after the load is removed. [27]

1.2.1.1 Tropoelastin

The full-formed polymer elastin structure is made up of soluble tropoelastin monomers that are self-assembled via coacervation and crosslinked with lysyl oxidase. Human tropoelastin is encoded by a single gene with 34 exons and can exist as multiple isoforms depending on the mRNA splicing pattern. The typical splicing pattern results in a mature protein with a molecular weight of 60 kDa. There are two main, hydrophobic and hydrophilic, domain types. Structural studies of tropoelastin have been challenging due to the molecules ability to self-associate and the limited source of pure tropoelastin [28]. Recently, the nanostructure of tropoelastin has been defined using small angle X-ray and

neutron scattering [29]. Specific regions of the molecule along with the full-length monomer were characterized elucidating the orientation of the structure defining the N and C termini. Tropoelastin's structure is asymmetric with a long gradual coil starting from the N terminus with a spur and bridge region connecting a protruding foot at the C-terminus (Figure 1.4). The coil region acts as the elastic axis of the molecule, and the spur region, containing exons 20-24, acts as a hinge between the bridge and coil regions. Domains 19-25 cluster between the spur and bridge regions indicating enriched cross-links. The cell contact C-terminal region is contained within the compact foot-like region of the molecule [29].

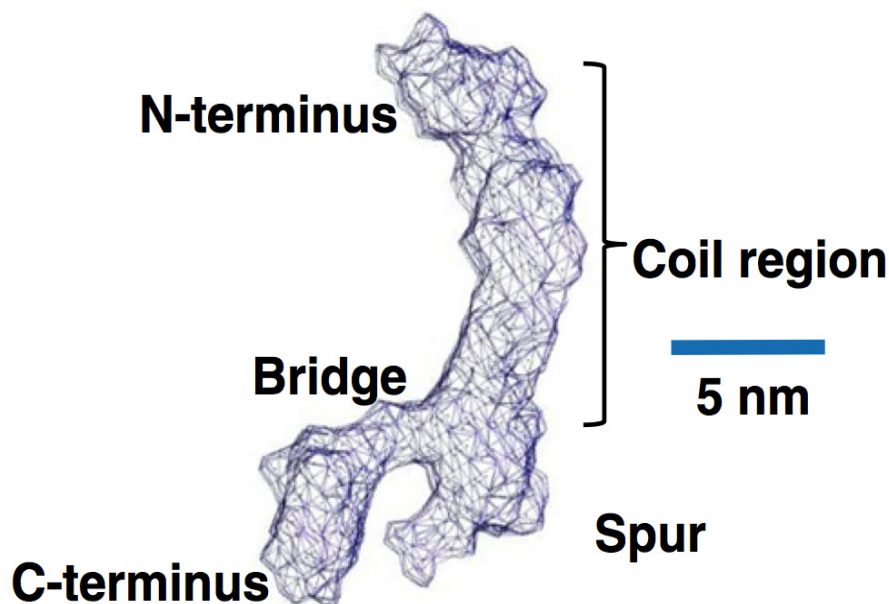


Figure 1.4. Structure of Tropoelastin: The structure of the full-length tropoelastin monomer is shown with the N-terminus leading to the coil region, which is responsible for the elasticity in the molecule, to the lower hinge region in the spur, and a bridge to the cell binding C-terminus. [28]

Tropoelastin has been commonly described as an unstructured or amorphous protein.

Theoretical structural models of elastin and tropoelastin contain an element of disorder,

due to the folding patterns between hydrophobic β -sheets within the protein's structure, and have been used to describe the mechanism for elastin's flexibility [28]. The elasticity of tropoelastin is likely not solely due to this disorder or chaos in the structure, but also imparted by the coiled region of the tropoelastin molecule [29]. Tropoelastin's unique molecular structure remains more hydrated and flexible, even when aggregated, than globular proteins of similar sizes [30], which allows for building hyper-elastic tissues. Tropoelastin's elastic molecular structure, along with its ability to self-organize, makes it a natural choice for building compliant elastic vascular graft biomaterial constructs.

The assembly process of tropoelastin into elastin occurs outside the cell [31].

Tropoelastin is chaperoned to the cell surface by the elastin binding protein and externalized from the cell. Tropoelastin monomers aggregate and are rapidly organized by coacervation in a self-assembly process. The coacervate remains tethered to the cell surface until it is released to newly forming elastic fibers, which are then cross-linked by lysyl oxidase to form the functional elastin polymer. Elastin is then linked by microfibrils to form the functional elastic fiber, which has bi-, tri-, and tetra-functional crosslinks in its final assembled state. The majority of elastin formation occurs early in development during the late fetal and early neonatal phases of development, with little to no elastin being formed after maturity.

For this research project, human tropoelastin was optimized and expressed from a synthetic gene codon in gram quantities in a 10-liter E.coli fermentation system. Gel electrophoresis determined that the purification procedure resulted in a greater than 99%

pure product (see Figure 2.1) as well as low endotoxin levels with an average of 0.2 EU/mg as determined by the Kinetic-QCL Assay (Cambrex). The purified human tropoelastin protein includes all of the functional exons with the exception of exons 1, 22, and 26A (see Figure 2.2). Exon 1 contains the signal sequence, while hydrophobic exon 22, and hydrophilic exon 26A are rarely expressed in mature elastin. The resultant tropoelastin exon structure used is the same as a natural isoform produced by normal human fetal heart cells. This purified human recombinant tropoelastin was cross-linked with the chemical cross-linkers DSS, BS3, and EDC/NHS to form structured elastin-like biopolymers. The goal of developing these polytropoelastin biomaterials was to determine the ability of these materials to mimic native elastic tissues mechanically, while maintaining vascular cell signaling.

1.2.1.2 Coacervation Dynamics of Human Recombinant Tropoelastin

The functional reactivity of the tropoelastin construct used in these studies was verified by evaluating its coacervation dynamics. Coacervation is a reversible process of phase separation of the bulk material from the solvent and is critical in elastin formation *in vivo*. *In vitro* human recombinant tropoelastin reversibly separates out of PBS as a coacervate at 37°C and physiologic pH. This process is dependent upon temperature, the amount of salt in the solution, and the tropoelastin concentration in solution [14, 32, 33]. The dynamics of this process was followed for the tropoelastin construct used in these studies by the Oregon Medical Laser Center in real time with a Zeiss Meta multi-photon confocal microscope. Tropoelastin was stained in solution with 2.5 µg/ml Oregon Green (Molecular Probes) for 1 hour. Tropoelastin was kept on ice prior to visualization to keep the tropoelastin in an uncoacervated state. Five microliter drops of 50 mg/ml tropoelastin

were then placed on glass coverslips and the temperature was raised to 37°C to view the dynamics of the coacervation process. Views were focused on the outside perimeter of the tropoelastin drop. A series of frames were extracted from a confocal movie to show the progression of the different coacervation stages (Figure 1.5). Spheroid aggregates of rTE started forming immediately as small bubbles (0 minutes). These then coalesced to form larger sphere aggregates (1 minute). A distinct transition was seen where the tropoelastin coalesced and only the stained tropoelastin could be seen (2 minutes). The tropoelastin then formed hollow spheres (2.5 minutes) that fused to ultimately form pocket-like structures of various sizes (3-6 minutes). In the final coacervated state, the PBS was observed to separate from the tropoelastin pockets. This whole process was complete within 6.5 minutes. It was also shown that the coacervation of rTE in PBS was highly dependent on rTE concentration--with higher concentrations forming larger pocket structures (data not shown). Verifying the ability of tropoelastin used in these studies to coacervate in solution demonstrates its capability to self-assemble in a manner similar to native tropoelastin, thus confirming its bioreactivity. This confirmation provides important validation for its use as a starting material for developing elastic vascular graft biomaterials.

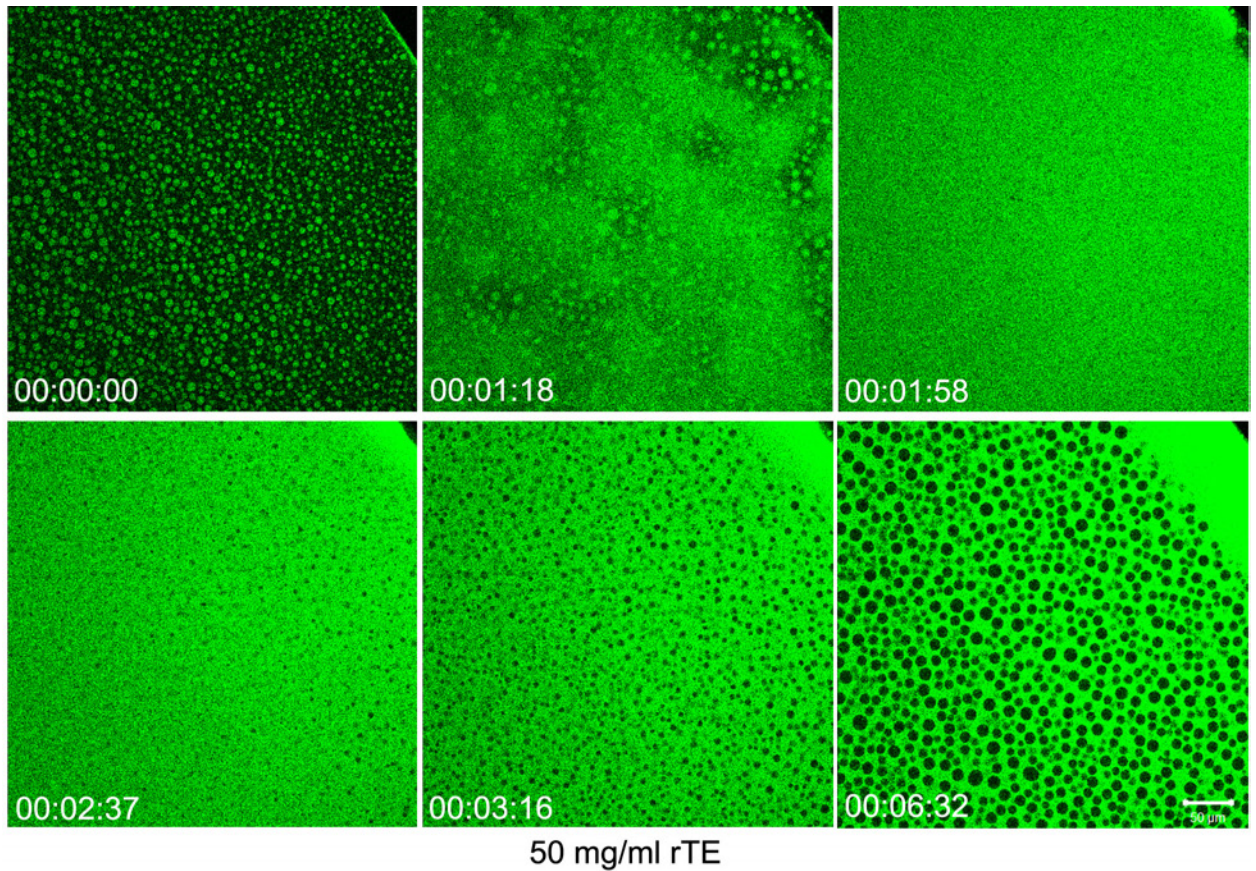


Figure 1.5. Time series (hh:mm:ss) of frames from a confocal movie showing the dynamic process of rTE coacervation at 50 mg/ml and 37°C. The 00:00:00 panel shows the initial solid sphere structure and the 00:06:32 panel shows the final hollow sphere-pocket structure. Tropoelastin was stained with Oregon Green for visualization. Tropoelastin is shown in green and the solvent PBS is shown in black. (Scale bar = 50 μ m). Dr. Robert Glanville, Rebecca Sarao, and Rose Merten at the Oregon Medical Laser Center Bioimaging Facilities obtained these images.

1.2.2 Collagen

Collagens are a family of fibrous proteins constituting 25% of the total protein in mammals and ranges from 20% of the dry weight of the aorta up to 51% in canine carotid arteries [13, 34]. There are 25 distinct collagen molecules. Collagens form the fibrillar and microfibrillar networks of the ECM. Collagen consists of three polypeptide chains with a nonpolar glycine at every third position. This regular structure allows the chains

to wind generating a triple helical structure (Figure 1.6). Collagen molecules bind to each other in a regular pattern in overlapping arrays to form collagen fibrils that give connective tissue their strength [27].

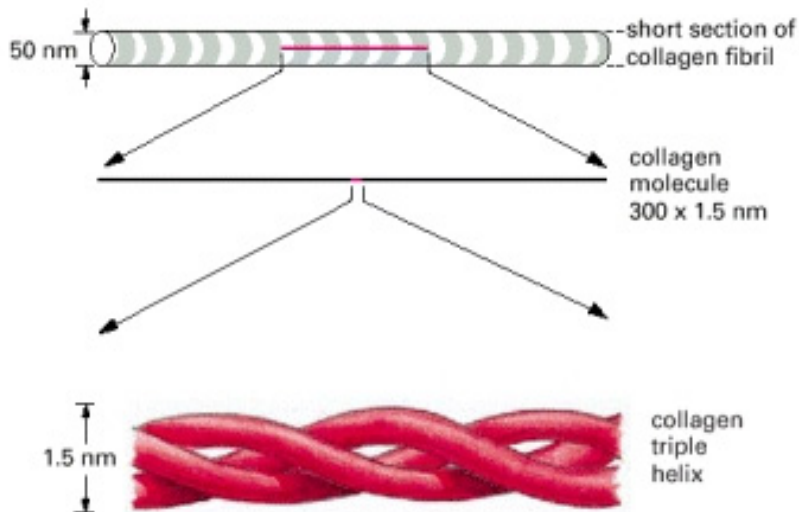


Figure 1.6. Collagen Structure. Collagen fibrils assemble to form a collagen triple helix structure. [27]

Type I collagen is the most abundant collagen and is a major component of connective tissues and the most abundant form of collagen in arteries. It has a triple helical structure and confers mechanical tensile strength to tissues. It is composed of two identical alpha 1 chains and one alpha 2 chain [35]. Mutations in type I collagen are linked to type VIIA and B Ehlers–Danlos syndrome [36], resulting in loose joints and skin, and osteogenesis imperfecta [37], commonly referred to as brittle bone disease. Type I collagen is a natural choice to use as a vascular graft biomaterial, due to its prevalence in the vasculature, ability to add mechanical tensile strength, and its cell biocompatibility.

Type IV collagen has a molecular weight of 540 kDa and is a structural component of the basement membrane that organizes other basement membrane components like the laminins and proteoglycans [38]. The structure has three domains: the N-terminal domain, the C-terminal globular domain, and a central flexible triple helical structure. Many mutations of type IV collagen are embryonically lethal, but mutations in the alpha-3 4 and 5 chains have been linked to forms of Alport syndrome, which is a kidney glomeruli disease [35]. Type IV collagen is the main structural organizer of the basement membrane and is closely associated with the EC monolayer, making it a natural choice for evaluating EC's functional responses on ECM based vascular graft biomaterials.

1.2.3 Fibronectin

Fibronectin is a cell interactive glycoprotein encoded by a single large gene with 50 exons, with in a number of variant isoforms, up to 20, due to alternatively splicing patterns. Fibronectin usually exists as a dimer with two nearly identical subunits, which are linked with disulfide bonds at the C terminus [39]. There are three types of repeating subunits; with 12 type I repeats, two type II repeats and 15-17 type II repeats in total accounting for 90 % of the protein [39]. Fibronectin can be found in multiple tissue types and can be classified as either “plasma” or “cellular” fibronectins. Plasma fibronectin exists as a significant proportion of the blood, 0.3 g/L, but remains freely soluble until incorporated into blood clots or tissue matrices. This is due to the precise regulation of fibril formation in a cellular matrix assembly system. Cellular fibronectins are produced by a variety of cell types, which secrete and organize them into an insoluble ECM [40]. Fibronectin acts as an important ligand for cells via the integrin family of receptors, with

best known of these being the RGD sequence. Fibronectin plays important roles in cell adhesion, growth, migration, differentiation, wound healing, and embryonic development [40]. Fibronectin is a well-studied substrate for EC attachment and growth making it a logical ECM substrate for comparing EC functional responses.

1.3 Vascular Graft Biomaterials

Natural biomaterial scaffolds based on ECM proteins have been proposed to address the failure of small diameter vascular grafts. The initial use of synthetic scaffolds, including ePTFE, poly(ethylene glycol) diacrylate, poly(caprolactone), and polyurethane as vascular graft biomaterials, has the advantage of controllable physical and mechanical properties, which are highly reproducible and easily manufactured in large scale quantities. Yet these synthetic scaffolds typically lack the elasticity of native arterial walls and the biocompatibility for long-term vascular cell functionality. Natural biomaterial scaffolds, including the most studied grafts of decellularized arteries, have had limited success. The two most successful examples of decellularized arteries without cell seeding have been Sawyer's ficin-digested glutaraldehyde-tanned bovine carotid graft [41] and Dardik's glutaraldehyde-tanned human umbilical vein graft [42]. While the 5-year patency rates were promising, aneurysm formation due to in vivo degradation limited their widespread use [42, 43]. Decellularized arteries are attractive scaffolds for tissue-engineered vascular grafts due to their mechanical and biological properties [44], yet these natural scaffolds are still limited by the lack of precise manufacturing control of the physical and mechanical properties.

Tissue-engineered vascular grafts incorporate vascular cells into the design of graft biomaterials. Autologous vascular cells have been used to produce and deposit ECM proteins to build tissue-engineered vascular graft matrix without using an initial scaffold. These tissue-engineered grafts have advanced from the research bench to clinical safety trials [4, 45], with promising results, in an arteriovenous shunt model, with primary patency rates of 78% at 1 month and 60% at 6 months. Failures were observed to be due to thrombosis, dilation, and aneurysm. These tissue engineered vascular grafts have lengthy production times of 24 weeks [4], which is a limiting factor in becoming a practical clinical option. Small diameter tissue-engineered vascular graft development has been the focus of many research groups, but a viable clinical option that structurally compares to native arteries, supports cell growth, and is functionally equivalent to autografts has not been found. Controlling the physical and biological properties of the ECM based vascular graft biomaterials, by defining the distribution, composition, and structure of the ECM, may be the key in developing a clinically relevant, highly reproducible vascular graft biomaterial.

1.3.1 Electrospinning of Extracellular Matrix Proteins

Electrospinning is a strategy that can be used to produce ECM based vascular graft biomaterials with controllable physical properties. This method draws sub-micron sized fibers from a polymer solution (both natural proteins or synthetic polymers) and deposits them on a grounded collection device, which can be any size length or shape of the desired biomaterial construct. This phenomenon is driven by the balance between surface charge and surface tension of the polymer solution. The fibers are drawn from the

solution when the surface charge overcomes the surface tension of the polymer solution. Electrospinning has proven to be a valuable tool to produce biomimetic scaffolds for use in tissue engineering. Electrospinning has been used to produce fibrous scaffolds from many biodegradable polymers, such as poly ϵ -caprolactone (PCL), poly lactic acid (PLA), poly glycolic acid (PGA), and poly lactide-co-glycolide (PLGA) [46-49]. These materials have been proposed for use in bone, cardiac, blood vessel, and wound dressing applications [50-56]. Mathews and Boland have used elastin and collagen co-electrospun matrices for tissue engineering applications [57, 58]. Huang was the first to electrospin collagen for use in wound repair [59, 60]. Many protein solutions have been electrospun successfully, including α -elastin, tropoelastin collagen, and gelatin [61]. While this technique can be used to produce fibrous scaffolds from a variety of starting materials, careful design must be implemented to optimize scaffold properties for vascular graft applications. Mechanically, these scaffolds require a balance between elasticity and tensile strength to respond to and withstand the vasculatures' dynamic fluid mechanical environment. Biologically, these materials must maintain an optimal environment for cell growth by promoting infiltration through the media while maintaining a stable structure for the luminal EC monolayer.

1.3.2 Modifications of Vascular Graft Biomaterials

Synthetic materials are easily manufactured with controllable physical properties but lack favorable biological properties. A promising way to integrate ECM proteins' biological signaling properties into vascular grafts is through the surface modification of synthetic materials. The two main determinants of vascular graft success have been the

thrombogenic potential of the material and the extent of intimal hyperplasia progression [62]. Early graft occlusion is primarily influenced by thrombosis with intimal hyperplasia affecting long-term results. Many variables modulate the thrombogenic potential of a graft construct. Considerable efforts have been made to develop a synthetic graft with favorable blood contacting properties [63]. The main strategy to develop a compatible synthetic surface has been to modify its interface properties. Strategies have included protein coatings such as collagen [64], heparin incorporation [65-68], anti-platelet factor incorporation [69-75], electrical surface charge modification, surface wettability, and graft endothelialization [63]. Treatments of conventional ePTFE grafts with ECM components (including fibronectin, collagen, and laminin) typically increase mature endothelial cell adhesion and retention.

Endothelialization as a surface modification strategy is the most promising for graft protection, because this does not simply mimic isolated functions of the endothelium rather it inherently provides the endothelium's regulatory functions. Endothelial cells (ECs) are potent regulators of thrombosis. They regulate the thrombotic response through three distinct yet interrelated systems: (1) The coagulation cascade is managed through receptors on the EC surface; (2) the complement cascade regulates fibrinolysis and vascular tone; and (3) cells in the blood such as leukocytes and platelets communicate with ECs to repair vascular injury [76], but can also respond to vascular graft materials as a perceived injury site thus initiating a thrombotic response. The conditions under which ECs are cultured can push the cellular response towards pro or anti-thrombotic pathways. Many strategies have been used to promote EC attachment to

synthetic surfaces. The first attempt to seed synthetic grafts with endothelial cells was done in 1980 [77]. These studies with canine ECs showed promising results, but have not translated to human studies. ECs do not readily attach to hydrophobic ePTFE grafts. The surface must be modified to make it adhesive for the cells. Methods of changing the microenvironment of the surface have included antibody and peptide sequence cell capture methods, protein adsorption, and growth factor incorporation. Synthetic grafts endothelialize from the anastomosis towards the middle of the graft, but this capability varies between animal models. Non-primate models have had reendothelialization rates of 0.1 mm per week in a rat aorta model [78], but primate models have proven more challenging as there is a limit to their ability to self-endothelialize of 1-2 cm from the anastomosis [62, 79].

1.4 Endothelial Cells

A monolayer of endothelial cells lines the inner walls of all arteries forming the first barrier between the bloodstream and the rest of the arterial wall. ECs have multiple functions in maintaining a normal physiologic environment. Under normal conditions, the endothelium maintains metabolic signaling functions that preserve the integrity of the arterial wall. Comparisons of the functions of normal and atherosclerotic prone vascular cells are outlined in Figure 1.7 for endothelial cells as well as other key cell types involved in the atherosclerotic disease process.






	Normal	Atherosclerosis
 Endothelial cells	<ul style="list-style-type: none"> • Vasodilation of smooth muscle cells • Antithrombogenic • Barrier • Synthesize inhibiting growth factors • Smooth muscle growth inhibitor 	<ul style="list-style-type: none"> • Increased vasoconstriction of smooth muscle cells • Thrombogenic • Increased permeability • Synthesize large amounts of stimulating growth factors
 Smooth muscle cells	<ul style="list-style-type: none"> • Contractile phenotype • Myofibrils • Respond to vasoactive substances 	<ul style="list-style-type: none"> • Synthetic phenotype • Golgi bodies • Secrete growth factors • Secrete connective tissue matrix
 Macrophages	<ul style="list-style-type: none"> • Not present or present in very small numbers in the subintimal space 	<ul style="list-style-type: none"> • Take up lipid to form foam cells • Chemotactic factors • Growth factors • Proteases
 Platelets	<ul style="list-style-type: none"> • Not present 	<ul style="list-style-type: none"> • If activated, recruit more platelets • Chemotactic factors • Growth factors
 T lymphocytes	<ul style="list-style-type: none"> • Not present 	<ul style="list-style-type: none"> • Activate macrophages • Chemotactic factors • Growth factors • Interleukin-2

Figure 1.7. Normal versus abnormal function for key cell types [8]

As the initial barrier for the transport of macromolecules from the bloodstream into the arterial wall, the endothelium is thought to play a key role in the atherosclerotic disease process. The description of the disease thus far has centered on phenotypic classifications. The specific mechanisms behind the initiation of atherosclerosis remain incompletely understood. It is thought that specific events within the endothelium constitute the initial events in the development of the disease. A key component in understanding atherosclerosis is to understand the mechanisms leading to the endothelial dysfunction that compromises the endothelium's protective capacity. Therefore, an understanding of endothelial cell biology promises to play a key role in elucidating the cardiovascular disease process.

Due to its anatomic location, the endothelium is exposed to greater mechanical forces than any other mammalian tissue [80]. Endothelial cells are subjected to three primary mechanical forces as a result of blood flow: hydrostatic pressure acting normal to the surface, biaxial tensile stretch acting circumferentially, and shear (or frictional) stress acting tangentially (Figure 1.8). Among these forces, shear stress is the most extensively studied and is thought to play an important role in regulating endothelial cell function. Vasoactive substances, gene expression, cell metabolism, and cell morphology have all been shown to be sensitive to shear forces [81].

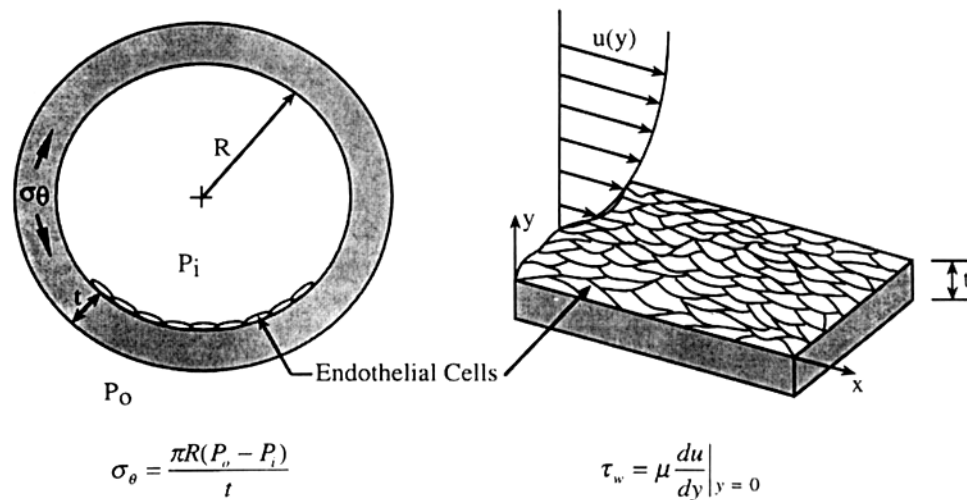


Figure 1.8. Blood flow-mediated mechanical stresses acting on the arterial wall. Hoop stress (σ_θ) and wall shear stress (τ_w) are defined and illustrated above. [82]

1.4.1 Endothelial Outgrowth Cells

Vascular graft biomaterials can be seeded with ECs to inherently provide the EC's barrier function. Autologous cells must be used to avoid host rejection. Endothelial outgrowth cells (EOCs) have been considered a promising source of autologous endothelial cells

[83, 84] because they can be readily isolated from whole blood and expanded *in vitro*. EOCs were identified in 1997 [85] and the isolation from peripheral blood first described in 2000 [86]. Other potential autologous cell sources are omental and subcutaneous fat, bone marrow, veins, and arteries [87]. While these sources yield viable ECs, they also require more invasive surgical procedures for isolation. Peripheral blood EOC isolation requires a simple venipuncture removing a relatively small volume of blood (40mL). Additionally, EOCs are increasingly recognized to play important roles in hemostasis, angiogenesis, and arterial injury repair [88-90]. This cell population has been shown to stain positive for typical EC markers of vWF, CD31, VE-cadherin, VEGF-R2, Thrombomodulin, and E-selectin, and have shown reduced eNOS expression [91]. EOCs can be incorporated into vascular graft biomaterial designs to reduce thrombosis and intimal hyperplasia.

1.4.2 Endothelial Cell Adhesion

Cell adhesive interactions play important roles during many normal physiological processes such as embryonic development, wound repair, and progression of diseases such as cancer. Cell adhesion is mediated by the specific interactions of cell surface receptors with extracellular glycoproteins. Tropoelastin has been shown to be a good substrate for cell adhesion and spreading [92]. It is known that the C-terminus is the region of tropoelastin responsible for cell adhesion, but the exact receptor involved in cell binding to tropoelastin remains to be defined [92-94]. The protein sequence or isoform and protein conformation must be considered in defining the binding mechanisms. Further work needs to be done to elucidate the specific mechanism and adhesion receptor for cell adhesion to tropoelastin. Three specific candidate mechanisms for cell adhesion

to tropoelastin are: integrins, G-protein coupled receptors, and elastin binding protein mediated adhesion.

1.4.2.1 Integrin Mediated Adhesion

Integrins are well-characterized adhesion receptors. There are 23 heterodimeric complexes of alpha and beta subunits within this family of receptors. Each subunit is a glycoprotein with a large, globular extracellular domain and a transmembrane domain. The cytoplasmic domain is a much smaller domain of approximately 60 amino acids. The $\alpha_v\beta_1$ is the major fibronectin receptor on most cells. It has two main cell adhesive regions. The cell adhesive region toward the center of the protein chain is the Arg-Gly-Asp or RGD sequence. This sequence promotes optimal binding to the $\alpha_v\beta_1$ integrin. These integrins are not passive structures, but are active in cell adhesion, migration, assembly of ECM, and signal transduction through the assembly of focal contacts and the F-actin cytoskeleton [95]. Elastin does not contain an RGD sequence and has not been shown to interact with most RGD-binding integrins. Mecham's group ruled out integrins as the receptor class responsible for cell adhesion [92]. However, the $\alpha_v\beta_3$ integrin has been shown to bind to tropoelastin in solid phase binding assays [96] and could be a possible binding partner for tropoelastin.

1.4.2.2 G-Protein Coupled Receptor Mediated Adhesion

G protein coupled receptors (GPCRs) are a protein family of transmembrane receptors that transduce extracellular signals such as ligand binding to an intracellular signal through G-protein activation. Pertussis toxin-sensitive G-protein-coupled pathway (stimulating $G\alpha_i$) has been shown to be activated by an elastin derived peptide,

VGVPAG [97]. Pertussis toxin, inhibiting G_i , blocked tropoelastin-mediated migration and vascular smooth muscle cell actin polymerization. This elastin derived peptide was also found to inhibit adenylate cyclase, reduce cAMP levels, and stimulate Rho-induced actin polymerization [97]. This suggests that elastin (as a signaling molecule) activates the G-protein coupled receptor pathway that ultimately leads to Rho induced actin polymerization in vascular smooth muscles. This shows a direct link between elastin and the G-protein-coupled receptor pathway and could play a role in adhesion of cells to tropoelastin, but remains to be proven.

1.4.2.3 Elastin Binding Protein Mediated Adhesion

There have been several elastin binding proteins (EBP) identified. The primary one is a 67-kDa protein that is also identified as a galactoside-binding lectin [93, 98-100]. This receptor has also been shown to have functional similarities to laminin receptor [101]. A 120-kDa protein (elastonection) and a 59-kDa VGVPAG-binding protein have also been identified [102]. Elastonection was shown to be up-regulated in mesenchymal cells in the presence of fragments of insoluble elastin [103]. The sequence in elastin assumed responsible for these activities is the hexapeptide VGVPAG [104, 105] located in the middle of the molecule. The VGVPAG sequence has been used in multiple studies to study elastin interactions, but has not been shown to promote cell adhesion. Full-length tropoelastin actively promotes cell attachment and spreading, thus suggesting that the VGVPAG sequence is not the critical sequence in cell adhesion. Broekelmann and Mecham have shown that cells do not bind through the EBPs but are associated with the COOH terminus of elastin [92]. Studies using the elastin derived sequence VGVPAG are

not sufficient in explaining the adhesion of cells to tropoelastin. Consequently, a full-length tropoelastin isoform should be evaluated in cell binding assays.

1.4.3 Endothelial Cells as Force Transducers

The ECM plays an important role in transducing mechanical forces to the cell through the cell's cytoskeleton. Force transduction can act through direct signaling by luminal surface deformation (Figure 1.9-A) such as ion channel activation, or between cell junctions (Figure 1.9-B) by transmitting the applied forces through the filamentous cytoskeleton. The cytoskeleton also transmits signals directly to adhesion sites on the ECM (Figure 1.9-C). These deformation signals are received by membrane bound integrins, which induce the phosphorylation of FAK leading to activation of MAP kinases. Integrin mediated signal transduction can also alter actin assembly and subsequent transmission of mechanical stimuli. Transduction signals can also transmit directly through the nucleus (Figure 1.9-D). [106]. The ECM can signal cell contractility and quiescence in the presence of these signals. The proper balance of ECM proteins at the EC attachment surface can impart a protective EC phenotype on ECM based vascular graft biomaterials.

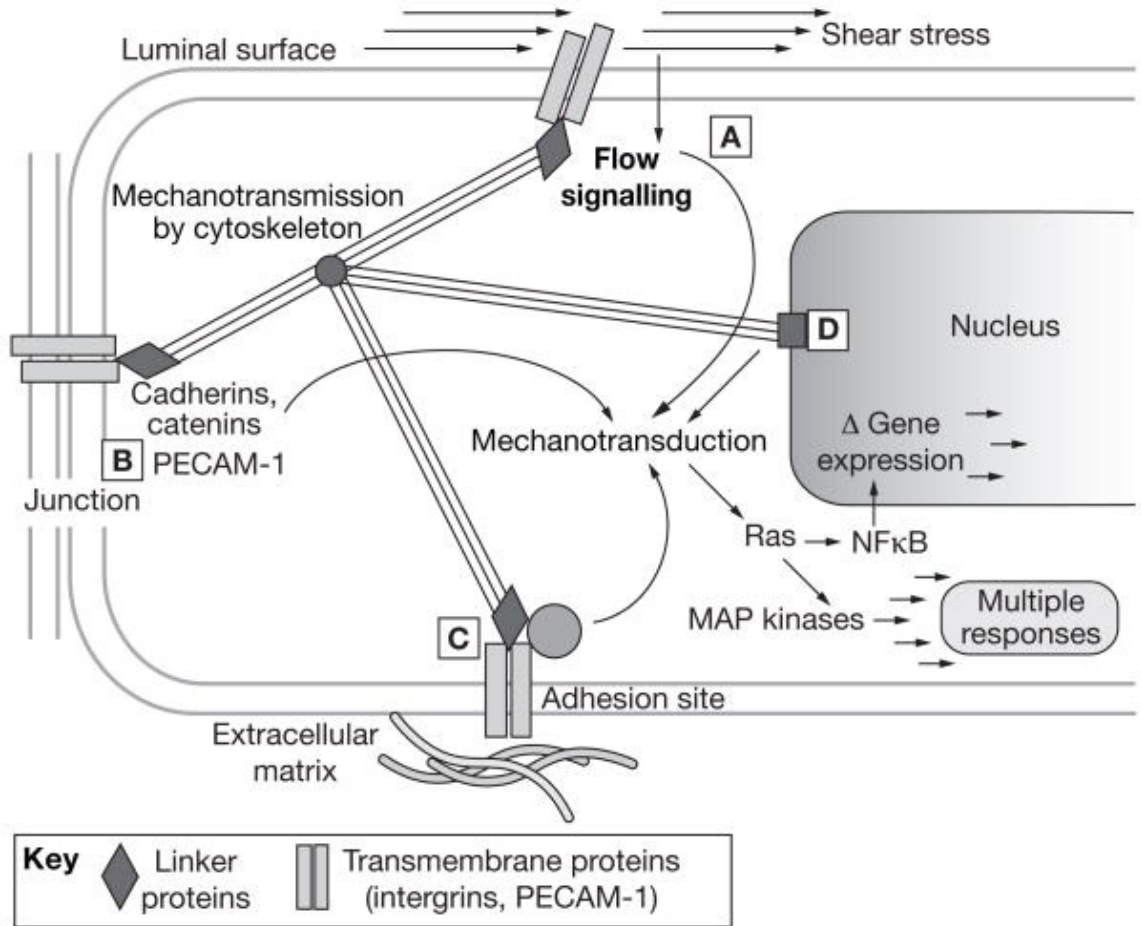


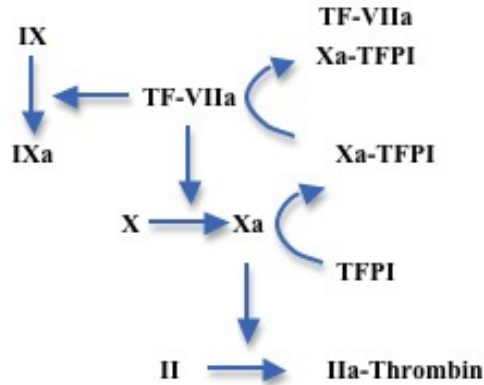
Figure 1.9. Model of endothelial mechanotransduction by mechanical shear stress. Signal can be transduced at the luminal surface (A) between cell junctions (B) directly to adhesion sites on the ECM matrix (C), and to the nucleus (D). [106]

1.4.4 The Role of Endothelial Cells in Thrombosis and Coagulation

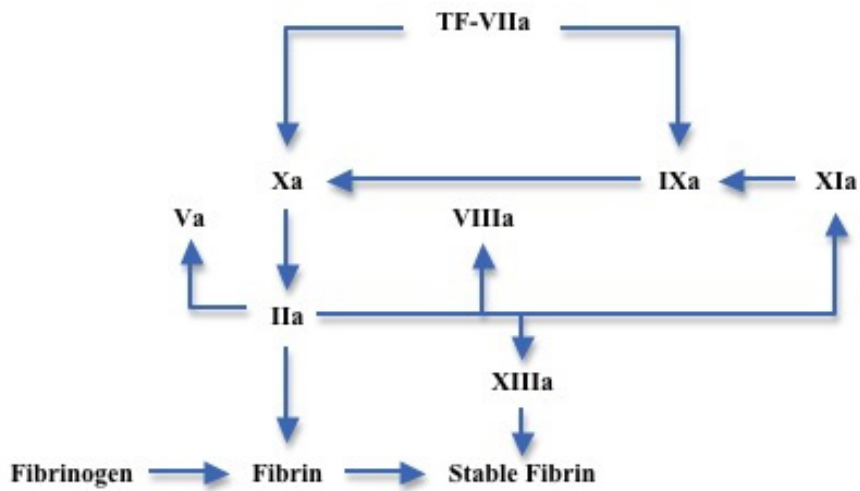
Endothelial cells are potent regulators of thrombosis and coagulation. Understanding how ECs and the ECM work together to regulate thrombosis and coagulation helps to define how these components can be combined to protect vascular graft biomaterials. Under normal conditions, there is a delicate balance between pro and anticoagulant functions. The thrombotic response can be broken down into three distinct phases; initiation, propagation and termination. The primary initiator of the coagulation cascade is tissue factor (TF). TF is a potent procoagulant molecule, which normally resides at low levels,

but is released and amplified by endothelial cells as a response to vascular injury. Tissue factor binds to factor VIIa, and this complex activates factor X thus producing factor Xa. Factor Xa then converts prothrombin (factor II) to thrombin (factor IIa). Tissue factor pathway inhibitor (TFPI) is an antithrombotic molecule that binds factor Xa. This Xa-TFPI complex then reacts with the TF-VIIa complex to form an inactive quaternary complex (Figure 1.10-A). The propagation phase results in a marked increase in thrombin generation. Thrombin activates platelets, which support procoagulant actions. Thrombin also activates factors V, IXa, VIII, which in turn stimulates tenase (factor IXa) and prothrombinase (factor Xa). Activation of factor IX on platelets increases thrombin generation. The activation of factor XIII forms fibrin cross-links to strengthen the clot. Fibrin has anticoagulant properties that allow it to act as a brake in the pathway by binding thrombin, thus acting as a temporary thrombin reservoir (Figure 1.10-B). The termination phase involves the removal of activated coagulation factors. Thrombin acts to downregulate itself by activating protein C. The endothelial protein C receptor (EPCR) acts with thrombomodulin (TM) to bind thrombin to the endothelial membrane. TM increases the efficiency of this reaction. Thrombin then cleaves protein C to form activated protein C (APC). APC then inactivates factors Va and VIIa (Figure 1.10-C) [107]. ECs acting through their released and membrane bound factors TF, TFPI, EPCR, and TM play critical roles in the initiation, propagation, and termination of the coagulation cascade. Individual coagulation factors can be assessed on ECM proteins to determine the best formulation to create a protective environment for EOC seeded cells on tissue-engineered vascular grafts.

A: Initiation



B: Propagation



C: Termination

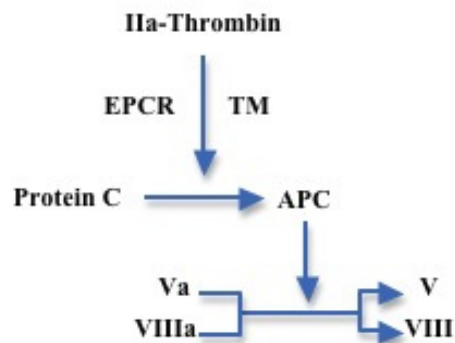


Figure 1.10. Three phases of the coagulation cascade in thrombosis. (A) The initiation phase is started with the release of TF leading to thrombin generation. (B) The propagation phase amplifies the response to form cross-linked fibrin clots. (C) The termination phase inactivates coagulation factor through the action of APC.

1.5 Dissertation Overview

The primary goal of cells, tissues and organisms is to maintain homeostasis to promote an environment consistent with sustaining life. This requires regulation of specific cellular pathways that recognize diseased or damaged tissue, subsequently remove the damaged tissue, and finally rebuild the tissue with healthy new cells [27]. Vascular injury induces thrombotic response and creates an imbalance between the vascular cell function, ECM and dynamic mechanical environment thus disturbing vascular homeostasis. The central theme of this dissertation explores how the ECM influences vascular cell function and thus homeostasis.

Chapters 2 and 3 describe novel vascular biomaterials that can be used as a medial layer of vascular graft constructs. Chapter 4 describes and validates a model for deriving strain energy density functions for tubular constructs that could be applied to the materials developed in Chapters 2 and 3. Chapter 5 characterizes the thrombotic and inflammatory responses of EOCs on different ECM components in *in vitro*, *ex vivo* shunt, and *in vivo* test systems. In Chapter 6, the key findings from this dissertation are summarized and areas of interest for future work highlighted.

Chapter 2: Structural and Cellular Characterization of Electrospun Recombinant Human Tropoelastin Biomaterials

Kathryn A. McKenna, Kenton W. Gregory, Rebecca C. Sarao, Cheryl L. Maslen, Robert W. Glanville, and Monica T. Hinds

2.1 Abstract

An off-the-shelf vascular graft biomaterial for vascular bypass surgeries is an unmet clinical need. The vascular biomaterial must support cell growth, be non-thrombogenic, minimize intimal hyperplasia, match the structural properties of native vessels, and allow for regeneration of arterial tissue. Electrospun recombinant human tropoelastin (rTE) as a medial component of a vascular graft scaffold was investigated in this study by evaluating its structural properties, as well as its ability to support primary smooth muscle cell adhesion and growth. rTE solutions of 9, 15, and 20 wt% were electrospun into sheets with average fiber diameters of 167 ± 32 , 522 ± 67 , and 735 ± 270 nm, and average pore sizes of 0.4 ± 0.1 , 5.8 ± 4.3 , and 4.9 ± 2.4 μm , respectively. Electrospun rTE fibers were cross-linked with disuccinimidyl suberate (DSS) to produce an insoluble fibrous polymeric recombinant tropoelastin (prTE) biomaterial. Smooth muscle cells attached via integrin binding to the rTE coatings and proliferated on prTE biomaterials at a comparable rate to growth on prTE coated glass, glass alone, and tissue culture plastic. Electrospun tropoelastin demonstrated the cell compatibility and design flexibility required of a graft biomaterial for vascular applications.

*The final, definitive version of this paper has been published in the
Journal of Biomaterials Applications, Online May 17th 2011, by SAGE Publications,
Inc., All rights reserved. © <http://online.sagepub.com>*

doi:10.1177/0885328211399480

Reprinted with permission

2.2 Chapter Overview

Studies conducted in this thesis were designed to investigate the effect of ECM proteins on vascular cell function. Electrospinning was used to develop novel tropoelastin biomaterials. The electrospinning parameters including: excitation voltage; solvent used to suspend the protein; protein concentration; gap distance; and the cross-linking methods, affect the final properties of the biomaterial. How these parameters influenced the structure of the biomaterials as well as the cell compatibility of the matrix are investigated in this chapter.

2.3 Introduction

Cardiovascular disease remains one of the leading causes of morbidity and mortality in the Western world, affecting nearly 81 million people in the United States alone in 2006 [108]. Treatment options for bypass grafts are limited to either autologous vessels, which are often not available and can be affected by preexisting disease, or synthetic grafts, which are limited to vessels larger than 6 millimeters in diameter [109]. Small diameter

vascular grafts have been under development for more than 50 years with limited clinical success. Vascular grafts often fail due to thrombosis, intimal hyperplasia, and aneurysm formation [7].

To address the failure of small diameter vascular grafts, tissue engineered vascular grafts have been extensively studied using both synthetic and natural biomaterial scaffolds. Synthetic scaffolds, including ePTFE, poly(ethylene glycol) diacrylate, poly(caprolactone), and polyurethane, have the advantages of controllable physical and mechanical properties while being highly reproducible and easily manufactured in large scale quantities. Yet these synthetic scaffolds typically lack the elasticity of native arterial walls and the biocompatibility for long term vascular cell functionality. Natural biomaterial scaffolds, including the most studied grafts of decellularized arteries, have also had limited success. The two most successful examples of decellularized arteries without cell seeding have been Sawyer's ficin-digested glutaraldehyde-tanned bovine carotid graft [41] and Dardik's glutaraldehyde-tanned human umbilical vein graft [42]. While the 5 year patency rates were promising, aneurysm formation due to in vivo degradation limited their widespread use [42, 43]. Decellularized arteries are attractive scaffolds for tissue-engineered vascular grafts due to their mechanical and biological properties [44], yet these natural scaffolds are still limited by the lack of precise manufacturing control of the physical and mechanical properties.

Tissue-engineered vascular grafts which are produced from autologous cells without a scaffold have recently advanced from the research bench to clinical safety trials using an

arteriovenous shunt model, with ten reported patients [4, 45]. These tissue-engineered grafts have shown promising results with primary patency rates of 78% at 1 month and 60% at 6 months with failures due to thrombosis, dilation, and aneurysm, but their lengthy production times of 24 weeks [4] will be a limiting factor in becoming a practical clinical option. Small diameter tissue-engineered vascular graft development has been the focus of many research groups, but a viable option that structurally compares to native arteries, supports cell growth, and is functionally equivalent to autografts, the gold standard treatment option, has not been found.

Electrospinning suspensions of monomers or polymers from both natural proteins and synthetic polymers can produce sub-micron sized fibers, which can then be cross-linked to produce stable polymeric structures [110, 111]. The structural properties of the electrospun fibers, primarily fiber shape and diameter, can be controlled by varying the gap distance, accelerating voltage, solution viscosity, and solution delivery rate [57, 110]. Adding this degree of control to a natural protein such as elastin is clearly advantageous. Elastin is a key extracellular matrix protein responsible for energy storage and recovery in native elastic arteries [112]. End stage aneurysm disease and supravalvular aortic stenosis have been associated with the lack of elastin and deficiency in elastin expression [19-22, 24-26]. Elastin has been proposed as an essential component in vascular graft design [113, 114]. Elastin has been electrospun for use in tissue-engineered grafts [57, 61, 115-119], but the elastin protein has primarily been extracted from assembled and crosslinked animal-sourced tissues. These forms of elastin may maintain critical elastin biochemical signaling, but are likely to elicit an immuno-rejection response leading to

graft degradation and ultimate aneurismal graft failure. The electrospinning of human tropoelastin, the monomer unit of elastin, is promising[61, 120] as a medial component of tissue engineering vascular grafts, but the limited analysis of the effects of crosslinking as well as the interactions with vascular cells, necessitates further study.

In this study, we created an electrospun biomaterial entirely from recombinant human tropoelastin and used a unique cross-linker to create fibrous polymeric recombinant tropoelastin (prTE) that mimics native elastin fibers and supports vascular cell adhesion and growth. This unique biomaterial can be a scaffold for vascular tissue engineering applications with customizable dimensions in terms of both individual fiber size and gross graft dimensions.

2.4 Materials and Methods

2.4.1 Materials

A codon optimized synthetic gene for human tropoelastin was expressed in gram quantities in a 10 liter *E.coli* fermentation system. The expression construct includes all of the functional exons except exon 1, which encodes the signal sequence, exon 22 and exon 26A, which are rarely if ever expressed in natural elastin. This produces an elastin isoform that is the same as one of the natural isoforms produced by normal human cells. The purification procedure resulted in a >99% pure product as determined by gel electrophoresis. Control materials of extracted elastin were obtained using a hot alkali digestion method on native carotid arteries from domestic swine (Animal Technologies, Tyler, TX) [121, 122]. All chemical reagents were acquired from Sigma-Aldrich unless otherwise noted.

2.4.2 Electrospinning of rTE

A 2 mL glass syringe was loaded with 9, 15, or 20 wt% rTE in 1,1,1,3,3,3-hexafluoro-2-propanol (HFP). An 18-gauge stainless steel blunt tip needle was connected to the glass syringe and loaded onto a syringe pump (Harvard Apparatus). A high voltage power supply (Glassman High Voltage, Inc., High Bridge, NJ) was electrically coupled to the end of the needle. A gap distance of 12.5 cm was set from the end of the needle to the center of the collection device. Fibers were spun onto grounded collection devices of either copper foil covered plates for fiber analysis or Poly-D-Lysine coated coverslips (Fisher) attached to copper foil covered plates for cell studies. Mandrels rotated at 4000-6000 rpm and translated longitudinally 6-8 cm with a rate of 8 cm/sec on a custom-built

device for electrospun tube formation. The solution was charged at 18.5 kV with the high voltage power supply. The syringe pump advanced the protein solution at 2 mL/hr. All electrospinning was conducted within a fume hood.

2.4.3 Cross-linking of electrospun rTE

All samples of electrospun rTE were cross-linked using the organic cross-linker disuccinimidyl suberate, DSS, (Pierce Biotechnology-Thermo Fisher Scientific Inc.) to produce the polymer, prTE. Samples were cross-linked in a two-stage process. The electrospun rTE samples were incubated for 4 hours in DSS, in 50 mL anhydrous ethyl acetate, at a ratio of 0.072 mg of DSS per mg of rTE protein at room temperature. A second incubation occurred for 12-18 hours at a concentration of 0.108 mg of DSS per mg of rTE protein at room temperature. prTE samples were then rinsed in anhydrous ethyl acetate for 5 minutes with a second 5 minute rinse in 70% ethanol, and a final 10 minute rinse in deionized water. The final product was stored in 70% ethanol.

2.4.4 Electrospun rTE fiber characterization

Electron microscopy was used to determine the electrospinning consistency, fiber characterization, and to evaluate the internal nanostructure of electrospun fibers. rTE solutions were electrospun onto copper foil covered plates. Electrospun rTE and prTE samples were mounted onto scanning electron microscopy (SEM) stubs and sputter-coated with 250 Å of gold/palladium. Micrographs were taken at magnifications from 1000 to 10000X and viewed at 5-30 kV on either a Zeiss Model 960 Analytical SEM or a FEI Sirion XL30 SEM. For transmission electron microscopy (TEM) analysis the

electrospun rTE samples were adhered to copper TEM slot grids using silver paint. Carbon ($\sim 200\text{\AA}$) was coated onto both sides of the sample on TEM grids using an evaporation coater. Samples were viewed with a JOEL Model 2000fx Analytical TEM/Scanning TEM at 200 kV.

The fiber diameters and pore sizes of rTE flat materials were measured from SEM micrographs using ImageJ software (NIH). Twenty measurements were taken for each picture with three pictures analyzed per electrospinning run. Five separate lots of rTE were analyzed for the 15 wt% rTE samples. Matlab analysis (Appendix A) was used to determine the degree of fiber orientation [123].

2.4.5 Smooth muscle cell adhesion to adsorbed rTE

Baboon carotid artery smooth muscle cells (SMCs) were isolated [124] and used to assess the adhesion of vascular cells on adsorbed rTE. SMCs were maintained in a media consisting of minimum essential media (MEM), 10% Fetal Bovine Serum (FBS), 5mM L-glutamine, and a 1% penicillin, streptomycin, and fungizone mix (Invitrogen). SMCs were maintained and passaged in culture using standard techniques. For all adhesion assays, the SMCs were plated in adhesion media (MEM with 1 mg/ml of BSA).

To determine the optimal rTE concentration for SMC adhesion, rTE solutions from 0 to 5 mg/ml in PBS were prepared and added to 12 wells of a 96 well plate. Plates were sealed and incubated at 4°C overnight. Plates were then rinsed twice with PBS and seeded with 2×10^4 SMCs per well and incubated at 37°C for 90 minutes. Plates were then rinsed twice

to remove loosely adhered and non-adherent cells and subsequently frozen at -80°C. Cell numbers were then evaluated using the CyQUANT® GR assay (Invitrogen). Fluorescence units were converted to cell numbers using standard curves generated from known cell numbers. Studies were repeated three times.

The adhesion mechanisms of SMCs to adsorbed rTE were determined and compared to SMC adhesion to adsorbed coatings of fibronectin and collagen, as well as uncoated tissue-culture treated plastic (TCP). 96-well plates were coated with 50 µg/ml of each protein overnight at 4°C. Plates were rinsed with PBS and incubated for 1 hour with 10 mg/ml BSA in PBS. Cells were removed gently from flasks with Versene (2% EDTA in PBS) and 0.05% Trypsin. Trypsin was deactivated following cell removal with 0.5 mg/ml soybean trypsin inhibitor. Plates were rinsed with PBS and SMCs were subsequently seeded at 2×10^4 cells per well on each substrate in each of the following media: adhesion media, adhesion media supplemented with EDTA (5 mM), pertussis toxin (0.5 µg/ml), or lactose (5 mM). Cells were incubated at 37°C for 90 minutes. Plates were then rinsed to remove loosely adherent cells with PBS and frozen at -80°C for subsequent analysis with CyQUANT® GR. Studies were run in 10 wells per condition and repeated three times.

2.4.6 Smooth muscle cell growth on electrospun prTE

Growth curves were constructed for SMCs grown on TCP coverslips as well as Poly-D-Lysine glass coverslips that were either untreated, coated with prTE, or electrospun with prTE. Three separate lots of rTE were tested with a sample size of 6 per condition. prTE

samples were electrospun from 15 wt% rTE solutions onto Poly-D-Lysine coated glass coverslips and cross-linked. prTE fibers were fluorescently stained with 2.5 µg/mL Oregon Green® 488-X, succinimidyl ester *6-isomer* (Invitrogen) for 1 hour at room temperature. Coated prTE coverslips were prepared by adding 0.2 wt% rTE solutions in HFP onto 12 mm diameter Poly-D-Lysine coverslips. Samples were air-dried, cross-linked, and soaked in 70% ethanol overnight. prTE samples were rinsed twice for 5 min with PBS and then incubated for 20 min in media.

SMCs (5×10^3 cells/cm²) were seeded onto coverslips and evaluated at 1, 2, 3, 5, and 7 days. Media was replaced at each timepoint with 500 µL of a 10% alamarBlue® solution (Invitrogen) in media and incubated at 37°C for 2 hours. 200 µL of the reduced alamarBlue® solution was removed from each well and transferred to a 96-well plate for immediate analysis on a SPECTRAFluor Plus plate reader (TECAN) at an excitation wavelength of 560 nm and an emission wavelength of 590 nm at 37°C. Any remaining alamarBlue® solution was aspirated from the wells and 500 µL fresh SMC media was added to each well. Measurements were normalized to the 24-hour timepoint for each condition. Doubling times of metabolic activity were calculated as $(t_2 - t_1) / (\log(\text{AB fluorescence at } t_2) - \log(\text{AB fluorescence at } t_1)) * 3.32$, where $t_2 = 120$ hours and $t_1 = 72$ hours.

At day 8 a CyQUANT® NF cell proliferation assay (Invitrogen) was performed. Media was removed from the wells and 500 µL 1X dye binding solution, which consisted of 2 µL of dye reagent per mL of Hank's balance salt solution (HBSS) buffer, was added to

each well. The plates were covered and incubated for 1 hour at 37°C. 200 µl of the dye solution was then transferred to a 96-well plate for immediate analysis on a SPECTRAFluor Plus plate reader with an excitation wavelength of 485 nm and an emission wavelength of 535 nm at 37°C. Measurements for each surface were normalized to the TCP condition.

Cell attachment and spreading were evaluated at 24 and 48 hours post seeding. SMCs (2×10^3 cells/cm²) were seeded onto electrospun prTE samples prepared in the same manner as the growth curves. Cells were fixed at each timepoint with 2.5% paraformaldehyde for 1 hour at room temperature. SMCs were permeabilized with 0.1% Triton-X 100 for 5 minutes and subsequently stained with rhodamine phalloidin (1 unit/sample) and 300nM DAPI (Invitrogen) to visualize the cytoskeleton and nuclear structures. Confocal images were taken with a 63X oil objective on a Zeiss Multiphoton Confocal microscope using 488, 543, and 780 nm excitation wavelengths.

2.4.7 Statistical analyses

All data are expressed as the mean \pm standard deviation. Student's *t*-test, linear regression, and one-way ANOVA with Tukey's post hoc test were used for hypothesis testing, with $p < 0.05$ as the measure for statistical significance. The number of independent tests is listed for each experiment.

2.5 Results

2.5.1 Morphology and substructure of rTE and prTE fibers

Human tropoelastin was successfully electrospun onto flat collection plates at concentrations of 9, 15, and 20 wt% rTE (Figure 2.1) to produce fibrous sheets, which were comparable in structure to extracted porcine elastin (Figure 2.2). The average fiber diameter was dependent on the rTE concentration (Table 2.1). For each concentration of rTE, the electrospun fiber diameters were consistent with no statistical differences between production lots (ANOVA, $P=0.16$). Extracted porcine carotid elastin had an average fiber diameter of 870 nm, which was larger and more variable (323 to 1843 nm) than the electrospun samples. The fiber sizes were significantly different from the native extracted elastin for the 9 wt% (Tukey, $p < 0.01$) and 15 wt% solutions (Tukey, $p < 0.01$), but not significantly different from the 20 wt% solution (Tukey, $p = 0.32$). While the gross morphology of the 9 and 15 wt% fibers was rounded, many of the rTE fibers spun from 20 wt% solutions were ribboned and contained voids within their fibers (Figure 2.3).

The pore sizes of the electrospun rTE scaffolds were quantified and compared to native elastin. The electrospun 15 and 20 wt% rTE had pore sizes of $5.8 \pm 4.3 \mu\text{m}^2$ and $4.9 \pm 2.4 \mu\text{m}^2$, respectively, which is similar to the native elastin with $3.7 \pm 1.6 \mu\text{m}^2$ (ANOVA, Tukey). The 9 wt% rTE had smaller pore sizes, but not significantly different from native elastin (ANOVA, Tukey). The random orientation of fibers was confirmed for these electrospun samples (data not shown).

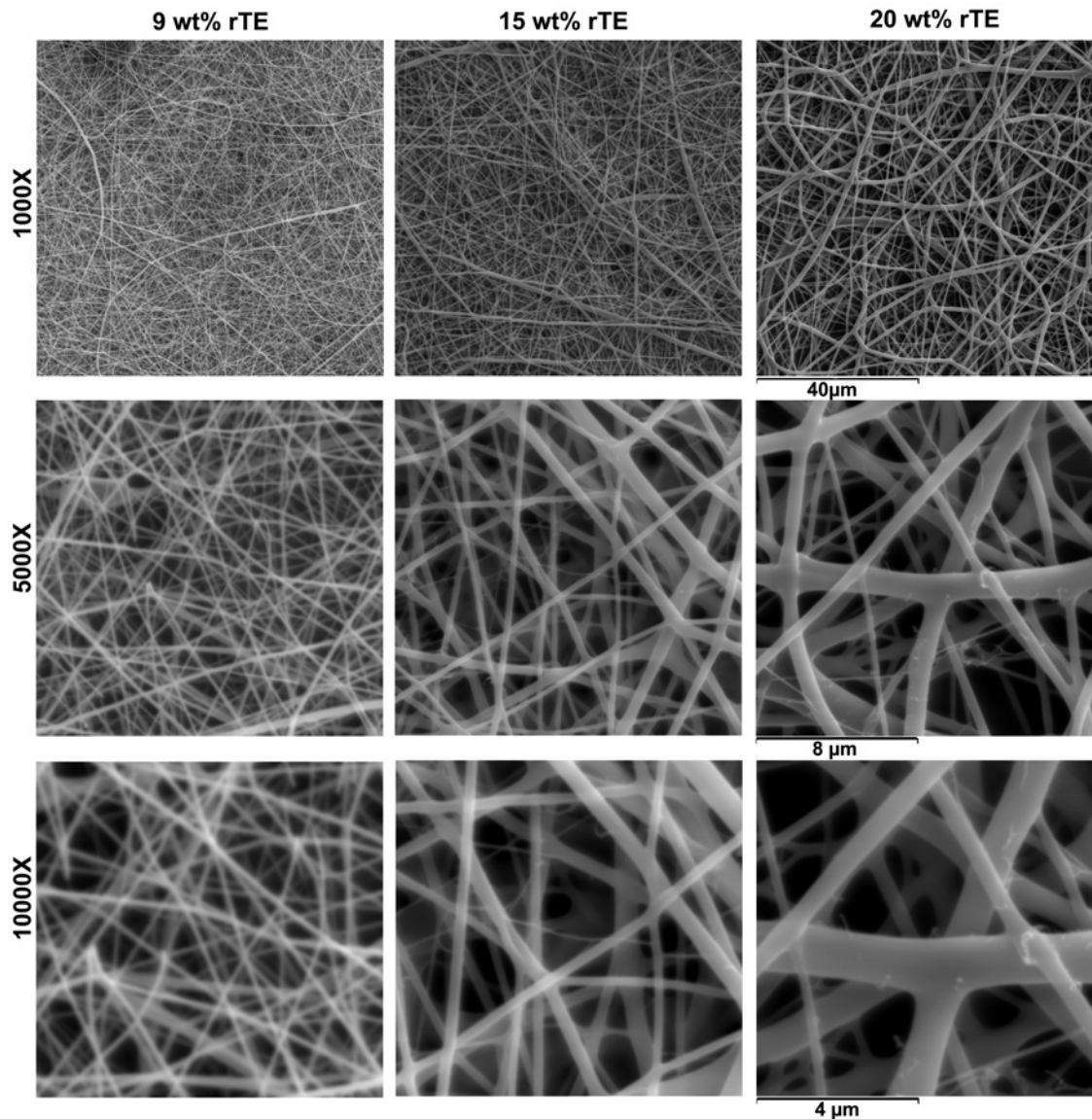


Figure 2.1. Comparison of electrospun rTE fibers from 9, 15, and 20 wt% solutions. The rTE fibers were randomly oriented. Fiber diameters were directly proportional to the concentration of the rTE solution. The electrospun rTE fibers from 9 and 15 wt% solutions had only round cross-sections, while isolated electrospun rTE fibers from 20 wt% solutions had flat cross-sections. SEM micrographs at magnifications of 1000X, 5000X, and 10000X.

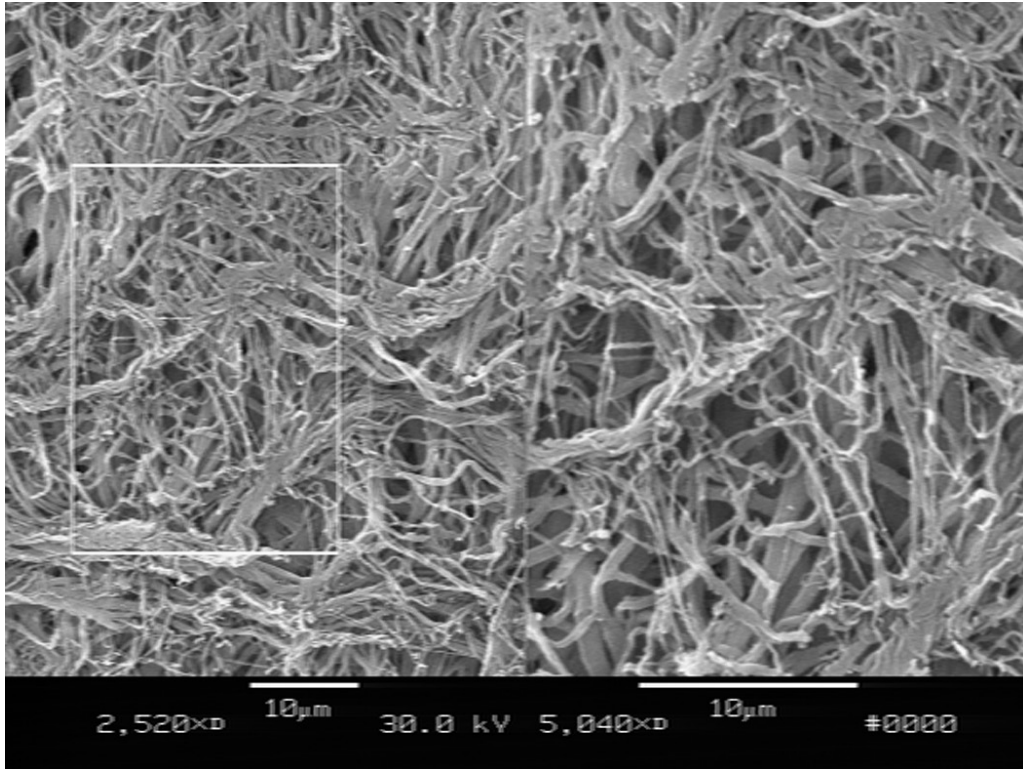


Figure 2.2. SEM micrograph of extracted native elastin from a porcine carotid artery. Scale bars indicate 10 µm.

Table 2.1: Fiber diameter and pore size for electrospun rTE and extracted porcine elastin

Material	Fiber Diameter Ave. ± SD n=20	Range of Fiber Diameters	Pore Size Ave. ± SD n=10
Extracted Porcine Elastin	870 ± 450 nm	323 - 1843 nm	3.7 ± 1.6 µm ²
9% electrospun rTE	167 ± 32 nm*	95 - 214 nm	0.4 ± 0.1 µm ²
15% electrospun rTE (5	522 ± 67 nm*	261 - 1174 nm	5.8 ± 4.3 µm ²
20% electrospun rTE	735 ± 270 nm	336 - 1430 nm	4.9 ± 2.4 µm ²

*p<0.01, compared to extract porcine elastin

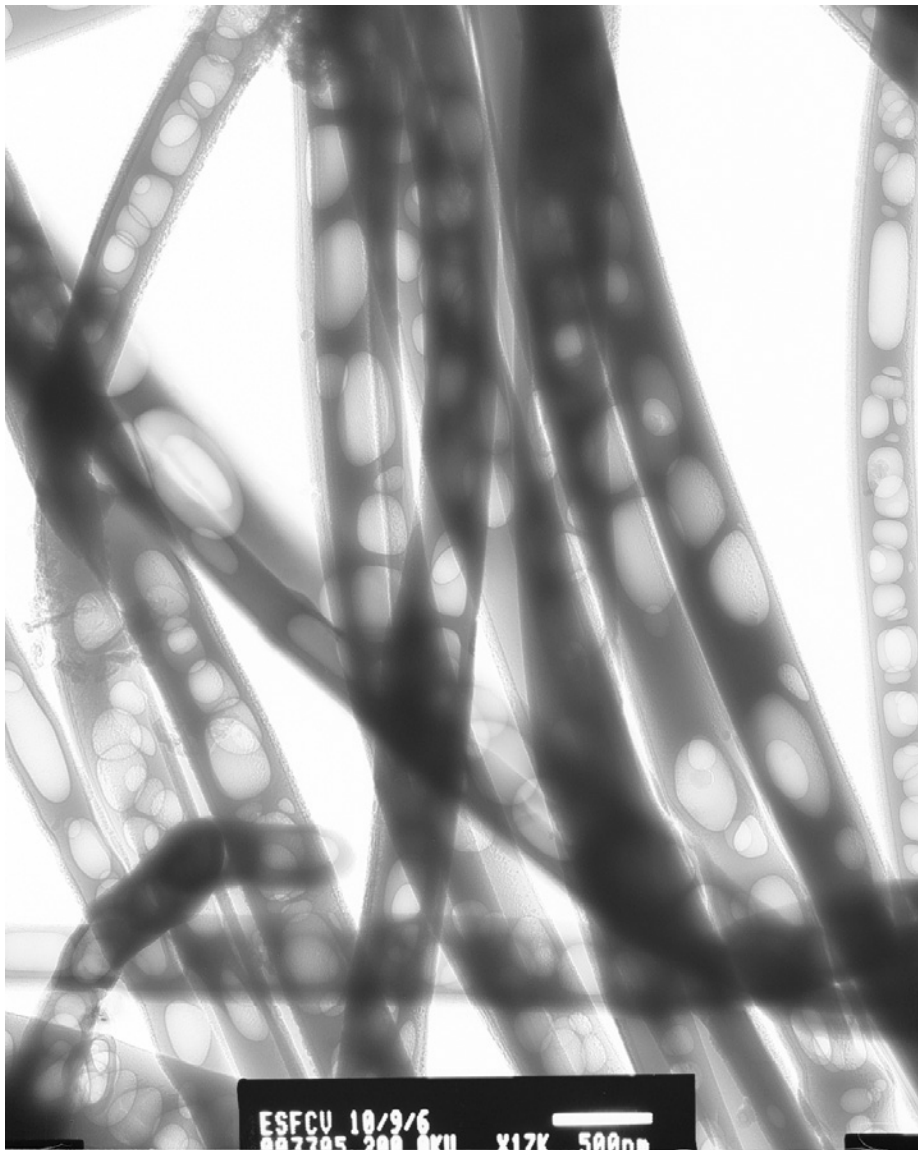


Figure 2.3. TEM micrograph of substructure of 15 wt% electrospun rTE fibers. Voids are visualized within the fibers. Scale bar indicate 500nm. Dr. Jack McCarthy assisted with the TEM imaging of this material.

The cross-linked 15 wt% prTE had the same fiber structure as the uncross-linked rTE samples (Figure 2.4). Electrospun fibers that were not cross-linked and rinsed in PBS dissolved and lost their fiber structure, due to rTE's solubility in aqueous solutions.

Cross-linking of 9 and 20 wt% rTE electrospun fibers also produced no visible alterations in fiber structure (data not shown).

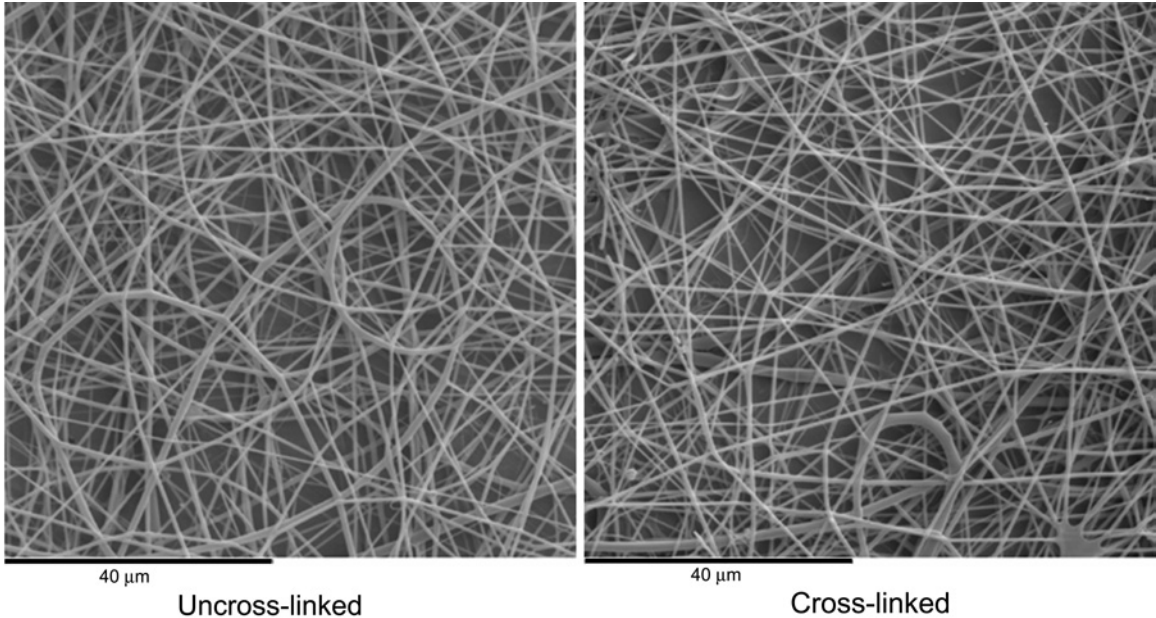


Figure 2.4. SEM micrograph of uncross-linked electrospun rTE (left) and cross-linked electrospun prTE (right) fibers produced from a 15 wt% rTE solution. No change in fiber structure was seen using the DSS cross-linker.

2.5.2 Smooth muscle cell adhesion to adsorbed rTE

In the absence of serum, SMC adhesion to adsorbed rTE increased exponentially between rTE coating concentrations of 0.05 $\mu\text{g/ml}$ and 50 $\mu\text{g/ml}$, where the number of adhered SMCs reached a plateau of 1.7×10^4 cells. There was no significant difference in the number of adhered SMCs for rTE coating concentrations between 50 $\mu\text{g/ml}$ and 5000 $\mu\text{g/ml}$. Thus all subsequent adhesion studies were performed at the 50 $\mu\text{g/ml}$ adsorbed rTE coating concentration.

Adsorbed coatings of rTE, fibronectin, and collagen type I significantly increased SMC adhesion compared to uncoated tissue culture plastic (Figure 2.5). SMCs adhered to each of the protein coatings without significant differences between them. EDTA significantly

reduced SMC adhesion to the adsorbed rTE and fibronectin coated wells, but had no effect on the collagen coated wells. The pertussis toxin and lactose had no significant effect on SMC adhesion to any of the tested surfaces.

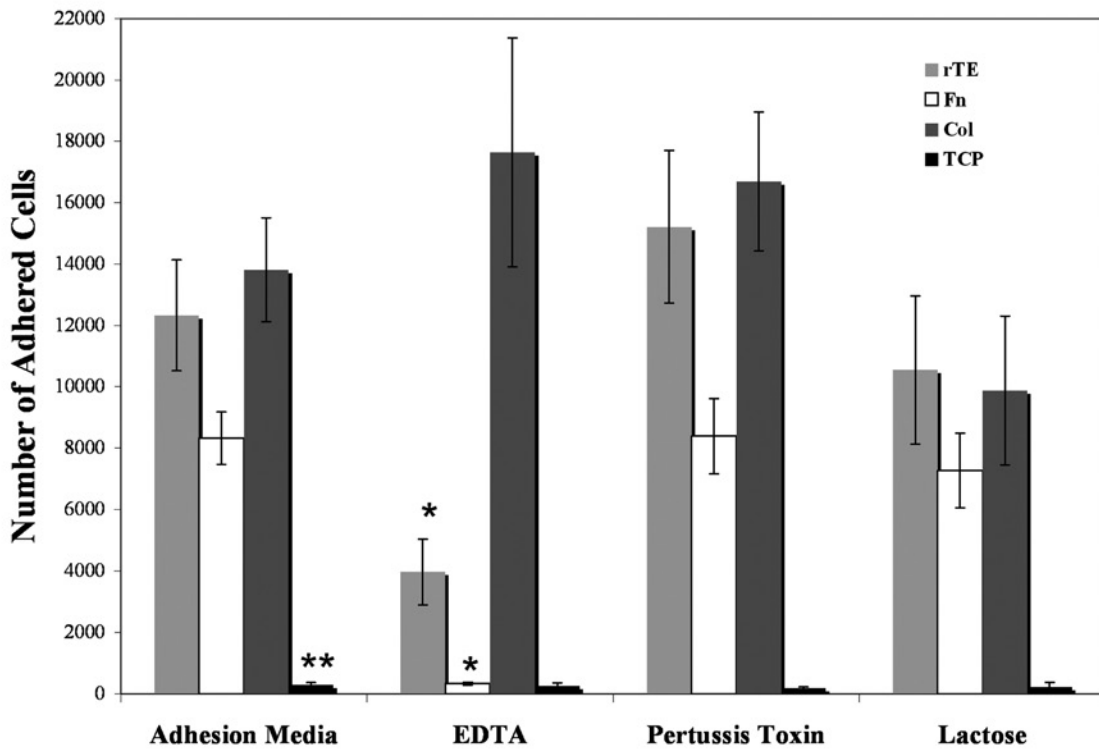


Figure 2.5. Characterization of the adhesion of SMCs to adsorbed rTE. SMCs were allowed to adhere to rTE, fibronectin (Fn), collagen type I (Col), or tissue culture treated plastic (TCP) in either adhesion media or adhesion media with a blocking reagent: EDTA, Pertussis toxin, or lactose. EDTA significantly reduced SMC adhesion to the rTE and Fn coated wells. * $p < 0.05$, compared to the same coating with adhesion media, ANOVA with a Tukey post-hoc test.

2.5.3 Smooth muscle cell morphology and proliferation on electrospun prTE

SMCs adhered and proliferated on 9, 15 and 20 wt% electrospun prTE. Confocal images taken at 24 and 48 hours showed cells spreading across the fibrous substrate and forming multiple attachment points to individual 15 wt% prTE fibers (Figure 2.6). These images

also indicated an increase in cell concentration between 24 and 48 hours post-seeding. Confocal images of SMCs on 9 and 20 wt% electrospun prTE confirmed similar responses in terms of cell attachment and spreading across the range of prTE fiber diameters (data not shown).

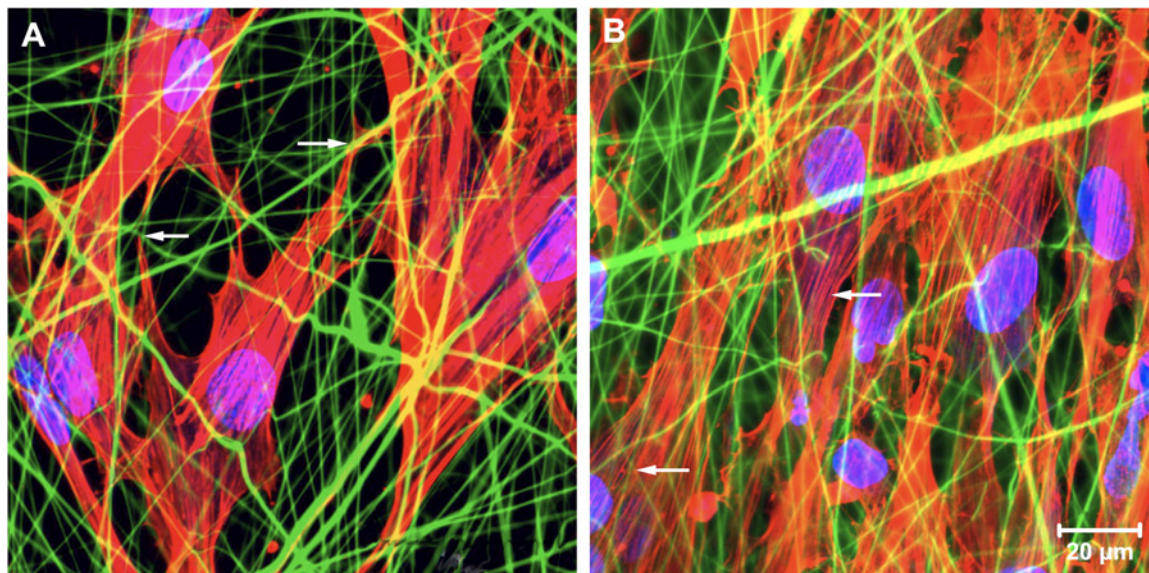


Figure 2.6. Morphology of SMCs seeded onto electrospun 15 wt% prTE for (A) 24 and (B) 48 hours. Confocal images of prTE fibers (green) with actin cytoskeleton-phalloidin (red) and nuclei (blue) of SMCs. SMC pseudopodia made attachments to individual prTE fibers (arrows in A), SMC concentrations increased between 24 and 48 hours, and SMCs formed actin stress fibers (arrows in B). Scale bar indicates 20 μm.

Growth curves were conducted using an alamarBlue® metabolic activity assay. The smooth muscle cells proliferated and were metabolically active on each of the four substrates (Figure 2.7). Logarithmic growth occurred between days 3 and 5 with growth reaching a plateau at day 5. Normalized alamarBlue® fluorescence values for day 5 were 1.82 ± 0.2 , 1.79 ± 0.2 , 1.88 ± 0.17 , and 1.73 ± 0.18 for electrospun prTE, coated prTE, Poly-D-Lysine glass, and TCP substrates, respectively. Doubling times were determined

to be 84 ± 14 , 86 ± 3.6 , 72 ± 6.9 , and 78 ± 9.2 hours for electrospun prTE, coated prTE, Poly-D-Lysine glass, and TCP substrates, respectively. There were no significant differences in doubling times between substrates (ANOVA).

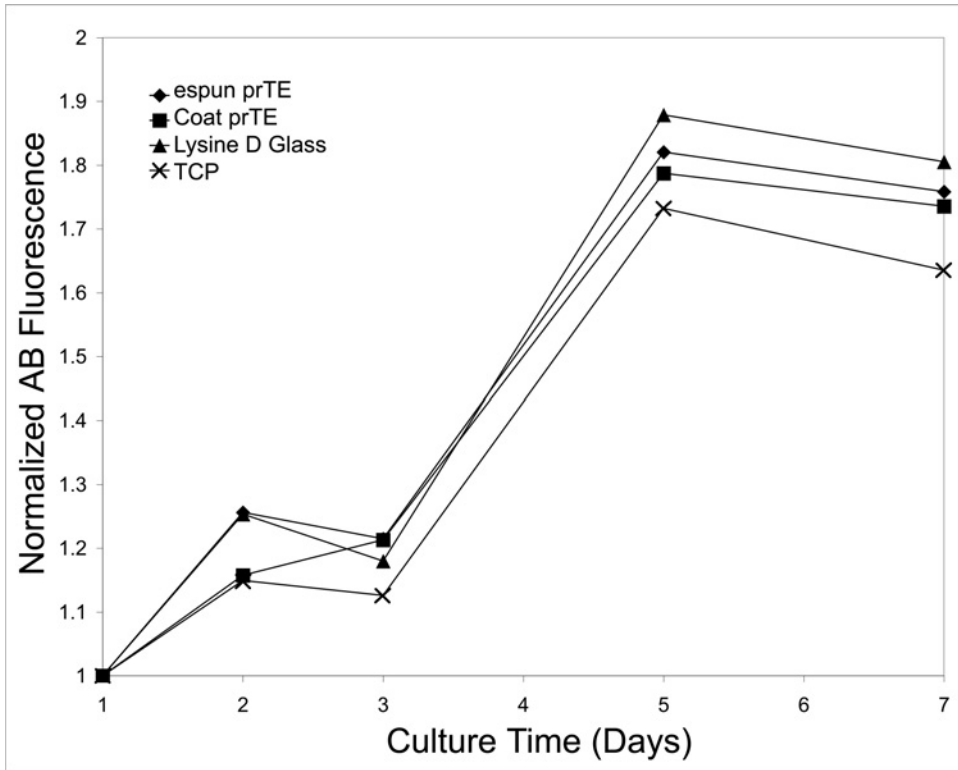


Figure 2.7. SMC proliferation on electrospun prTE, coated prTE, Poly-D-Lysine (Lysine D glass), and tissue culture plastic (TCP) over a 7 day time course. Note: Cell metabolic activity was quantified using alamarBlue assay and the data normalized to the fluorescence reading at day 1. Data are the average of 3 lots of rTE solutions.

A CyQUANT® assay was performed to quantify cell number on Day 8. Normalized cell numbers compared to TCP were $188 \pm 5.9\%$, $172 \pm 11.1\%$, and $158 \pm 16.9\%$, for electrospun prTE, coated prTE, and Poly-D-Lysine glass, respectively. The cell numbers on each of the three substrates were significantly higher compared to the number of cells

on TCP, but no differences were seen between electrospun prTE, coated prTE and Poly-D-Lysine glass (ANOVA, Tukey post-hoc, $p < 0.01$).

2.6 Discussion

Electrospinning was selected as the method to construct a reproducible, physiologically relevant human tropoelastin vascular medial biomaterial. Electrospinning of tropoelastin produced a vascular medial layer scaffold with highly controllable structural properties comparable to the native extracellular matrix protein. The fiber and pore sizes of the prTE electrospun scaffolds were optimized to mimic the structural properties of native arterial elastin. Cross-linking using DSS enabled stabilization that prevented the fibers from dissolving in aqueous media without affecting the structural properties of the fiber. The electrospun prTE scaffolds were capable of supporting vascular SMC growth at rates comparable to coated-prTE and tissue culture plastic.

Electrospinning has advanced the tissue engineering field and proven to be a valuable tool to produce biomimetic scaffolds from both biodegradable polymers and natural proteins. The majority of current research has focused on the use of biodegradable polymers which lack the relevant cell signaling of natural matrix proteins. Elastin and collagen have been used to electrospin vascular grafts, yet these matrix proteins are frequently electrospun from solutions with fully crosslinked polymer fragments or from solutions containing a mixture of natural and synthetic polymers [57, 125].

Electrospinning of these blended solutions leads to an unknown amount, distribution, and structure of elastin in the final electrospun material. An alternative approach to

electrospinning proteins in organic solvents has been the incorporation of synthetic polymers. Synthetic polymers such as poly(ethylene oxide) (PEO), poly(epsilon-caprolactone) (PCL), poly(lactic-co-glycolic acid) (PLGA), polydioxanone (PDO) have been combined with protein blends (collagen, gelatin, and elastin) to electrospin scaffolds [116, 117, 125-129]. These scaffolds do not mimic the native arterial structure of separate elastin and collagen fibers and therefore are unlikely to support vascular cell functions. Li et al. has electrospun calfskin type I collagen, bovine gelatin, extracted bovine α -elastin and the first published instance of human tropoelastin in HFP [61]. The use of the elastin monomer, tropoelastin, provides an opportunity to control material properties and deliver solely “elastin” fibers by crosslinking the final structure.

Optimizing the structure of the electrospun fibers requires balancing the fiber diameter, spacing, shape, and orientation. Our 20 wt% rTE fibers had fiber diameters and pore sizes that matched the diameters of *in vivo* elastin fibers yet their configuration of ribboned fibers differed from the cylindrical *in vivo* fibers. Similarly, using 20 wt% protein solutions and flow rates that ranged from 1 to 8 mL/hr, electrospun bovine α -elastin and human tropoelastin fibers were “ribbon-like” in appearance, with ribbon widths ranging from 0.6 to 3.6 μm and 1.4 to 7.4 μm [61]. This ribboning phenomenon was seen in the larger spun fibers of our electrospun 20 wt% rTE fibers. The ribboning results as the bulk material and solvent separated during fiber formation [130], followed by the subsequent collapsing of fibers forming the flattened ribbons. Additionally, the 20 wt% human tropoelastin fibers from Li et al. had average fiber diameters of approximately 2.2 μm [61], which was significantly greater than our average diameter of

735 nm for a flow rate of 2 mL/hr. This was likely due to differences in their electrospinning parameters, most notably a lower accelerating voltage of 10 kV vs 18.5 kV and a larger gap distance of 14 cm vs 12.5 cm, as well as the variability induced by the measurement of the larger dimension (width vs thickness) of the ribboned fiber. Due to the ribboned-structure in our 20 wt% rTE scaffolds, the 15 wt% rTE solutions were used for all subsequent studies. Using 15 wt% rTE solutions, we were able to produce cylindrical prTE fibers (Figure 2.1), a structure similar to native medial elastin structure.

Using monomer protein solutions necessitates the use of cross-linking to stabilize the electrospun fibers. The monomer tropoelastin is soluble in aqueous solutions and would therefore lose its macro fiber structure upon introduction to aqueous media. This cross-linking has a significant effect on the structural properties of the electrospun materials [131] and can lead to complications of calcification and cytotoxicity. This is the first reported use of DSS to cross-link tropoelastin electrospun materials. DSS was selected to cross-link the rTE due to the low reported cytotoxicity of its aqueous equivalent *bis*(sulfosuccinimidyl) suberate (BS³) and its ability to react with amine groups on lysine residues of adjacent molecules to form amide bond cross-links [132-134]. The prTE was cross-linked with DSS in anhydrous ethyl acetate at a concentration sufficient to attain 100% cross-linking based upon a molecular weight of 62,500 and 35 lysines per molecule. Monomeric rTE maintains its fiber structure in ethyl acetate giving the DSS cross-linker time to stabilize or lock the fiber structure in place. Use of high concentrations of cross-linker can lead to blocking of amine groups resulting in fewer cross-links being formed. DSS forms an 8-atom bridge (11.4Å) between tropoelastin

monomers to form polytropoelastin, and has proven to be an effective method for cross-linking rTE electrospun materials. Electrospun tropoelastin alone or elastin with collagen have previously been cross-linked with glutaraldehyde vapor [120, 125], hexamethylene diisocyanate (HMDI) [61, 135], or BS³ [132, 134, 136]. The glutaraldehyde vapor caused melting of the collagen/elastin fibers [125] and may lead to calcification of the fibers and a cytotoxic environment. HMDI binds lysine or hydroxylysine residues and has been used primarily with collagen biomaterials (eg., Permacol, Covidien). BS³ uses the same mechanism of cross-linking as DSS. Thus DSS, HMDI, and BS³ are promising as cross-linkers of protein monomers but their full biological effects on cell proliferation, mechanical properties, and host reactions are unknown. The proliferation of SMCs on the DSS cross-linked prTE supports the cytocompatibility of the DSS crosslinker. The mechanical properties and host reactions will depend on the concentration of the electrospinning solution, as well as the configuration of the final biomaterial as a flat or tubular scaffold. For vascular applications, the appropriate mechanical evaluations (e.g. burst pressure, compliance) of DSS-cross-linked prTE in the tubular configuration should be determined.

Support of vascular cell adhesion and growth is required for tissue-engineered scaffolds. Elastin is an important regulator of SMC phenotype. Karnik et al. demonstrated an increase in vascular SMC proliferation rates in cells unable to synthesize elastin [97]. Yet the addition of exogenous tropoelastin to the growth culture recovered normal proliferation rates, equivalent to wild type cells [97]. It has been suggested that elastin (as a signaling molecule) activates the G-protein coupled pathway that ultimately leads to

Rho-induced actin polymerization in vascular smooth muscle cells [137]. Our study, where pertussis toxin was unable to block adhesion, suggests that the G-protein coupled pathway does not play a role in the initial cell adhesion to rTE. There have been several elastin binding proteins (EBP) identified, including a 67-kDa protein that is also identified as a galactoside-binding lectin [93, 99, 100, 138], a 120-kDa protein (elastonection) and a 59-kDa VGVAPG-binding protein [102]. These EBPs act as chaperones during elastin assembly by preventing intracellular aggregation of tropoelastin as well as protecting tropoelastin and mature elastin from proteolysis. EBP binds elastin through the VGVAPG motif within exon 24 [92] and signaling through this receptor may influence SMC proliferation and differentiation [137]. Fetal bovine chondrocyte adhesion was associated with the COOH terminus of tropoelastin and dependent on glycosaminoglycans, while integrin and EBP inhibitors had no effect on chondrocyte adhesion and spreading on the COOH terminus of tropoelastin [92]. Thus, the EBPs do not appear to play a role in cell adhesion to tropoelastin, which was confirmed in this study with the inability of lactose to block SMC adhesion to rTE. A direct link between cell adhesion to tropoelastin and the $\alpha_3\beta_3$ integrin has been demonstrated with human dermal fibroblasts [139]. Similarly, in this current study the adsorbed rTE, as well as the adsorbed fibronectin, supported SMC adhesion through cationic binding, which was blocked by EDTA. This integrin-mediated adhesion is likely due to $\alpha_3\beta_3$ integrin interaction with GRKRK motif [139]. Differences in cell binding mechanisms to tropoelastin are likely due to the utilization of different cell types.

Coatings of rTE can be used to modify devices such as stents and vascular graft materials. Optimal cell adhesion occurred on substrates coated with 50 $\mu\text{g/ml}$ or greater and consequently, this value can be used as the baseline value for designing rTE modified surfaces. The three-dimensional electrospun prTE supported SMC proliferation indicating the cytocompatibility of the DSS-cross-linked prTE. SMC metabolic activity (as indicated by the alamarBlue® assay) on electrospun prTE increased between day 1 and day 7 similar to the activity of SMCs on coated prTE, Poly-D-Lysine, and TCP. While the alamarBlue® assay does not quantify exact cell numbers, rather cell metabolic activity, it is correlated to the growth rates of cells in culture. After 8 days of growth, the cellular DNA content on the electrospun prTE, coated prTE, and Poly-D-Lysine (CyQUANT® assay) were equivalent and greater than the DNA content on TCP. The ability of electrospun tropoelastin to support cell growth agrees with the results of Li et al., who demonstrated human embryonic palatal mesenchymal cell (HEPM) growth on both electrospun elastin and tropoelastin [61]. Similar to the HEPM cells, SMCs formed distinct organized cytoskeletal fibers with multiple pseudopodia attachments to the prTE fibers. Likewise, human dermal fibroblasts attached and proliferated on electrospun tropoelastin [120]. Though a direct comparison is difficult to make due to differences in study conditions, our SMC growth data was similar to Karnik's data for wild-type SMCs, which demonstrated a 2-fold increase in cell numbers at 72 hours [97]. Modest cell growth rates, the presence of distinct stress fibers, and multiple attachment points on each of the three biomaterials of prTE tested suggests that SMCs grown on prTE adopt a contractile phenotype, which could ultimately provide physiologic vascular compliance and vasomotor tone. Further investigation into the three-dimensional growth patterns of

SMCs on electrospun prTE and their remodeling effect on the protein scaffold in long-term cultures is warranted.

2.7 Conclusion

An electrospun cross-linked recombinant human tropoelastin vascular scaffold material has been developed. This novel tissue engineered scaffold has structural properties similar to native elastin within the medial layers of elastic arteries. The diameter, length, fiber size, and fiber spacing of the electrospun prTE scaffold were easily manipulated providing a high degree of control for tissue engineering. The electrospun prTE biomaterial supported SMC attachment (via an integrin-mediated pathway), spreading, and growth. A cross-linked stable polymer produced from recombinant human tropoelastin, which matched the structure of medial elastin, may provide the optimal environment needed for a functional tissue-engineered scaffold. The development of this technology provides a tool for tissue engineers, which can ultimately lead to natural protein-based vascular grafts.

Chapter 3: Mechanical Property Characterization of Electrospun Recombinant Human Tropoelastin for Vascular Graft Biomaterials

Kathryn A. McKenna, Monica T. Hinds, Rebecca C. Sarao, Ping-Cheng Wu, Cheryl L. Maslen, Robert W. Glanville, Darcie Babcock, and Kenton W. Gregory

3.1 Abstract

The development of vascular grafts has focused on finding a biomaterial that is non-thrombogenic, minimizes intimal hyperplasia, matches the mechanical properties of native vessels and allows for regeneration of arterial tissue. In this study, the structural and mechanical properties and the vascular cell compatibility of electrospun recombinant human tropoelastin (rTE) were evaluated as a potential vascular graft support matrix. Disuccinimidyl suberate (DSS) was used to cross-link electrospun rTE fibers to produce a polymeric recombinant tropoelastin (prTE) matrix that is stable in aqueous environments. Tubular 1 cm diameter prTE samples were constructed for uniaxial tensile testing and 4 mm small-diameter prTE tubular scaffolds were produced for burst pressure and cell compatibility evaluations from 15 wt% rTE solutions. Uniaxial tensile tests demonstrated an average ultimate tensile strength (UTS) of 0.36 ± 0.05 MPa and elastic moduli of 0.15 ± 0.04 MPa and 0.91 ± 0.16 MPa, which were comparable to extracted native elastin. Burst pressures of 485 ± 25 mmHg were obtained from 4 mm ID scaffolds with 453 ± 74 μm average wall thickness. prTE supported endothelial cell growth with typical endothelial cell cobblestone morphology after 48 hours in culture. Cross-linked electrospun recombinant human tropoelastin has promising properties for utilization as a

vascular graft biomaterial with customizable dimensions, a compliant matrix, and vascular cell compatibility.

This work is published by Elsevier

Acta Biomaterialia, Online August 6th 2011

doi:10.1016/j.actbio.2011.08.001

Reprinted with permission

3.2 Chapter Overview

Chapter 2 focused on the structural characteristics of electrospun human recombinant tropoelastin and its cellular compatibility. Chapter 3 evaluates the mechanical properties of tubular constructs produced from materials evaluated in Chapter 2. These materials can be incorporated into vascular graft constructs to provide both the biochemical signaling of elastin and mechanical compliance. Both compliance and elastin signaling are critical factors for successful implementation of vascular graft designs.

3.3 Introduction

Heart disease remains the leading cause of death in the Western world with nearly 81 million people affected in the United States in 2006 [140]. Bypass surgery using autografts of saphenous veins or mammary arteries remains the gold standard treatment for severe cases, but can be limited by previous vessel harvest or preexisting disease. Synthetic graft materials, such as expanded poly(tetrafluoroethylene) (ePTFE) and poly(ethylene terephthalate) (PET or Dacron[®]), work well for large diameter vessels, but are not viable options for grafts smaller than six millimeters in diameter [141].

The failure modes of small diameter vascular grafts have primarily been thrombosis, aneurysm, and intimal hyperplasia [7]. To address these failure modes many researchers have studied both synthetic and natural biomaterial scaffolds. Synthetic biomaterials have controllable physical and mechanical properties that are highly reproducible and are easily manufactured in large-scale quantities, but many lack the elasticity of native arteries and biocompatibility for long-term vascular cell functionality. Considerable efforts have been made to functionalize synthetic surfaces [63, 76]. Natural biomaterial scaffolds, including well-studied grafts of decellularized blood vessels [6-8], have had limited success. The decellularized bovine [41] and human [42] blood vessels had promising 5-year patency rates, yet aneurysm formation due to *in vivo* degradation limited their widespread use [42, 43]. Decellularized arteries, from allogenic and xenogenic sources are attractive scaffolds for tissue-engineered vascular grafts due to their mechanical and biological properties [44], yet these natural scaffolds are limited by the lack of precise manufacturing control of the physical and mechanical properties, as well as problems with inflammation and calcification [142]. To reduce concerns of inflammation of the allogenic and xenogenic sourced vascular biomaterials, the biomaterials are frequently cross-linked; yet this has led to problems of limited cell repopulation and increased stiffness of the biomaterials [143]. While stiffness and compliance mismatch alone may not lead to vascular graft failure [144-146], graft compliance has correlated to the formation of intimal hyperplasia and should be considered in biomaterial scaffold design along with the potential of cellular remodeling of the graft and cell signaling capability [147-153]. The search for a viable off-the-shelf small diameter vascular graft that can match an autograft's performance in terms of

mechanical properties, cell compatibility, and vascular healing has been the focus of many research efforts, but has remained an elusive target.

The incorporation of vascular cells with biomaterial scaffolds to produce tissue engineered grafts have been successful in animal and, recently, human trials [153]. Production of the scaffold by the vascular cells has been accomplished using both *in vivo* [154-156] and *in vitro* [4, 45] methods. The *in vivo* methods require the graft to be grown in the recipient's peritoneal cavity. Recent advancements of this technique include improved scaffold design to produce multilayered scaffolds and the use of cyclic stretch to improve the assembly time and organization of the extracellular matrix [4, 45, 154, 157-159]. Yet these *in vivo* methods require a second surgical site for autologous use. The *in vitro* methods of L'Heureux et al., where the tissue-engineered vascular grafts were produced from autologous cells without a scaffold, have advanced to clinical trials using an arteriovenous shunt model [155, 156]. These autologous tissue-engineered grafts have promising results with primary patency rates of 78% at 1 month and 60% at 6 months and the limited failures due to thrombosis, dilation, and aneurysm [4, 45]. The *in vitro* cell produced scaffolds are elegant in design, but require lengthy production times potentially limiting their clinical use.

The use of electrospinning to make biomaterials has the capability of combining natural proteins with controllable physical and mechanical properties. Electrospinning produces sub-micron sized fibers from suspensions of monomers or polymers from both natural proteins and synthetic polymers [4]. Fibers produced from monomer suspensions can

then be cross-linked to produce stable polymeric structures with customizable dimensions in terms of fiber diameter and overall graft dimensions. Electrospun fibrous scaffolds made from biodegradable polymers, such as poly(ϵ -caprolactone) (PCL), polylactic acid (PLA), polyglycolic acid (PGA), and poly(lactide-co-glycolide) (PLGA) [111, 160-163] have been proposed for use in bone, cardiac, blood vessel, and wound dressing applications [46-49]. Several groups have successfully electrospun elastin for use in tissue-engineered grafts [50-56] and support material for vein grafts [57, 61, 115-119]. Most, however, have used animal sourced elastin that is [164] extracted from already assembled and cross-linked protein forms. While these forms of elastin may provide the biochemical signaling of elastin, they remain an animal sourced material with the associated potential for immuno-rejection leading to structural degradation and ultimate aneurismal graft failure.

Our aim is to electrospin small diameter vascular grafts containing recombinant human tropoelastin, the monomer unit of elastin, that when cross-linked mimics native elastin fibers. Elastin is the principal structural component of elastic arteries responsible for energy storage and recovery, and contributes to their unique mechanical properties [126, 153, 165, 166]. End stage aneurysm disease and supra-aortic stenosis have been associated with the pathologic loss of elastin or deficiency in elastin expression [112]. Elastin, as a blood-contacting surface on stents and grafts, reduced thrombus adherence and demonstrated good long-term patency [19-26]. Establishing an elastic fiber structure in a vascular scaffold that is similar to the arterial wall has been well recognized, as the depletion or loss of elastin has been correlated to both aneurysmal progression and severe

smooth muscle cell hyperplasia in both animals and humans.[97, 167]. Thus, elastin is a promising, and perhaps necessary, component in vascular graft development [19, 22, 23, 25, 97, 168-170]. Recent work has examined a class of elastin-like recombinant polymers with self-assembly properties and cross-link sites designed into the peptide sequence [113, 114]. The elastin-like polymer has been used to produce organized multilayer collagen reinforced vascular grafts and abdominal wall repair tissue constructs with customizable mechanical properties, which make this technology promising for many soft tissue applications [171]. Our use of electrospinning will enable the customization of the dimensions and mechanical properties for the vascular graft biomaterial, and the use of tropoelastin may impart critical cell signaling to the biomaterial.

3.4 Materials and Methods

3.4.1 Materials

Human tropoelastin was optimized and expressed from a synthetic gene codon in gram quantities in a 10-liter *E.coli* fermentation system. Gel electrophoresis determined that the purification procedure resulted in a greater than 99% pure product (Figure 3.1) as well as low endotoxin levels with an average of 0.2 EU/mg (1 EU = 100 pg of endotoxin) as determined by the Kinetic-QCL Assay (Cambrex). All chemical reagents were acquired from Sigma-Aldrich unless otherwise noted.

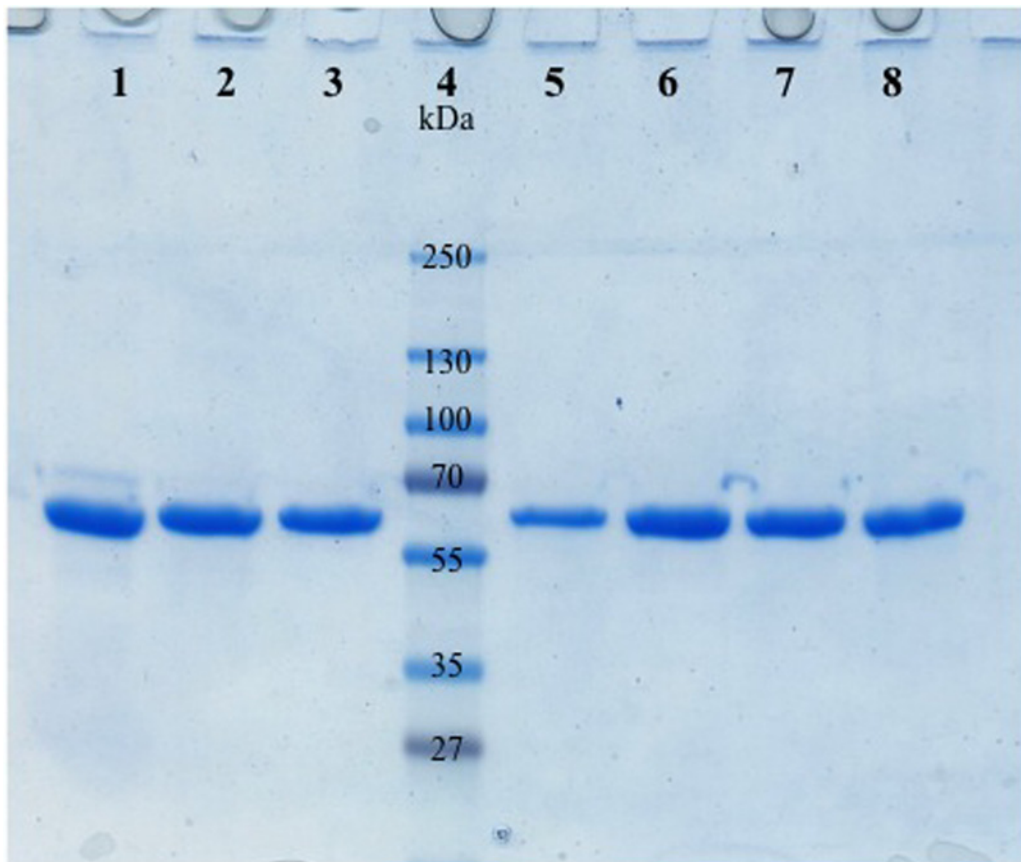


Figure 3.1. Stained electrophoresis gel showing purified human tropoelastin from 7 different batches (lanes 1-3 and 5-8) illustrating the purity of the product and reproducibility of the purification process. Lane 4 is a molecular weight standard. This gel was provided by Dr. Robert Glanville at the Oregon Medical Laser Center.

The purified human tropoelastin protein includes all of the functional exons with the exception of exons 1, 22, and 26A (Figure 3.2). Exon 1 contains the signal sequence, while hydrophobic exon 22, and hydrophilic exon 26A are rarely expressed in mature elastin. The resultant tropoelastin exon structure used is the same as a natural isoform produced by normal human fetal heart cells.

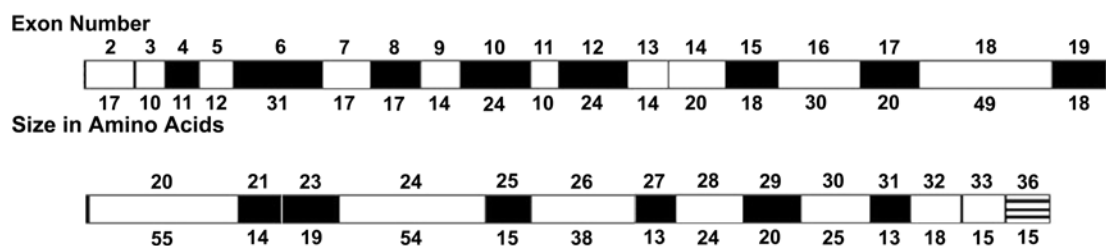


Figure 3.2. Diagrammatic representation of human tropoelastin protein domains. The number of the corresponding exons and the sizes of the domains are shown. The exon numbering system is based upon the bovine elastin gene sequence. The human gene has no exons 34 and 35, while exon 26A is rarely expressed in human tropoelastin. Cross-linking domains are shaded black and hydrophobic domains are white. This structure was identified and produced by Dr. Cheryl Maslen, Dr. Robert Glanville, Darcie Babcock and the Oregon Medical Laser Center research team.

Extracted porcine elastin was isolated as previously described [172, 173]. Briefly, porcine carotid arteries were obtained from domestic swine of 250 lb and 6–9 months of age (Animal Technologies, Tyler, TX) to size match the diameters. The arteries were shipped overnight in phosphate-buffered saline (PBS) on ice. The gross fat was dissected away and, using aseptic techniques, the arteries were placed in 80% ethanol for a minimum of 72 h at 4°C and subsequently treated with 0.25M NaOH for 70 min with sonication at 60°C, followed by two 30-min, 4°C washes in 0.05M HEPES (pH 7.4). The extracted elastin tubular conduits were then autoclaved at 121°C for 15 min and stored at 4°C in 0.05M HEPES buffer.

3.4.2 *Electrospinning of rTE*

Tropoelastin solutions of 15 wt% rTE in 1,1,1,3,3,3-hexafluoro-2-propanol (HFP) were prepared and loaded into 2 or 5 mL glass syringes depending on the volume needed for each application. 18-gage stainless steel blunt tip needles were connected to the syringes and electrically coupled to a high voltage power supply (Glassman High Voltage, Inc.,

High Bridge NJ). A gap distance of 12.5 cm was set from the end of the needle to the center of the collection device. A syringe pump (Harvard Apparatus) was used to advance the protein solution at 2 mL/hr to refresh the solution at the tip of the syringe needle. Fibers were spun onto mandrels of either 1 cm diameter copper tubes for mechanical testing or 4 mm diameter stainless steel rods for small diameter graft production. Mandrels were connected to ground to complete the circuit. The collection system was set to rotate at 4400 rpm and translate longitudinally 6-8 cm with a rate of 8 cm/sec driven by a custom-built device with separate drives for longitudinal and rotational control. The solution was charged to an 18.5 kV excitation potential. All electrospinning was conducted within a chemical fume hood.

3.4.3 Cross-linking of Electrospun rTE

Disuccinimidyl suberate, DSS, (Pierce Biotechnology-Thermo Fisher Scientific Inc.), an organic amide bond cross-linker, was used to link electrospun rTE monomers to produce polymeric tropoelastin, prTE. Cross-linking was performed in a two-stage process. The electrospun rTE samples were incubated for 4 hours in DSS suspended in 50 mL anhydrous ethyl acetate, at a ratio of 0.072 mg of DSS per mg of rTE protein at room temperature in glass tubes. A second incubation occurred for 12-18 hours at a concentration of 0.108 mg of DSS per mg of rTE protein at room temperature. prTE samples were then rinsed in anhydrous ethyl acetate for 5 minutes with a second 5 minute rinse in 70% ethanol and a final 10 minute rinse in DI water. Final products were stored in 70% ethanol.

3.4.4 Electrospun rTE Fiber Characterization

The tubular scaffolds electrospun from 15 wt% prTE were analyzed with electron microscopy to determine fiber diameters and evaluate the degree of fiber orientation and consistency through the thickness of the graft. Electrospun prTE samples were mounted onto scanning electron microscopy (SEM) stubs and sputter-coated with 250 Å of gold/palladium. Micrographs were taken at magnifications from 3000 to 5000X and viewed at 5 kV on an FEI Sirion XL30 SEM. Image analysis of fibers was done with a custom MATLAB® program (MathWorks®) using a Laplacian edge detection algorithm followed by a Radon transform to determine the probability distribution of fiber orientation angles relative to horizontal.

3.4.5 Mechanical Properties of prTE

The mechanical properties of electrospun prTE samples were compared to extracted porcine elastin and native porcine carotid arteries. All uniaxial tensile tests were conducted on dogbone shaped specimens with a gage length of 10 mm and 4 mm grip ends. The tubular 1 cm diameter prTE samples were opened longitudinally, laid flat, and cut with a dye cutter. Four circumferential and four longitudinal sections were cut from each of the three electrospun samples. Eight longitudinal and eight circumferential samples were tested for native carotid arteries and extracted elastin conduits. All specimens were rehydrated in PBS for at least 15 minutes prior to testing. The thickness, width, and gage length were recorded. The samples were mounted on custom tensile grips on a Chatillon Vitrodyne V1000 system with a 500 gram load cell or on a MTS 858 Mini Bionix II mechanical tester with a 5 lb load cell using spring action grips. All

dogbone prTE samples were tested in tension at room temperature with a crosshead speed of 2 mm/sec until failure. Force and displacement measurements were acquired at 0.1 sec intervals. Engineering stress (force/cross-sectional area, F/A_{cs}) and strain (change in length/original length, $\Delta L/L_o$) were calculated and plotted. Linear regression of the slope in the stress-strain plots was used to calculate the elastic modulus (stress/strain, σ/ϵ). Elastic modulus 1 was measured between 10 and 30% strain, while elastic modulus 2 was measured between the maximum strain minus 20% and the maximum strain with linear curve fits to these regions of the stress strain curve. Peak stress (MPa) and strain (%) were taken as ultimate tensile strength (UTS) and percent elongation (ultimate strain). Compliance measurements were calculated using the stress and strain data between 50 and 100 kPa. Calculated values were based on the ANSI/ISO 7148 standard for “Cardiovascular implants – tubular vascular prostheses” [167]. Radius values at these stress values were calculated using a thin-walled cylinder approximation relating pressure to stress scaled by wall thickness and initial radius (Equation 3.1). Compliance was measured as the change in radius relative to the initial radius over the change in pressure or stress at 100 kPa and 50 kPa for each material (Equation 3.2).

Equation 3.1:

$$\sigma_{\theta\theta} = \frac{P_i r_i}{t}$$

Equation 3.2:

$$\frac{\%compliance}{100mmHg} = \frac{R_2 - R_1}{R_1} \frac{1}{P_2 - P_1} * 10^4$$

Where σ_{θ} = circumferential Cauchy stress, P = pressure, t = wall thickness, r = radius, R_2 = radius at P_2 , and R_1 = radius at P_1 .

3.4.6 Burst Pressure of prTE Scaffolds

Three 4 mm inner diameter, 5 cm long electrospun prTE scaffolds were fabricated for burst pressure analysis. Scaffolds of rTE were electrospun, cross-linked and stored in 70% ethanol prior to analysis. Wall thickness was measured using handheld digital micrometers and recorded. Scaffolds were cannulated onto barbed nylon connectors and secured using cotton umbilical tape. Samples were rehydrated in PBS for at least 30 minutes prior to testing. The ends of the scaffolds were fixed in position under zero longitudinal strain/load and saline was subsequently infused at a rate of 100 mL/min until failure occurred. The pressure (mmHg) was continuously monitored by an inline pressure transducer (Cole Parmer) and recorded with a custom built LabVIEW (National Instruments) data acquisition program.

3.4.7 Endothelial Cell Growth on prTE Scaffolds

Porcine bone marrow derived endothelial outgrowth cells (BMEOCs) were isolated and used to assess the growth of vascular cells on the luminal surface of electrospun prTE vascular grafts. Porcine bone marrow mononuclear cells were collected and separated as previously reported [174]. Isolated cells were differentiated into BMEOCs in endothelial cell growth media (EGM2) at 37°C and 5% CO₂ in a tissue culture incubator. BMEOCs were passaged and maintained in endothelial cell growth media (EGM2) using standard

techniques. BMEOCs were stained with endothelial cell specific von Willebrand factor (vWF, DAKO).

Tubular prTE grafts were rehydrated in growth media for 1 hour. Vessels were inoculated with BMEOCs (5×10^3 cells/cm²) and held at 90 mmHg for 1 hour. Grafts were then maintained in a cell culture incubator for 48 hours in standard conditions. Grafts were fixed with 2.5% paraformaldehyde at 48 hours and evaluated for cell engraftment with DAPI nuclear stain and rhodamine phalloidin f-actin stain. Confocal images were taken with a 63X oil objective on a Zeiss Multiphoton Confocal microscope using 543 and 780 nm excitation wavelengths.

3.4.8 Statistical analyses

All data are expressed as the mean \pm standard deviation. Student's *t*-test, linear regression, and one-way ANOVA with Tukey post hoc tests were used for hypothesis testing, with $p < 0.05$ as the measure for statistical significance. The number of independent tests is listed for each experiment.

3.5 Results and Discussion

Electrospinning has proven to be a valuable tool to produce biomimetic scaffolds for use in tissue engineering. Electrospun vascular graft materials have included natural proteins, such as collagen and elastin, and biodegradable polymers either as stand alone materials or as blends with other polymers or natural proteins [175]. The number of materials used for electrospinning is increasing as well as the design complexity with multilayered

constructs [126, 162, 176] and materials with tunable mechanical properties [155, 172, 173, 177, 178]. Elastin is emerging as an important component of vascular graft development with our increased understanding that synthetic polymers alone pose problems with compliance mismatch and foreign body response [173, 178, 179]. Elastin has unique properties making it a natural choice as a component in vascular scaffold biomaterials that require long-term durability, antithrombogenic properties, and elasticity. Elastin is highly insoluble with a half life of greater than 70 years; it modulates cell function reducing the thrombogenic potential of the surface; and it is highly elastic thus adding compliance to the structure of the biomaterial [126]. Electrospinning of tropoelastin into a biomaterial was first reported in 2005 [180]. Widespread use of tropoelastin for biomaterial development has been limited by the availability of monomeric tropoelastin. Since 2005, the use of tropoelastin has increased and has been incorporated into additional vascular graft scaffolds [61] and coatings on stent struts [178, 180]. The current work describes methods of electrospinning recombinant human tropoelastin into tubular grafts, cross-linking the material into a stable polymer, and characterizing its structural, mechanical, and cell compatibility properties.

3.5.1 Morphology and Substructure of prTE Fibers

To produce purely electrospun prTE tubular scaffolds, 15 wt% solutions of rTE were electrospun onto rotating mandrels and cross-linked. Conduits were 4-10 cm in length, 4 mm in diameter, with wall thicknesses of 0.43-0.65 mm (Figure 3.3A). The wall thickness was dependent on the volume of the rTE solution used. The prTE fibers were randomly oriented as determined using image analysis to calculate the probability

distribution function of fiber orientation angles relative to horizontal (Figure 3.4). The average fiber diameters (580 ± 94 nm) and fiber structure (Figure 3.3B) of the electrospun protein was maintained throughout the thickness of the graft (data not shown).

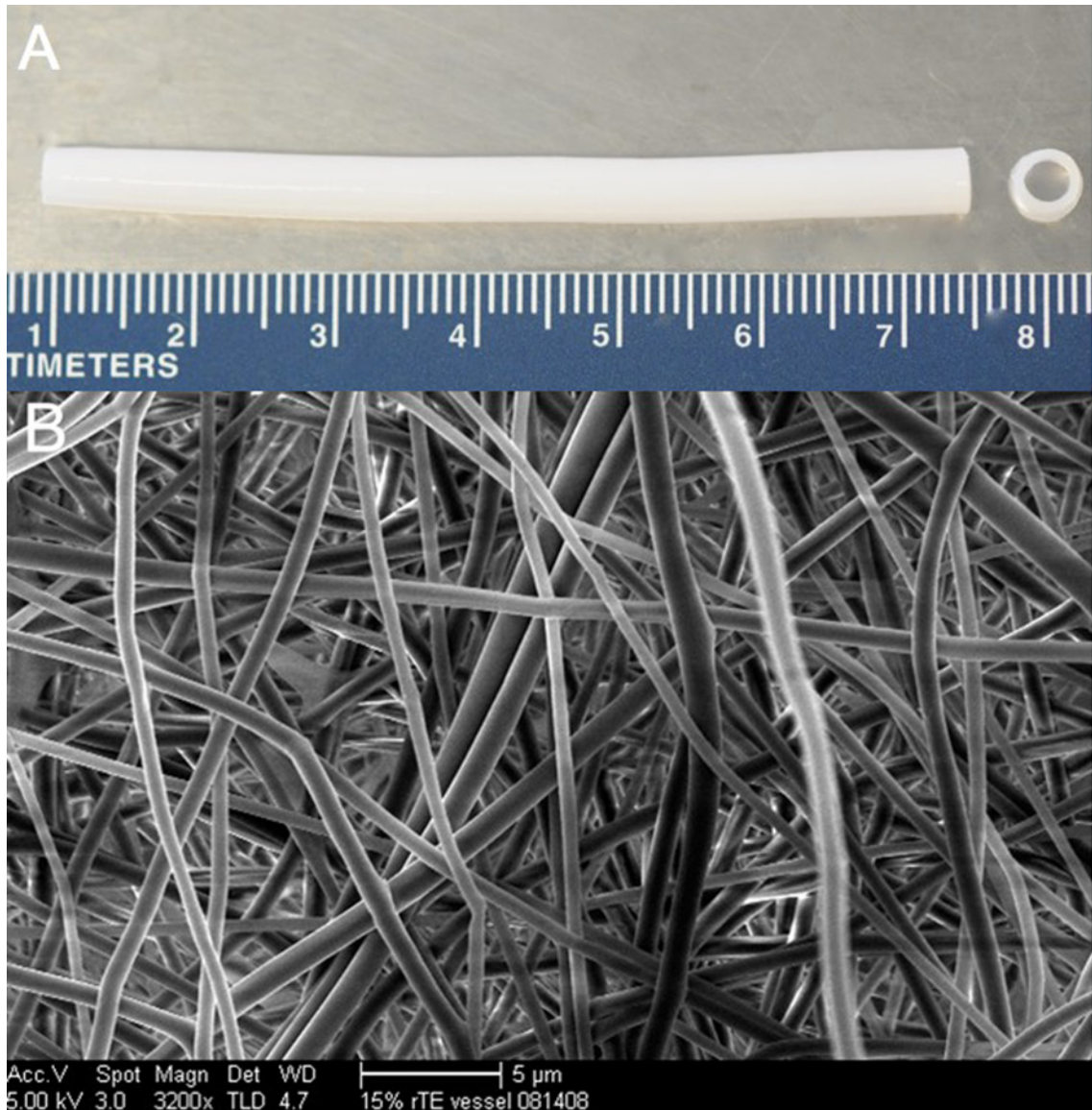


Figure 3.3. Electrospun tubular prTE vascular scaffold. (A) The vascular scaffold was 7 cm in length, 4 mm internal diameter, and consisted of pure prTE fibers. (B) The prTE fibers were randomly oriented with average fiber diameters of 580 ± 94 nm. The scale bar indicates 5 μ m.

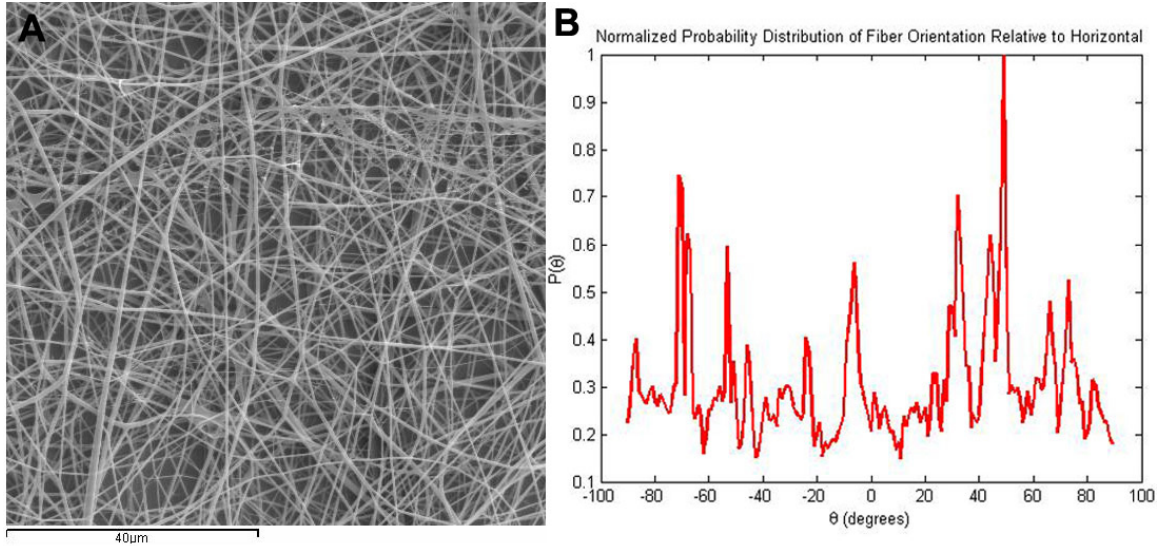


Figure 3.4. MATLAB image analysis of fiber orientation. (A) Image of electrospun prTE fibers (B) Normalized probability distribution function plotted as probability of the feature orientation versus angle. Fibers were randomly oriented in these samples. Dr. Sean Kirkpaterick wrote the original MATLAB code that was modified for this analysis.

3.5.2 Mechanical Properties of prTE

Uni-axial tensile testing of prTE samples from 15 wt% rTE produced stress-strain curves (Figure 3.5) for both the longitudinal and circumferential sample orientations. The curves were similar for the two orientations showing a bimodal stress-strain relationship in which the modulus was dependent on the percent strain. The transition in moduli values occurred between 40 and 50% strain. The only mechanical property that was significantly different between the longitudinal and circumferential orientations of electrospun prTE was the elastic modulus 2 (t-test, $p < 0.01$). The remaining mechanical properties (UTS, % elongation, and elastic modulus 1) were not significantly different (t-test, $p > 0.05$) between the two orientations (Figure 3.6). Combining electrospun prTE's longitudinal and circumferential orientations measurements, the average UTS, elastic modulus 1 and

percent elongation were 0.36 ± 0.05 MPa, 0.15 ± 0.04 MPa, and $77 \pm 5\%$, respectively. Elastic modulus 2 values were not combined because they were significantly different between orientations.

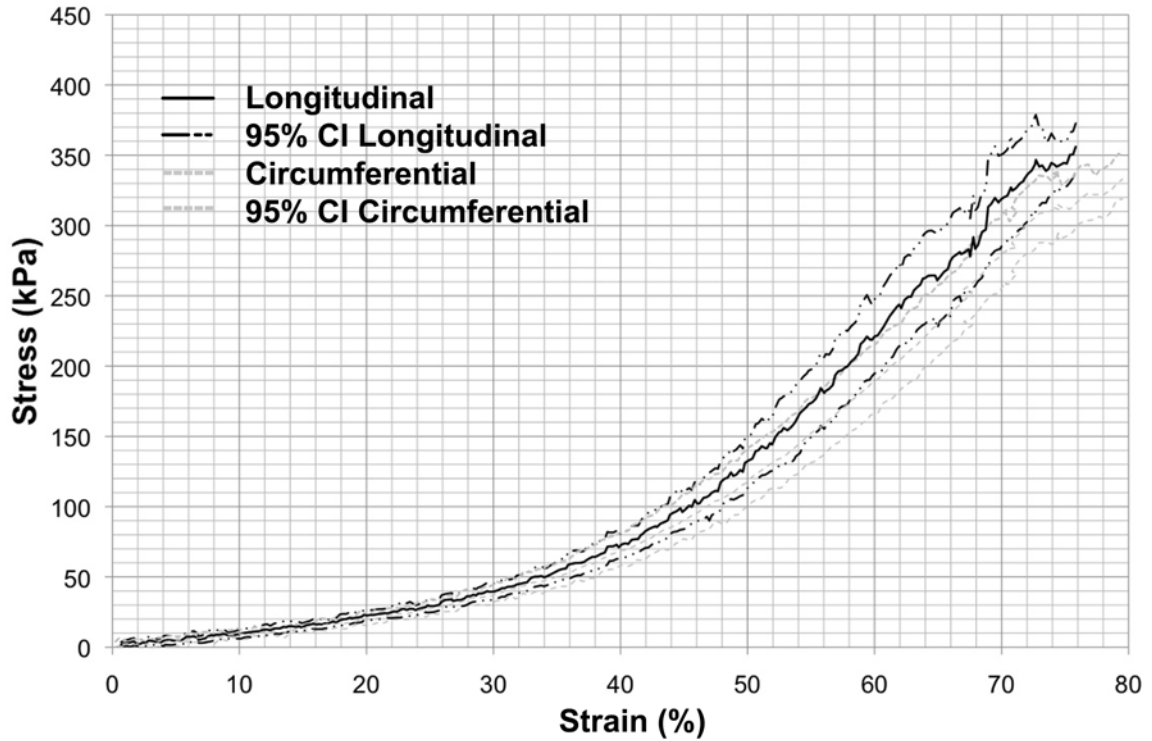
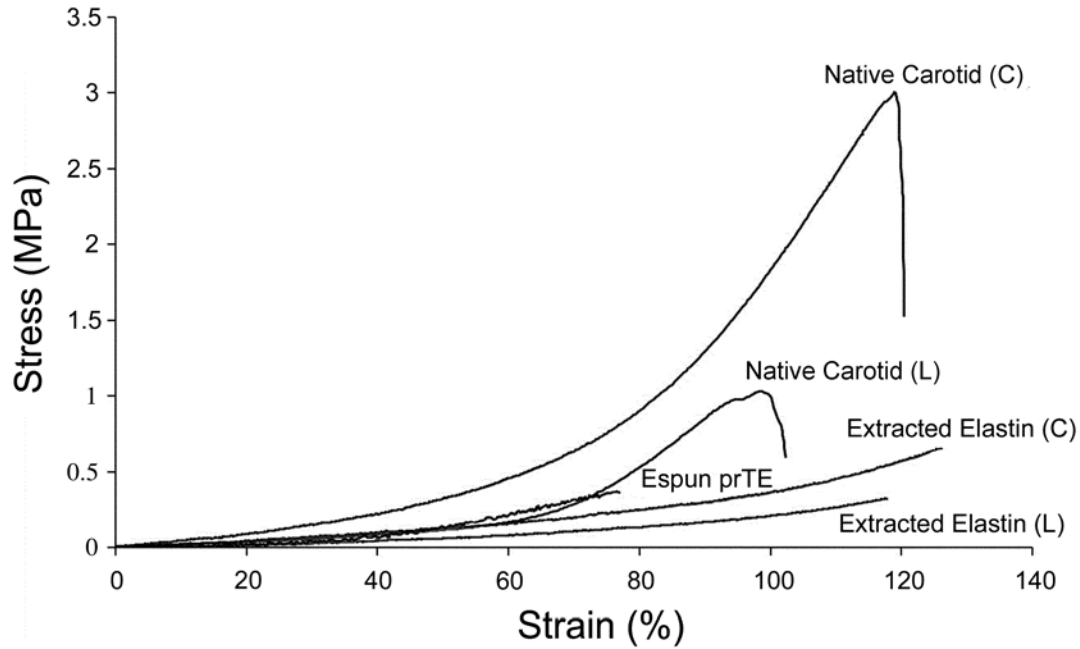


Figure 3.5. Average stress-strain curves for electrospun prTE fibers from a 15 wt% solution for both circumferential and longitudinal orientations (average with 95% confidence interval). The only significant difference in mechanical properties was in the elastic modulus 2 of the tested orientations. Mechanical data was obtained with the excellent technical assistance of Ping Cheng Wu at the Oregon Medical Laser Center.

Ultimate tensile strength (UTS), percent elongation, and elastic moduli for electrospun prTE were compared to extracted porcine elastin and native porcine carotid arteries for the longitudinal (L) and circumferential (C) orientations (Figure 3.6). The electrospun prTE samples had UTS values of 0.34 ± 0.14 MPa (C) and 0.38 ± 0.05 MPa (L). The UTS values for the electrospun prTE were comparable to extracted porcine elastin in the

longitudinal direction, yet significantly different to circumferential extracted elastin and both native carotid artery specimens (ANOVA, Tukey post hoc, $p < 0.05$). The percent elongation at failure of the electrospun prTE was $79 \pm 6\%$ (C) and $75 \pm 5\%$ (L), which was significantly lower than the control materials in both orientations (ANOVA, Tukey post hoc, $p < 0.01$). The average elastic moduli of electrospun prTE were 0.15 ± 0.05 MPa (C) and 0.15 ± 0.03 MPa (L) for elastic modulus 1 and 0.82 ± 0.11 MPa, (C) and 0.99 ± 0.17 MPa (L) for elastic modulus 2 which were comparable to extracted elastin in the longitudinal direction for elastic modulus 1 and in both orientations for elastic modulus 2. Both prTE elastic moduli were significantly different from the native carotid materials (ANOVA, Tukey post hoc, $p < 0.05$)



Specimen	UTS (MPa)	Percent Elongation (%)	Elastic Modulus 1 (MPa)	Elastic Modulus 2 (MPa)
Espun prTE (L)	0.38 ± 0.05	75 ± 5	0.15 ± 0.03	0.99 ± 0.17**
Espun prTE (C)	0.34 ± 0.14	79 ± 6	0.15 ± 0.05	0.82 ± 0.11**
Extracted Elastin (L)	0.29 ± 0.06 ^a	107 ± 14*	0.16 ± 0.05 ^a	0.53 ± 0.16 ^a
Extracted Elastin (C)	0.59 ± 0.11*	119 ± 11*	0.24 ± 0.04*	1.05 ± 0.37 ^a
Native Carotid (L)	0.95 ± 0.13*	105 ± 11*	0.20 ± 0.06*	2.39 ± 0.84*
Native Carotid (C)	2.59 ± 0.31*	125 ± 15*	0.41 ± 0.09*	5.72 ± 0.79*

Figure 3.6. Mechanical properties of the electrospun prTE scaffolds. (Top) Representative stress-strain curves of electrospun prTE, extracted porcine elastin, and native porcine carotid arteries. (Bottom) Table of mechanical properties including ultimate tensile strength (UTS), percent elongation at failure, and elastic moduli of electrospun prTE compared to extracted porcine elastin and native porcine carotid arteries. The UTS and elastic moduli of electrospun prTE were not significantly different from the extracted elastin in the longitudinal direction. Note: ^aindicates no significant difference (ANOVA, Tukey post hoc, $p > 0.05$), compared to electrospun prTE in the same orientation, *indicates a significant difference (ANOVA, Tukey post hoc, $p < 0.05$) for comparisons to electrospun prTE in the same orientation, and **indicates $p < 0.01$, t-test. Mechanical data was conducted with the excellent technical assistance of Ping Cheng Wu at the Oregon Medical Laser Center.

Average compliance values for electrospun prTE, extracted elastin, and native carotid arteries were 20.2 ± 2.6 , 32.0 ± 3.1 and 3.4 ± 0.5 % respectively, which were all significantly different (ANOVA, Tukey post hoc, $p < 0.01$). Extracted elastin lacks collagen and therefore is expected to have greater compliance. The compliance of electrospun prTE fell between extracted elastin and native carotid arteries. This allows for the addition of stiffer materials, such as collagen, to the biomaterial to both strengthen the vessel in terms of UTS while maintaining compliance equivalent to native vessels.

The mechanical properties of electrospun proteins are dependent on the specific proteins selected, the protein concentration, electrospinning parameters, cross-linkers, and fiber orientation [181]. The mechanical properties of the circumferential and longitudinal orientations of the prTE materials were similar, where the only measured significant difference was in the elastic modulus 2 of electrospun prTE. UTS values of prTE electrospun materials were between the values of native extracted elastin in the longitudinal and circumferential directions and were much lower than the native carotid artery [58, 60, 61, 176, 182]. These results were expected due to the random (non-oriented) nature of the electrospun prTE fibers compared with the oriented fibers of native elastin [183-188], and due to the presence of collagen in the native matrix.

Additionally, the elastic modulus 1 of electrospun prTE, measured on the initial linear slope of the stress-strain curve, were comparable to the extracted elastin. Native elastic fibers (composed of elastin and fibrillin-1) contribute significantly to the material properties of native elastic arteries [189] in this initial linear slope region of the stress-

strain curve. Native arteries are true composites of matrix proteins and the transition in elastic modulus is primarily due to elastin and collagen's unique mechanical contributions working in concert. Therefore, the incorporation of prTE into a collagen scaffold is likely to increase the compliance of the vascular graft. The material properties of the electrospun prTE biomaterials were significantly different from the electrospun human tropoelastin by Li et al. [190]. The prTE had lower average UTS (0.36 MPa vs. 13 MPa) and average elastic moduli (0.15 MPa (elastic modulus 1) and 0.91 MPa (elastic modulus 2) vs. 289 MPa), yet a higher average percent elongation at failure (77% vs. 15%). It should be noted that only a single mechanical test was reported for Li's electrospun tropoelastin due to limited availability of protein [61]. The prTE materials were more elastic with a lower failure stress than Li's previously reported electrospun tropoelastin [61]. These disparities could be due to significant differences in electrospinning methods, testing methods, and cross-linking strategies. Our electrospinning parameters differ from Li et al., in several ways, including lower concentration of tropoelastin, higher accelerating voltage, and a smaller gap distance, which resulted in smaller and cylindrically-shaped fibers [61] for our prTE. The mechanical property evaluation by Li et al. utilized a unique testing system designed to evaluate textiles, which included the measured material weight to calculate stress. This measurement can be variable due to differences in the hydration of the tropoelastin. Our engineering stress calculations were based on the measured initial cross-sectional area. Additionally, to crosslink the tropoelastin Li et al. used hexamethylene diisocyanate (HMDI), which binds lysine or hydroxylysine residues, but may also react with nucleophilic functional groups such as amines, alcohols, and protonated acids. HMDI has

been shown to react with side chains of lysine, cysteine, histidine and tyrosine and may as well react to arginine, and aspartic acid. Nonspecific binding of residues by HMDI may affect the functionality and water content [191], thus altering the mechanical properties of cross-linked tropoelastin. DSS in comparison is specific to amines on lysine residues with an 8 atom bridge resulting in a 11.4 Angstrom crosslink arm. The specificity of DSS to lysine [192] leaves the cell binding domains available on the molecule as well as results in improved consistency of mechanical properties.

The mechanical properties were comparable to extracted elastin scaffolds, but still lack the tensile strength to support *in vivo* arterial pressures. For vascular graft applications, the tensile strengths of the prTE scaffolds must be further increased by reinforcement or co-spinning with either collagen or synthetic materials.

3.5.3 Burst Pressure of prTE Scaffolds

The electrospun prTE tubular scaffolds (n=3) had an average wall thickness of 453 ± 74 μm and an average burst pressure of 485 ± 25 mmHg. Scaffolds increased in size both longitudinally and circumferentially throughout the burst pressure test and test samples failed longitudinally in all cases. Saphenous vein and internal mammary artery grafts, the gold standard treatments, have reported burst pressures of 1599 ± 877 and 3196 ± 1264 mmHg, respectively [193]. Extracted porcine carotid elastin has a reported burst pressure of 162 ± 36 mmHg [194], which is significantly lower than the electrospun prTE, however, the UTS measurements were comparable between our electrospun and extracted elastin samples. Burst pressure differences could be due simply to differences

in wall thickness or a more complex mechanism involving variations in fiber architecture, which would lead to altered loading on individual fibers during biaxial deformation of the matrix. While an average burst pressure of 485 mmHg for our electrospun graft is sufficient for initial *in vivo* testing of host response, higher failure pressures of at least 1500 mmHg would need to be achieved to give an ample safety factor (>10) for its widespread clinical use.

3.5.4 Endothelial Cell Growth on prTE Scaffolds

Organic solvents, such as HFP, facilitate the electrospinning of pure protein solutions, due to improved protein solubility and solvent volatility. HFP has been shown to affect the conformation of electrospun collagen [167], which could have a drastic effect on its stability and mechanical properties. Tropoelastin is unlikely to be affected, as it is a single chain molecule that easily regains its secondary structure on removal of denaturants. The similarity in mechanical properties of prTE and extracted native elastin indicate minimal conformational changes in the prTE. The cytotoxic effects of HFP must be considered in construct design. HFP at concentrations above 250 ppm is toxic to cells [195]. The residual solvent HFP can be present in electrospun materials, but is likely removed through post processing (heat/vacuum treatments) of the material [196]. Our electrospun materials have been shown to support vascular cell growth [196], thus indicating low residual solvent levels, but a full evaluation of residual HFP should be conducted prior to conducting *in vivo* implant studies.

Bone marrow derived endothelial outgrowth cells (BMEOCs) attached, spread, and grew on the 15 wt% prTE tubular scaffolds. BMEOCs stained positive for vWF indicating an endothelial cell population (Figure 3.7A & B). Confocal images taken at 48 hours showed cells well attached and spread on the electrospun fiber matrix. Cells formed a confluent monolayer with typical endothelial cell cobblestone morphology (Figure 3.7C). This supports the hypothesis that prTE is a cell compatible matrix for both endothelial cells as well as, previously reported, smooth muscle cells [191], which demonstrated positive SMC growth and proliferation on prTE over a week with logarithmic cell growth between 3 and 5 days via integrin mediated binding mechanisms.

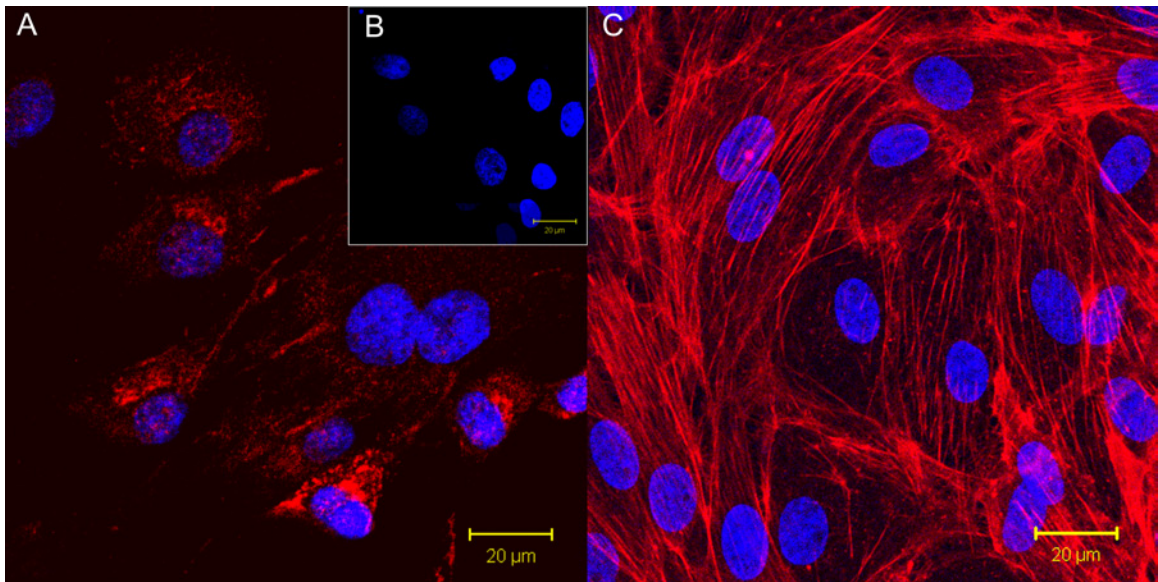


Figure 3.7. (A) BMEOCs stained for vWF (red) with a DAPI (blue) nuclear stain. (B) Control for vWF stain with the DAPI nuclear stain. (C) Endothelial cell monolayer on 15 wt% prTE after 48 hours in culture. Nuclei are stained with DAPI and the cytoskeleton (f-actin) is stained with rhodamine phalloidin (red). BMEOCs attached and spread on the prTE scaffold.

3.6 Conclusions

An electrospun tubular vascular scaffold material has been developed, composed of cross-linked recombinant human tropoelastin, which has physical and mechanical properties similar to extracted arterial elastin. The graft architecture, i.e. length and diameter, of the prTE scaffold can be precisely designed and controlled. A cross-linked stable polymer assembled from recombinant human tropoelastin provides both the compliance and support of endothelial cell adhesion for a component of a vascular graft biomaterial. While the mechanical strength of the prTE scaffolds are insufficient for implantation alone, the relatively lower compliance compared to native arteries will allow for the addition of stronger, but stiffer biomaterials. This technology holds great promise for incorporation in small diameter vascular graft biomaterials.

Chapter 4: Burst Pressure Based Analysis Method for Tissue Engineered Vascular Constructs: A Constitutive Model Development

Kathryn A. McKenna, Samuel Jensen-Segal, Sean J. Kirkpatrick, Monica T. Hinds,
Kenton W. Gregory

4.1 Abstract

This work focuses on the development of a method to derive two-dimensional constitutive equations for vascular biomaterial tubular constructs. The testing method is modified from standard burst testing systems and can be affordably implemented by most laboratories not equipped with biaxial testing systems. The vascular constructs are modeled as cylindrical tubes and can be tested in their tubular form, which ultimately simplifies analysis by maintaining a physiologically relevant coordinate system. Strain energy density functions are developed via this testing scheme. The proposed model was verified by testing extracted elastin tubular constructs using this system to define a strain energy density function for this material. The strain energy function for extracted elastin was derived and took the form:

$$\rho_o W = AE_{\theta\theta}^2 + BE_{\theta\theta}E_{zz} + CE_{zz}^2 + DE_{\theta\theta}^3 + EE_{\theta\theta}^2E_{zz} + FE_{\theta\theta}E_{zz}^2 + GE_{zz}^3 \text{ where } A=1.92e5, \\ B=1.43e6, C=4.73e6, D=-1.38e5, E=-2.77e7, F=1.12e7, \text{ and } G=-2.77e7.$$

Ultimately, the proposed method could be used as a tool for evaluating a myriad of vascular graft designs, thus, giving researchers an additional method for making comparisons between biomaterial designs.

4.2 Chapter Overview

In Chapters 2 and 3, novel biomaterials were developed and characterized for their structural, cell compatibility, and mechanical properties. This chapter describes a method for evaluating the biaxial mechanical properties of vascular graft materials that can be applied to the materials developed in Chapters 2 and 3. This model provides a method for developing strain energy density functions for tubular biomaterials tested in their final configuration with a modified burst pressure system. This can be particularly valuable when there is a limited supply of a biomaterial, because multiple mechanical properties can be assessed for each test sample.

4.3 Introduction

The development of vascular grafts is a major focus area for many research groups [4, 41, 42, 53, 55, 117, 119, 191, 197, 198]. As more of these grafts are developed they are getting more sophisticated in their design with sometimes only subtle differences between them. An additional tool for analyzing their mechanical properties can be instituted to enable meaningful comparisons between constructs. This paper will propose and outline a protocol for testing and subsequent analysis by which other vascular grafts can be evaluated.

This is not a simple proposition when the complexity and variability of the types of constructs in development are considered. Constructs take many forms such as amorphous collagen gels, fibrous protein conformations with highly variable fiber orientations, and multi-layered composite materials [197, 199-204]. These are also formed from naturally occurring proteins such as elastin, collagen [57, 113, 115, 116, 125, 205], and proteoglycans, as well as synthetic materials such as Dacron and Gore-Tex [206, 207]. Both the natural and synthetic materials vary greatly in their physical composition. They vary in their dimensions, radius and thickness, as well as their physical properties, such as mechanical properties, porosity and permeability. This proposed unification of testing schemes is reasonable, because the final proposed use and configuration, i.e. tubes, is consistent between constructs. Though they vary in their specific dimensions, they can all be modeled as cylinders. The final unifying parameter is that all of these constructs follow and can be analyzed via Newtonian mechanics.

Raymond Vito and Michael Sacks have outlined the importance of and considerations required for blood vessel constitutive equations and multiaxial mechanical behavior of biological materials in their review articles, respectively [208, 209]. Vito summarizes model assumptions and derivations required for blood vessel modeling. These factors must be considered in this development. First, the issue heterogeneity vs homogeneity must be determined. Most vascular grafts are heterogeneous. The walls are comprised of combinations of cells, elastin, and collagen. The distribution and orientation of the vessel components changes through the thickness of the wall. It is known that the orientation of the protein fibers are also load dependent. Though this is true, the following model will

be considered homogeneous. This implies that the macroscopic response is described by locally averaging properties. The second consideration is the incompressibility of the material. This assumption requires that the wall volume of the material is conserved during deformation. This assumption is reasonable due to the large percent of water in the materials, which remains incompressible within the loading ranges. The consequence of this assumption is that the determinant of the deformation vector \mathbf{F} is equal to 1. The deformation vector is defined in Equation 4.1 and the affect on the stretch ratios is given in Equation 4.2 where x is the reference state and X is the deformed state for a generic coordinate system. Direct tensor notation will be used in this text. Bold characters indicate vectors and normal text refers to scalars.

Equation 4.1: Deformation vector

$$\mathbf{F} = \begin{bmatrix} \frac{\partial x_1}{\partial X_1} & \frac{\partial x_1}{\partial X_2} & \frac{\partial x_1}{\partial X_3} \\ \frac{\partial x_2}{\partial X_1} & \frac{\partial x_2}{\partial X_2} & \frac{\partial x_2}{\partial X_3} \\ \frac{\partial x_3}{\partial X_1} & \frac{\partial x_3}{\partial X_2} & \frac{\partial x_3}{\partial X_3} \end{bmatrix}$$

Equation 4.2: Stretch Ratio for an incompressible material

$$\lambda_1 \lambda_2 \lambda_3 = 1$$

Uniaxial mechanical testing is important in analyzing the material properties of a homogeneous material but can be limiting when bulk fiber orientation is complex and uncharacterized. Uniaxial testing does not account for the contribution of deformation changes in the untested orientations on the derived material properties. The tissue being tested is a three-dimensional body and should be tested as such. Biaxial testing solves

many of these problems by accounting for the stress/strain state in two loading orientations, but many labs developing tissue constructs are not equipped to run biaxial tests. Labs that are equipped with biaxial testers are still faced with challenging issues involved with determining fiber orientation and an appropriate coordinate system orientation. Therefore, a readily actualizable testing scheme can be considered.

Burst pressure testing is a standard method implemented to evaluate vascular constructs. This is a powerful and simple testing approach providing the ultimate failure stress of the construct. These data can be used for comparing designs to each other and to native arteries. However, most researchers simply report the final burst pressure value in mmHg and forgo thorough stress tensor analysis. This makes analysis of and comparisons between construct materials impossible. The thickness of the material has a direct affect on burst pressure and is usually reported, but the circumferential dimensional changes are usually not tracked which is necessary for tracking and defining the stress state of the material.

Failure stress or burst pressure is not the only parameter of interest when evaluating vascular grafts. It has been postulated that matching the elastic modulus of the material to that of the native modulus leads to the ultimate success or failure of a graft [147, 152, 210]. The elastic modulus is not evaluated with standard burst pressure methods. A standard burst pressure test is performed by occluding one end of the vessel and rapidly increasing internal pressure of the vessel with compressed gas or liquid from the open end while measuring internal pressure until failure. The loading rates are normally not accounted for nor are the changes in the vessel's dimensions. Burst testing is valuable

and gives researches a tool for determining maximum failure pressures, but further testing analysis should be implemented to derive constitutive equations and consequently the two-dimensional material properties of construct designs.

A simple modification of a burst pressure testing system can be made to account for both loading rates and dimensional changes. These methods will be explored along with the appropriate analysis techniques in this paper. This apparatus can be used in both simple loading and dynamic modes.

4.4 Methods

Graft constructs are modeled as cylinders in this analysis. A cylindrical coordinates system will be used in the vessel testing analysis. The cylindrical coordinate system is defined in terms of z , θ , and r , correlating to the longitudinal, circumferential and radial directions respectively (Figure 4.1).

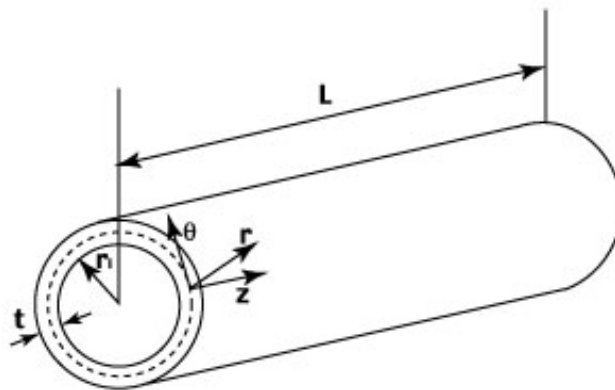


Figure 4.1. Graphical representation of the coordinate system used for this model. A cylindrical coordinate system was used. r is the radius, z is the axial or longitudinal displacement along the length, t is the wall thickness, and θ is the circumferential orientation of the cylinder.

4.4.1 Model Development

The vascular graft can be modeled as a membrane, which can be considered a two dimensional continuum. The cylindrical polar coordinate system can be seen in Figure 4.1. Axes are defined as r , θ , and z relating to the radial, circumferential and longitudinal/axial directions respectively. The stretch ratios for the circumferential and longitudinal directions are defined by Equation 4.3 and Equation 4.4, respectively. The stretch ratios (λ_i) are defined in terms of the initial dimensions. Thus, careful measurements are required of the initial dimensions. L_z and r_i , longitudinal length and inner radius, are measured test variables. The following model was developed based on Fung's treatment of constitutive modeling of pseudo-elastic materials [211].

Equation 4.3: Longitudinal Stretch Ratio

$$\lambda_z = \frac{L_z}{L_{z0}}$$

Equation 4.4: Circumferential Stretch Ratio

$$\lambda_\theta = \frac{r_i}{r_{i0}}$$

Stains are derived in terms of Green's Strain (E_{ij}) and are defined by Equation 4.5 and Equation 4.6.

Equation 4.5: Longitudinal Green's Strain

$$E_{zz} = \frac{1}{2}(\lambda_z^2 - 1)$$

Equation 4.6: Circumferential Green's Strain

$$E_{\theta\theta} = \frac{1}{2}(\lambda_\theta^2 - 1)$$

Strain values are calculated from dimensional measurements taken during the test.

Kirchhoff stresses are conjugate to Green strains and can therefore be used to develop the constitutive model formulation. The strain energy density function is defined in Equation 4.7. A polynomial function was chosen for this model, but an exponential function defined in Equation 4.8 can also be chosen due to the large strain/stress values applied to the vascular graft while taking it to failure. The tissue or material type will be the ultimate determining factor when determining the most appropriate curve fit. This is simply an example of one possible fitting regimen. A nonlinear least squares fitting algorithm such as a modified Marquarts's algorithm should be used to attain the strain energy density function constants [212].

Equation 4.7: Longitudinal Strain Energy Density Function

$$\rho_o W = AE_{\theta\theta}^2 + BE_{\theta\theta}E_{zz} + CE_{zz}^2 + DE_{\theta\theta}^3 + EE_{\theta\theta}^2E_{zz} + FE_{\theta\theta}E_{zz}^2 + GE_{zz}^3$$

Equation 4.8: Exponential Strain Energy Density Function

$$\rho_o W = \frac{C}{2}(e^{\varrho} - 1)$$

The equation used for will vary with different materials. The value of the constants relate to the elastic modulus of the material. The tissue/material of interest will dictate the most appropriate form of the function. The value of C in the exponential function is a constant and relates to the elastic modulus of the material. Q is a function that is specific to the material of interest. One proposed form for Q is given in Equation 4.9.

Equation 4.9: Material Function

$$Q = a_1 E_{\theta\theta}^2 + a_2 E_{zz}^2 + 2a_4 E_{\theta\theta} E_{zz}$$

The stress tensors can now easily be derived from the strain energy density function and the strain values for the graft material. Kirchhoff stresses (S_{ij}) are used in this model. $\rho_0 W$ is the strain energy density function and are given in Equations 4.10 and 4.11.

Equation 4.10: Circumferential Kirchhoff Stress

$$S_{\theta\theta} = \frac{\delta(\rho_0 W)}{\delta E_{\theta\theta}}$$

Equation 4.11: Longitudinal Kirchhoff Stress

$$S_{zz} = \frac{\delta(\rho_0 W)}{\delta E_{zz}}$$

Kirchhoff stresses can be derived from the Cauchy stresses. The equation forms are given in Equation 4.12 and Equation 4.13. Circumferential ($\sigma_{\theta\theta}$) and longitudinal stresses (σ_{zz}) are considered to be uniformly distributed in the test region.

Equation 4.12: Circumferential Kirchhoff to Cauchy Stress Conversion

$$S_{\theta\theta} = \sigma_{\theta\theta} \lambda_{\theta}$$

Equation 4.13: Longitudinal Kirchhoff to Cauchy Stress Conversion

$$S_{zz} = \sigma_{zz} \lambda_z$$

Average Cauchy stress values can be derived directly from the pressure diameter values acquired during the burst test. These calculations are given in Equation 4.14 and Equation 4.15, where P_o is the pressure outside the vessel, P_i is the internal vessel pressure, r_i is the inner radius, r_o is the outer radius, and t is the wall thickness, and F is the applied axial force. P_o is assumed to be zero in all testing conditions.

Equation 4.14: Circumferential Cauchy Stress

$$\sigma_{\theta\theta} = \frac{P_o r_o - P_i r_i}{t} = -\frac{P_i r_i}{t}$$

Equation 4.15: Longitudinal Cauchy Stress

$$\sigma_{zz} = \frac{F + P_i \pi r_i^2 - P_o \pi r_o^2}{\pi(r_o^2 - r_i^2)} = \frac{F + P_i r_i^2}{\pi r_o^2}$$

4.4.2 Model Verification

Extracted porcine elastin vessels were prepared from native carotid arteries with a hot alkali digestion method [167] to remove all endogenous cellular and protein components leaving a purely elastin structured matrix. These vessels were used as the test material for this system. This material was chosen because of its viscoelastic properties, it undergoes large dimensional changes during testing, has a complex fibrous structure, and is a major component of the normal vessel architecture. The test setup used a custom built stage to hold the test specimen (Figure 4.2). Vessels were cannulated to barbed tube connectors with umbilical tape suture for making connections to inlet tubing. The constructs were coupled to the stage by the barbed connectors to minimize loading effects

form the stage. The stage was equipped with motorized linear displacement control, which enabled fine control and measurement of axial displacement. A 150 gram force transducer was mounted at the fixed end of the mandrel to measure axial force. An inline pressure transducer was coupled to the flow loop to measure internal construct pressure (Figure 4.2). Measured parameters were acquired and recorded with a data acquisition system and a custom LabVIEW control program (National Instruments).

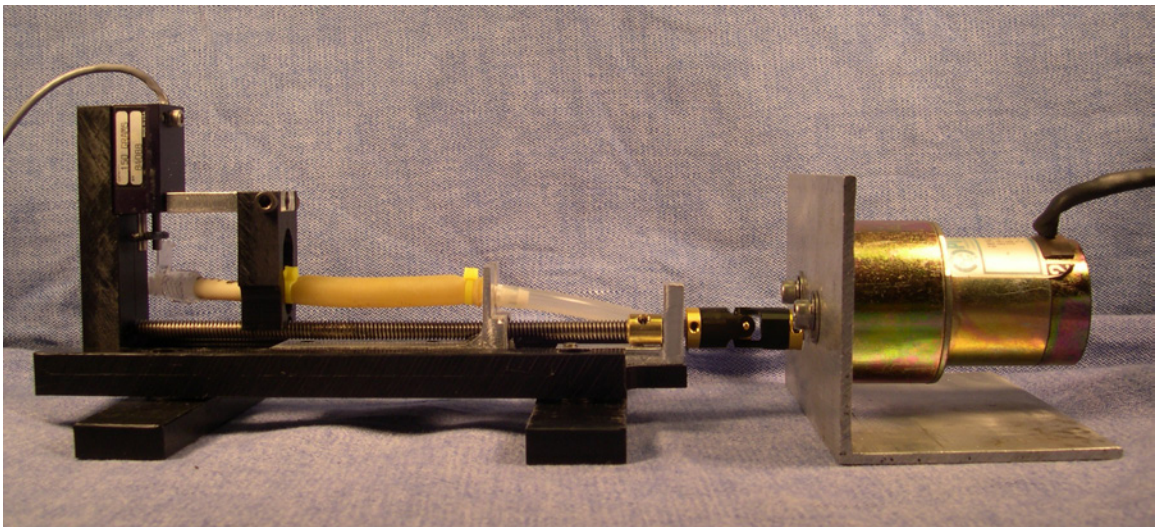


Figure 4.2. Biaxial testing device. A linear force transducer is coupled to the fixed end of the vessel (left hand side of this figure). The displacement is controlled with a motor and a linear slide on a custom built testing platform (right hand side of this figure).

A syringe pump was used to control internal hydraulic pressure. P_0 is zero in all test conditions. Circumferential strains were dynamically measured non-invasively with a video dimension analyzer (VDA), which used contrast changes between the vessel wall and a black background to dynamically track outer diameter (Figure 4.3). This system does not require the placement of markers on the tissue surface as is commonly done with biaxial tests. The output was converted to a voltage and was read into a data acquisition

system for recording and subsequent analysis. If a VDA is not available software packages can use video images to extract vessel dimensions. The test specimens were kept in a temperature controlled buffered saline bath at 37°C. and the pH of the solution was maintained at 7.4.

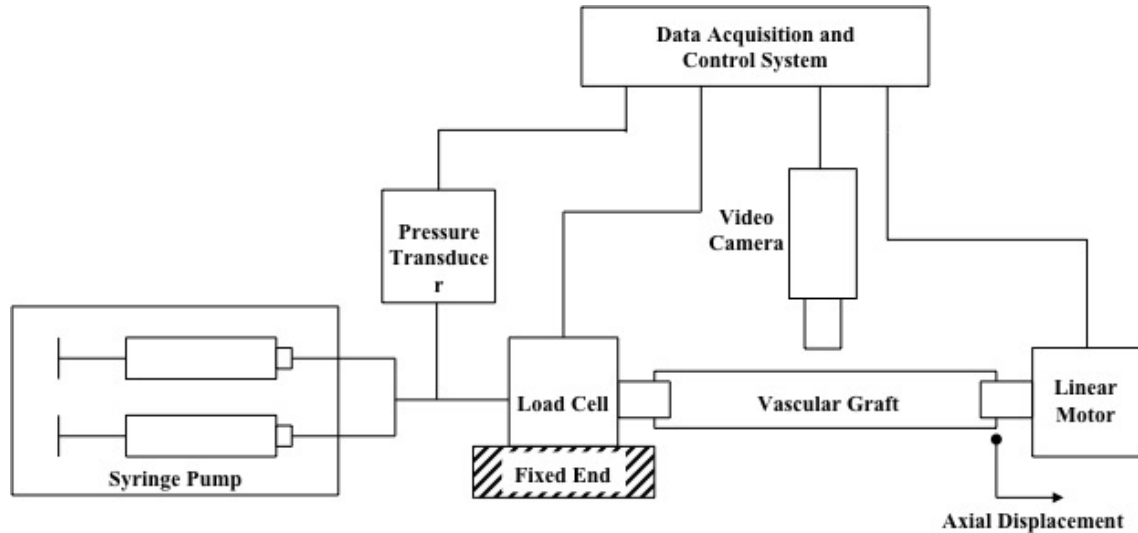


Figure 4.3. Schematic of testing apparatus

Test specimen constructs were modeled as cylinders with z , θ , and r , correlating to the longitudinal, circumferential and radial directions, respectively.

Three testing methods are possible. First, the longitudinal stretch ratio can be fixed at physiologic values, between 1.4 and 1.6, which is the standard range for native vessels. Once the longitudinal stretch ratio is set, the transmural pressure of the vessel can be increased to failure. The second testing method holds the transmural pressure at zero, relative to atmospheric/gage pressure, while varying the longitudinal displacement. Independent constitutive equations can be derived from these data. To fully understand

the material in the physiological ranges several conditions should be tested to attain a map or surface strain energy density function for the material. The third method varies both longitudinal and circumferential displacement simultaneously. This allows for a complete analysis of circumferential and longitudinal strains and subsequent derivation of stress states and constitutive models.

The third testing method was applied to extracted porcine elastin vascular constructs (n=6). The longitudinal extension rate was 1 mm/sec and the infusion rate was 40 mL/min. Equation 4.7 was used for the fitting algorithm. A custom MatLAB program (Appendix B) was developed to evaluate the acquired data and derive the strain energy density function.

4.5 Results

Extracted porcine elastin tubes were tested by varying both longitudinal and circumferential displacement simultaneously to attain stress strain relationships for both orientations simultaneously. Samples were tested to failure. Pressure and axial force measurements were converted to stress and measured displacements were converted to the corresponding strain values (Figure 4.4).

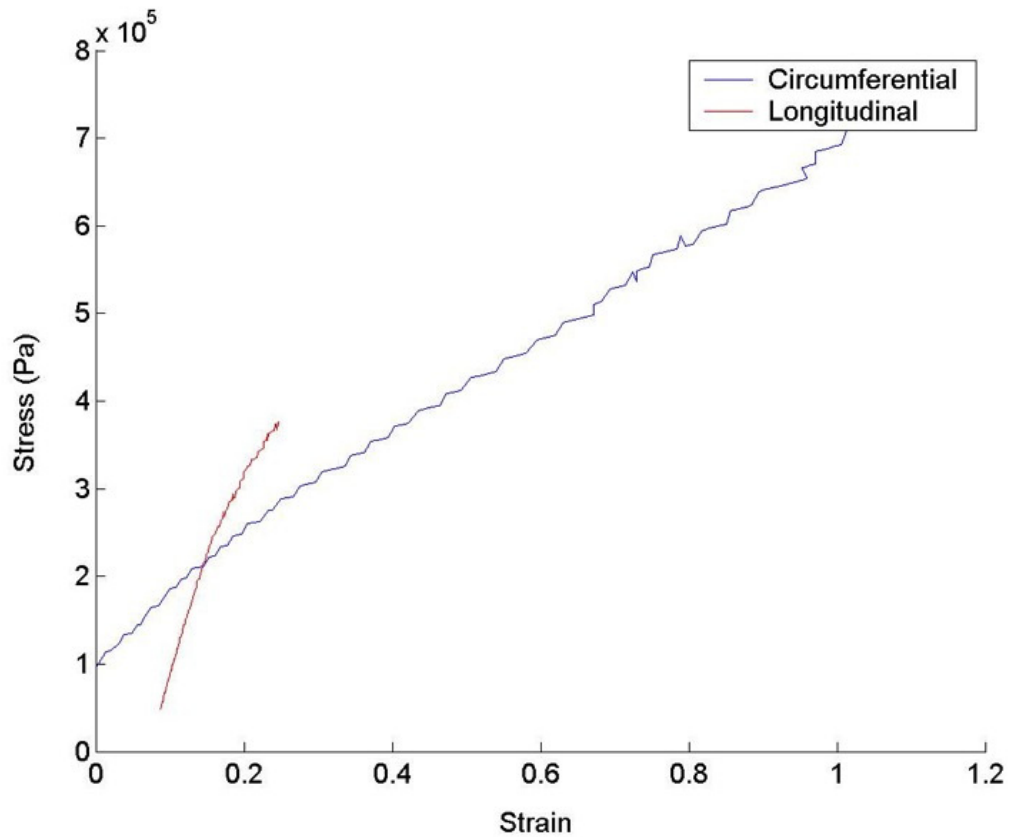


Figure 4.4. Stress strain plot for an extracted elastin graft for the circumferential and longitudinal orientations.

The stress-strain data was then fit to Equation 4.7 for deriving a strain energy density function for the material (Figure 4.5). A polynomial curve fit was used to define the function with low residuals. The constants for the curve fit were defined as $A=1.92e5$, $B=1.43e6$, $C=4.73e6$, $D=-1.38e5$, $E=-2.77e7$, $F=1.12e7$, and $G=-2.77e7$.

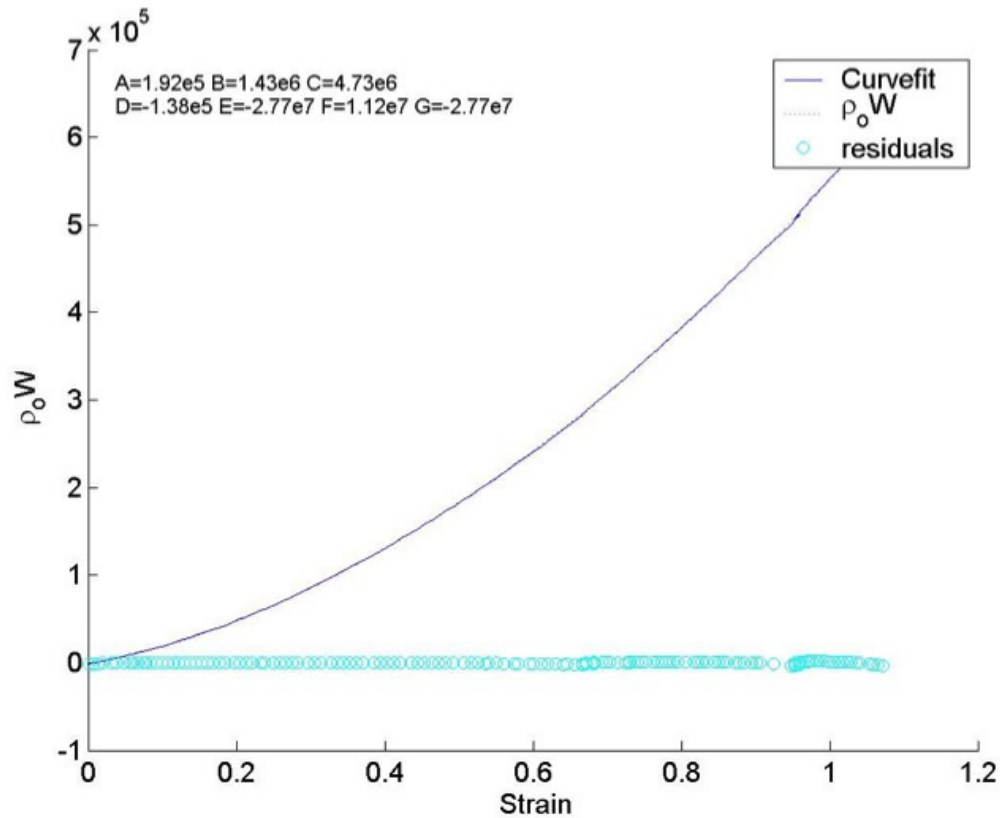


Figure 4.5. Polynomial curve fit for the strain energy density function.

4.6 Discussion

Mechanical properties of bioengineered vascular grafts are extensively studied. These studies have implemented a variety of methods from uniaxial testing, biaxial testing, biaxial testing including shear deformation, and modified burst pressure tests [213]. Burst pressure is an important parameter to define for any vascular graft construct. The ultimate failure pressure is a key indicator for a graft design to progress to *in vivo* testing. This scheme allows for acquisition of this parameter as well as additional load/deformation data. Burst pressure can change significantly with changes in axial loading and changes in wall thickness. This system considers these variables within the model. This system is also important if the material to be tested is scarce in quantity.

The mechanics of the material are acquired with the same test sample that would be used for burst pressure testing, thus eliminating the need for a separate test specimen for uniaxial/biaxial tensile testing.

This survey describes a simple modification of a burst testing apparatus and subsequent analysis for developing two-dimensional constitutive models for describing tubular vascular graft constructs. This model can be expanded to three dimensions when shear and bending forces are assumed to be zero. This application is easily employed and can be built inexpensively in most laboratories. Valuable comparisons could be made between construct designs if this method is utilized.

Careful considerations of the model assumptions must be made. The first is that the constructs can be modeled as a two-dimensional membrane continuum and as a cylinder. We know that there are factors to consider when making these assumptions. The first is that in order to perform these tests the ends of the construct must be cannulated to rigid tubes. This constrains the ends and causes stress concentrations and end effects. As the pressure inside the construct is increased the ends of the cylinder are constrained while the center of the tube expands. This results in the bulging of the cylinder. The equations described above assume that the cylinder is uniformly changing dimensions throughout the construct. In this situation r is a function of z , which is not considered in this analysis. This phenomenon can be ignored if the dimensional evaluations and measurements are made sufficiently far from the ends. The video image should be

focused on the central region of the vessel. Also, if the failure mode is deemed to be caused by or initiated from the ends the failure data should not be included.

Another assumption that could invalidate the analysis is the zero bend and zero shear stress assumption. These assumptions will generally hold true throughout the experiment. However, if there is not a sufficient longitudinal stretch applied to the construct the applied pressure will cause significant length changes in the axial direction. Since these vessels are constrained axially the vessels are unable to expand and thus, may result in bending or buckling of the material. This breaks basic assumptions and invalidates the model developed and data acquired under these conditions should not be used for the model development.

The strain energy density functions derived from these experiments describe the behavior of the material along a single line of a more complex surface. The surface gives a complete representation of the strain energy density surface function. Several lines along this surface should be determined and plotted to get a representation of this function throughout physiologic ranges and thus define a portion of the strain energy density surface.

The meaning of the strain energy density function constants is hard to define. They can change drastically do to small variations in the shape of the curve. The value of C is a representation of the elastic modulus. The constants A-G can be thought of as scalars for the modulus.

4.7 Conclusion

This work described a basic method for using a modified burst pressure testing system to measure and derive a strain energy density functions for vascular constructs. Extracted porcine elastin was tested and analyzed with this system and a strain energy density function defined. This scheme gives researchers an affordable and easily implementable tool for the testing of any tubular biomaterial constructs. Ultimately, the goal of this work was to provide a means by which researchers can acquire and meaningfully comparative mechanical properties for tubular designs.

Chapter 5: Comparison of effect of protein surface on thrombotic and inflammatory responses with comparative *in vitro*, acute *ex vivo* shunt, and chronic *in vivo* studies

Kathryn A. McKenna, Deirdre Anderson, Ulla Marzec, Howard Song, Stephen R. Hanson, and Monica T. Hinds

5.1 Abstract

There is a significant clinical need for viable small-diameter vascular grafts. There are many vascular graft biomaterials in development, but relatively few have been clinically successful. Evaluation of graft failure mechanisms in relevant primate models with a greater understanding of the factors that lead to *in vivo* success is necessary to push vascular graft development. We evaluated different extracellular matrix (ECM) proteins effect on thrombotic and inflammatory responses of endothelial outgrowth cells (EOCs). These responses were tested in two-dimensional flat plate studies and then moved to three-dimensional ePTFE graft studies in *ex vivo* shunt and *in vivo* implant test systems with corresponding *in vitro* controls. EOCs were evaluated for their functional phenotype on adsorbed coatings of type I and IV collagens, fibronectin, and α -elastin for flat plate studies and type I collagen and fibronectin for ePTFE *ex vivo* shunt graft studies and type I collagen for *in vivo* graft implants. Functional responses were evaluated with changes in gene expression at 48 hours for coagulation and inflammatory gene panels and also through activated protein C (APC) and factor Xa activity assays. The EOCs attached and proliferated more readily on type I collagen and fibronectin surfaces than on type IV

collagen and α -elastin as determined by total DNA. Two-dimensional studies showed significant differences in gene expression of endothelial protein C receptor (EPCR) between type I collagen and α -elastin and CD39 between type I collagen and α -elastin, and type IV collagen and α -elastin. The majority of the gene panel showed no significant differences. The activity of APC was dependent on surface coating with type I collagen (164 ± 20 ng/mL) and FN (164 ± 14 ng/mL) displaying a higher activity than both type IV collagen (61 ± 22 ng/mL) and α -elastin (61 ± 15 ng/mL). Factor Xa activity was independent of surface coating. Three-dimensional ePTFE graft studies showed differences between type I collagen and fibronectin for tissue factor pathway inhibitor (TFPI) and VCAM. Platelet adhesion and activity assays were not significantly different between substrates. There was no difference between EOC-seeded collagen modified ePTFE grafts and untreated controls in the implant studies. There were differences noted between implant animals. There was a distinct linear correlation between the number of adhered platelets in the *ex vivo* shunt and the *in vitro* control's factor Xa functional activity due to tissue factor without the influence of TFPI. Thus, the hemostatic phenotype of the EOCs displayed some differences between substrates, but were largely independent of the ECM surface coating. The importance of tissue factor (TF), through factor Xa generation, in determining *ex vivo* outcomes was demonstrated and could be used as a predictor for *in vivo* success.

5.2 Chapter Overview

Chapters 2 and 3 described novel biomaterials for vascular graft applications. Chapter 5 focuses on how individual ECM components affect thrombosis and inflammation using a

clinically relevant ePTFE synthetic graft model. Grafts are modified with ECM proteins and evaluated in *in vitro*, acute *ex vivo* shunt, and chronic *in vivo* test systems. This study demonstrates the importance of tissue factor evaluated with a factor Xa activity assay in the acute *ex vivo* thrombotic response. These studies can be used to drive the development of the materials developed in Chapters 2 and 3. Understanding how the ECM influences grafts success/failure is important in developing natural protein-based graft constructs and was pursued while further graft development of tropoelastin biomaterials was conducted to enable their *in vivo* testing.

5.3 Introduction

Heart disease remains the number one cause of morbidity and mortality in the Western world. In 2006, nearly 81 million people were affected by cardiovascular disease in the United States [1]. This has a significant effect on the health care system with total direct and indirect costs totaling 503.2 billion dollars, for 2010 in the United States, treating heart disease [1]. Treatments using vascular grafts have not significantly changed in 30 years, with mammary artery and saphenous vein autografts as the gold standard treatment for bypass surgery. Synthetic materials, such as expanded poly(tetrafluoroethylene) (ePTFE) and poly(ethylene terephthalate) (PET or Dacron[®]), have been successfully used for large diameter vessels, but are not appropriate for small diameter vessels under 6 millimeters.

The two main determinants of vascular graft success have been the thrombogenic and intimal hyperplasia potential of the construct. The primary failure modes for prosthetic

grafts are thrombosis in the central region of the graft, typically because of the lack of endothelium, and intimal hyperplasia at the graft anastomosis. Intimal hyperplasia requires a connection to the tissue which is the reason it is only present at the anastomotic regions [62]. Early graft occlusion is primarily influenced by thrombosis with intimal hyperplasia affecting long-term results. The thrombogenic potential of a graft construct is modulated by many variables. Considerable efforts have been made to develop a synthetic graft with favorable blood contacting properties [63]. The main strategy to develop a compatible synthetic surface involves the modification of its interface properties. Strategies have included protein coatings such as collagen [64], heparin incorporation [65-68], anti-platelet factor incorporation [69-75], electrical surface charge modification, surface wettability, and graft endothelialization [63].

Endothelialization as a surface modification strategy is the most promising for graft protection, because this does not simply mimic isolated functions of the endothelium rather it inherently provides the endothelium's regulatory functions. Endothelial cells (ECs) are potent regulators of thrombosis. They regulate the thrombotic response through three distinct yet interrelated systems. The coagulation cascade is managed through receptors on the EC surface, the complement cascade regulates fibrinolysis and vascular tone, and cells in the blood such as leukocytes and platelets communicate to repair vascular injury [76] but can also respond to vascular graft materials as a perceived injury site thus initiating a thrombotic response. The conditions under which ECs are cultured can push the response towards pro or anti-thrombotic pathways. Many strategies have been used to promote EC attachment to synthetic surfaces. The first attempt to seed

synthetic grafts with endothelial cells was done in 1980 [77]. These studies with canine ECs showed promising results, but have not translated to human studies. ECs do not readily attach to hydrophobic ePTFE grafts. The surface must be modified to make it “sticky” for the cells. Methods of changing the microenvironment of the surface have included antibody and peptide sequence cell capture methods, protein adsorption and growth factor incorporation. Non-primate models have had reendothelialization rates of 0.1 mm per week in a rat aorta model [78], but primate models have proven more challenging as there is a limit to their ability to self-endothelialize with a limit of 1-2 cm from the anastomosis [62, 79].

Endothelial outgrowth cells (EOCs) have been considered a promising source of autologous endothelial cells because they can be readily isolated from whole blood and rapidly expanded *in vitro*. EOCs were identified in 1997 [85] and the isolation from peripheral blood first described in 2000 [86]. Other potential autologous cell sources are omental and subcutaneous fat, bone marrow, veins, and arteries [87]. While these sources yield viable ECs, they also require more invasive surgical procedures for isolation. Peripheral blood EOC isolation requires a simple venipuncture removing a relatively small volume of blood (40mL). Additionally, EOCs are increasingly recognized to play important roles in hemostasis, angiogenesis, and arterial injury repair [88-90]. They are also promising as a potential autologous cell source for tissue engineered vascular grafts [83, 84]. This cell population has been shown to stain positive for typical EC markers of vWF, CD31, VE-cadherin, VEGF-R2, Thrombomodulin (TM), and E-selectin, as well as reduced eNOS expression [91].

The extracellular matrix (ECM) is the primary support for the vascular endothelium [9]. The main functions are adhesive interactions between integrins of endothelial cells and the matrix, which provides the organization of the EC monolayer [10]. The functions of ECs influenced by the ECM are complex and are regulated through multiple signaling pathways controlling apoptosis, proliferation, cell shape, and contractility [9]. Basement membrane proteins are spatially and temporally regulated during angiogenesis *in vivo*, and influence cell proliferation *in vitro*. While the stable basement membrane may provide anti-proliferative cues (laminin), provisional matrix proteins (collagens and fibronectin) may signal proliferation and the formation of new blood vessels [9]. Treatments of conventional ePTFE grafts with ECM components (including fibronectin, collagen, and laminin) typically increase mature endothelial cell adhesion and retention.

In this study, the haemostatic activity of EOCs on protein modified two- and three-dimensional surfaces was investigated. The effect of the ECM on EOCs hemostatic properties is just starting to be characterized. It can be postulated that their response will be similar to mature ECs, but that remains to be proven. Initial studies have been done investigating EOCs regulation of the inflammatory and coagulation pathways and their ability to be regulated by shear stress. EOCs respond to stimulation by tumor necrosis factor α (TNF α) with increased expression of IL-6, IL-8, MCP-1, ICAM1, and TF, and downregulate inflammatory and coagulatory responses upon the application of shear stress [214]. TNF α treated EOCs upregulate TF, which initiates factor VII/VIIa-dependent thrombin generation, but did not significantly alter the non-procoagulant

functions such as migration, proliferation, and tube formation [215]. Shear stress without TNF α stimulation has also been shown to upregulate gene and protein expression of anticoagulant and platelet inhibitory factors and demonstrated a significant functional change with an increased activated protein C level [216].

Our aim was to use a simple vascular graft model, based on Peter Zilla's work with endothelialized ePTFE grafts [204, 217], in which we coat 4 mm diameter ePTFE grafts with a ECM protein matrix and endothelialized the luminal surface with EOCs. This is the first reported evaluation of EOCs on ePTFE vascular grafts. The aim was not to produce an optimized vascular graft, but rather to use this as a model with variations in protein coatings to induce significant changes in *in vitro*, *ex vivo* and *in vivo* responses, thus we can better define how the ECM proteins affect the EOCs thrombotic potential, to ultimately understand which factors are important for *in vivo* clinical success.

5.4 Methods

5.4.1 Endothelial Outgrowth Cell Isolation

Baboon peripheral blood, was collected with a 1 to 7 dilution of acid citrate dextrose (ACD) to blood for anticoagulation. Tubes were mixed gently several times and transported to the cell culture facility. Anticoagulated blood was diluted with HBSS (1:1) at room temperature and gently mixed. The blood/HBSS mixture was layered onto Histopaque® 1077, avoiding any mixing of the layers at the interface. Samples were spun at 800g for 30 minutes, which separated the mixture into four distinct layers. The MNC layer was removed from each tube and collected. The MNCs were then diluted (1:1) with HBSS and mixed well. The MNC cells/HBSS mixture was then centrifuged

for 10 minutes at 400g. The supernatant was removed and the cells washed with 10mL of HBSS. The samples were then spun at 250g for 10 minutes. Cells were then washed a second time with 10 mL of HBSS and pelleted at 250g for 10 minutes. A cell count was performed and cells were resuspended in EGM-2 media supplemented with 20% FBS. 12-well plates coated with 5 $\mu\text{g}/\text{cm}^2$ bovine serum fibronectin (FN) (Sigma) for 1 hour at room temperature were seeded with 12-18 x 10⁶ cells per well. Cell cultures were maintained using standard techniques in a 5% CO₂/37 °C incubator. Media was changed every day using EGM-2 supplemented with 20% FBS for the first 2 weeks and every other day thereafter. Cultures were maintained until outgrowth colonies developed. Cells were then passaged and expanded on FN coated tissue culture flasks. Cells were expanded to passage 3. Passage 2 and 3 cells were frozen and stored in liquid nitrogen for experimental use.

5.4.2 Graft Construction

Grafts were constructed such that they could be used for *in vitro*, *ex vivo* shunt, and *in vivo* implant studies. Small diameter, 4mm, thin walled, non-ringed ePTFE vascular grafts (Gore[®]) were cut to 7 cm in length. The last 0.5 cm of length on both ends were coated with silicone (Si) glue. A 4.5 mm diameter thrombectomy probe was inserted into the graft leaving the last 0.5 cm open. The end of the graft was then filled with Si glue and the thrombectomy probe extracted leaving a thin layer of glue pushed into the inner surface of the graft which was then air-dried overnight. Grafts were then threaded onto 4 mm diameter and 8 cm long Teflon rods. Silicone tubing cut to 1 cm in length and opened longitudinally were secured with Si glue to the ends of the grafts to create cuffs.

Cuffed ends were then air dried overnight. The ends of each graft were trimmed at a right angle with a Teflon coated blade (Electron Microscopy Sciences). Rods were removed and new 33 cm rods were threaded into the cuffed grafts. Si tubing, 4 mm ID, was cut to 15 and 20 cm lengths for the distal and proximal connections respectively. The 15 cm Si tubing was fully threaded onto the rod positioned 1 cm from the end. The graft was then positioned adjacent to the distal Si tubing and the first 4 cm of the proximal Si tubing threaded onto the remainder of the rod. A bead of Si glue was added between each junction and the ends of the grafts pushed flush with the ends of the Si tubing. Additional glue was then added to the outer surface of the junctions and FEP heat shrink tubing cut to 1.5 cm in length was centered over the junction and gently shrunk with a heat gun.

5.4.3 Graft Coating

Grafts were impregnated with either bovine fibronectin (Sigma) or type I collagen (MP Biomedicals). All coating solutions were introduced from the distal end of the graft and not permitted to enter the proximal Si tubing. The ePTFE graft surface was first permeabilized by infusing 95% ethanol through the pores of the graft to wet the graft surface. Ethanol was then replaced with water and further rinsed with PBS for fibronectin coatings and 0.02 N acetic acid in H₂O for type I collagen modified grafts. Protein solutions of 4 mg/mL type I bovine collagen or 1 mg/mL bovine fibronectin were immediately pushed through the pores of the ePTFE until the outer surface was completely saturated with solution. The distal end of the Si tubing was then rinsed three times with PBS for fibronectin or 0.02 N acetic acid in H₂O for type I collagen.

5.4.4 EOC Flat Plate Culture

EOCs were plated on non-tissue culture treated polystyrene 96-well plates and 35 mm dishes coated with 5 $\mu\text{g}/\text{cm}^2$ of type I collagen, type IV collagen, fibronectin, or α -elastin. Cells (3×10^5) were plated and conditioned in 10% EGM-2 media for 24 hours followed by 24 hours in 15% Hyskon (dextran/dextrose) flow media (EBM media, 5% FBS, 1% PSF, 1% L-glut, and EGF).

5.4.5 EOC Seeding on Protein Modified ePTFE Conduits

EOCs were seeded onto ePTFE grafts modified with either type I collagen or fibronectin. Grafts are seeded with EOCs in a three-step process. EOCs were gently removed from flasks using TrypLE Express (Invitrogen). Cells were resuspended in EGM-2 media at a concentration of 3×10^5 cells/mL. Grafts were rehydrated in EGM-2 media for 30 minutes prior to introducing cells. Cells were introduced to the graft from the distal tubing and the solution advanced to the proximal end of the graft. The proximal tubing is not exposed to the cell seeding solution or growth media throughout the conditioning phases. Three separate inoculations of 3×10^5 cells/mL at 40-minute intervals were added to the graft lumens. The biochambers were rotated 120° prior to the 2nd and 3rd inoculations to ensure an even and confluent cell distribution around the circumference of the graft.

5.4.6 Platelet Aggregation

Platelet aggregation times and percent clearance for type I collagen, α -elastin, and fibronectin were determined and compared to a standard fibrillar type I collagen solution (Chronolog). Platelet rich and platelet poor plasma was isolated from baboon blood for this assay. The protein to be tested was added to the platelet rich plasma at various concentrations between 20 and 800 $\mu\text{g/mL}$. A dual aggregometer (Chronolog Corp) was used to measure the clearance time to attain a response plateau. The response is driven by platelets activating and dropping out of suspension in response to the tested protein. Percent clearance relates to the opacity of the solution as compared to platelet poor plasma. Aggregation response times and percent clearance were then compared between samples.

5.4.7 Gene Expression

RNA was isolated using the Mini RNA I Isolation Kit™ (Zymo Research) for flat plate studies and the Qigen kit (Qigen) for graft studies. RNA was treated with DNase I (Fermentas) and converted to cDNA using SuperScript® III Reverse Transcriptase (Invitrogen). Gene expression was measured using quantitative real-time PCR. In house designed primers (Appendix C) were used with Platinum® SYBR® Green and ROX reference dye (Invitrogen) to attain amplification curves. Ct values for each gene were subtracted from the housekeeping gene's GAPDH Ct to get dCt. The coagulation gene panel included TM, TF, EPCR, CD39, and TFPI and the inflammatory gene panel included ICAM, VCAM, PECAM and eNOS.

5.4.8 APC Functional Assay

EOCs were rinsed and incubated for 1 hr with a 5nM thrombin and 100nM protein C (Haematologic Technologies) in PBS with cations. Repludan (Berlex) was added after incubation to inhibit thrombin. Samples were visualized with 1mM S-2366 (Chromogenix) and compared to an APC standard (Haematologic Technologies, Inc). Absorbance was measured at 20 second intervals over 20 mins at 37°C and the concentration of APC determined.

5.4.9 Factor Xa Functional Assay

EOCs were incubated with 20nM factor VIIa and 200nM factor X (Enzyme Research Laboratories) in HBSS. Half of the samples were also incubated with 70uM TFPI antibody for 1 hr at 37°C. The reaction was quenched with 100mM cold EDTA and visualized with 0.667 mM Spectrozyme factor Xa, and compared to a factor Xa standard (American Diagnostica). TFPI activity was determined by subtracting quantity of factor Xa from samples with and without antibody (Ab). TF activity without the influence of TFPI was taken from the amount of factor Xa produced in the presence of TFPI Ab.

5.4.10 Total DNA

The amount of DNA in the sample was measured with the picogreen assay (Invitrogen) using standard techniques.

5.4.11 Baboon Arteriovenous (AV) ex vivo Shunt Model

Shunts were surgically implanted between the femoral artery and vein of 10-12 kg baboons (Figure 5.1A). Autologous platelets were labeled with $^{111}\text{Indium}$ prior to flow studies and reinfused into the animals. Homologous fibrinogen was also labeled with $^{125}\text{Iodine}$ and infused into the animal 5 minutes prior to flow initiation. Animals were trained/conditioned to the testing system/apparatus such that minimal to no sedation was required. Animals were not treated with anticoagulant or anti-platelet therapies. The permanent AV shunt was elongated with Silicone tubing and the test graft centered over a gamma scintillation camera (GE Model 400T Maxi-Camera), which temporally and spatially measured platelet deposition on the graft surface (Figure 5.1B). The graft was isolated in a custom-built flow chamber. A flow meter (Transonics Inc.) was used to monitor flow rates, which were maintained by adjusting a tubing clamp distal to the chamber at 100 mL/min throughout the study period (Figure 5.1C). As circulating blood flowed through the graft segment radiolabeled platelets and fibrin accumulate on the graft surface. Thrombus formation was quantified by dynamically measuring total platelet and fibrin deposition. Platelets adhering to the graft surface were dynamically quantified, both temporally and spatially, in 5 minute intervals. A blood sample was drawn prior to the study and analyzed for total platelet counts. The activity, counts per minute in each mL of blood (CPM/mL) of the standard was measured with the gamma camera in a 5 minute cumulative frame. The cpm per platelet was then determined and used to calculate the total platelets on the graft surface. The $^{125}\text{Iodine}$ labeled fibrin was measured in a 1480 Wizard Gamma Counter (PerkinElmer), 30 days after the study, once the $^{111}\text{Indium}$ activity had decayed.

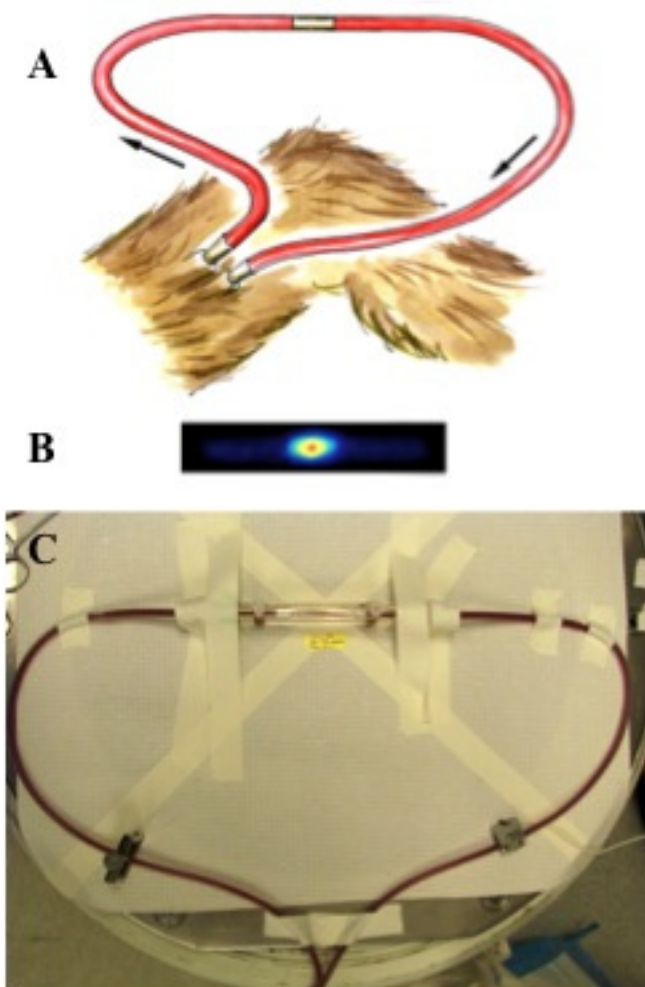


Figure 5.1. Arteriovenous Shunt model system (A). A dialysis type permanent shunt was placed between the femoral artery and vein. The shunt utilized the animal's blood flow as the driving force with a distal clamp to maintain a flow rate of 100 mL/min. All blood was recirculated back into the animal to minimize blood loss. (B) Typical image obtained from the gamma camera during the study. The image ranges from blue to red for low to high platelet numbers respectively with temporal and spatial resolution. (C) Flow loop positioned on the gamma camera with a flow probe and distal tubing clamp. Images A and B were obtained from Dr. Stephen Hanson who developed the shunt model system.

5.4.12 Baboon Arteriovenous (AV) *ex vivo* Shunt Durability Model

Durability shunts were run using the *ex vivo* shunt system to access the EOCs retention on the graft surface under *ex vivo* shunt and *in vivo* flow conditions. The EOCs used to seed the grafts were labeled with ¹¹¹Indium rather than labeling the animal's platelets and fibrin. Cells were passaged using standard techniques and resuspended at a high concentration of 8×10^6 cells/mL in PBS. Labeling buffer was prepared and consisted of 50 μ L of carbonate buffer, 1.3 μ L of 0.2 M tropolone and 50 μ L of ¹¹¹Indium (500 μ Ci). Labeling buffer was added to the concentrated cell solution at a ratio of 10 μ L (50 μ Ci) of buffer to 4×10^6 cells in 0.5 mL and incubated for 10 minutes at 37°C. Type I collagen and fibronectin modified grafts were then seeded with cells and conditioned with media as previously described. A T-75 flask and 9 wells distributed evenly on a 96 well plate were also seeded with a range of labeled EOCs to calibrate the number of seeded cells to CPM on the gamma camera. Prior to the start of flow calibration images of background (ambient) radioactivity and calibration flasks and plates were collected in 5 minute frames. A time zero frame was also collected of the seeded graft in the biochamber following a gentle rinse with PBS. The shunt study was then run in the same manner as the *ex vivo* platelet accumulation studies, except that a decrease in CPM, for detachment of EOCs, was evaluated rather than an increase due to adhering platelets. The first hour flow was run at 100 mL/min followed by 30 minutes of high *in vivo* flow rates of 250 mL/min. CPM were then converted to cell numbers and plotted over the course of the study.

5.4.13 Baboon Aorto-iliac *in vivo* Bypass Model

Type I collagen modified, autologous EOC-seeded ePTFE grafts were implanted in a bilateral aorto-iliac bypass position. Grafts were 7 cm between the Si tubing cuffed ends, which was 2 cm longer than the *in vitro* and *ex vivo* samples to ensure ample length for surgical implantation. This was the only difference in graft preparation from the *ex vivo* and *in vitro* samples. The grafts were sterilely removed from the biochambers in the surgical suite and cut to length by the surgeon. Animals were anticoagulated with a single dose of 300 units heparin prior to implantation. Implanted grafts were anastomosed to the aorta, proximal to the aortic ligation, and to each common iliac artery just proximal to the takeoff of the internal iliac arteries. End-to-side anastomoses were constructed using proline sutures (Figure 5.2).

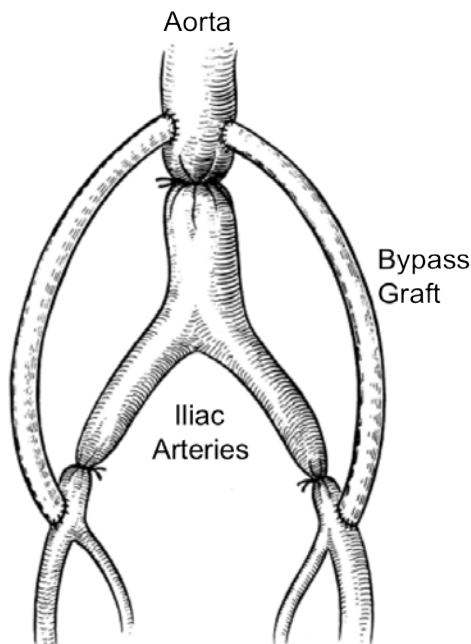


Figure 5.2. Illustration of the aorto-iliac bilateral bypass graft model. Grafts are implanted between the aorta and iliac vessels with an end to side anastomosis and the bypassed vessel ligated to direct flow through the shunts. This image was obtained from Dr. Stephen Hanson who developed this model.

Following graft placement, flow was re-established and hemostasis of the anastomosis verified. Blood flow rates through the grafts were measured to confirm flow through the graft lumen after implantation using a flow meter (Transonics, Inc). At the time of sacrifice, the patency of the grafts was first evaluated, and then the grafts were perfusion fixed with 10% formalin under arterial pressure (100 mmHg). Pressure was maintained by restricting flow through the perfused arteries distally. The aorta and graft segments were removed and dissected free of surrounding tissue, blocked, sectioned and stained. Grafts and adjacent proximal and distal segments were sectioned at the mid-point and between the heel and toe of each anastomosis. Sections were located 1-2 mm from the heel and toe, and at 5 mm intervals along the graft and vessel segments (Figure 5.3). Tissue sections were embedded in paraffin and stained with hematoxylin and eosin (H&E) to evaluate cell coverage and intimal ingrowth.

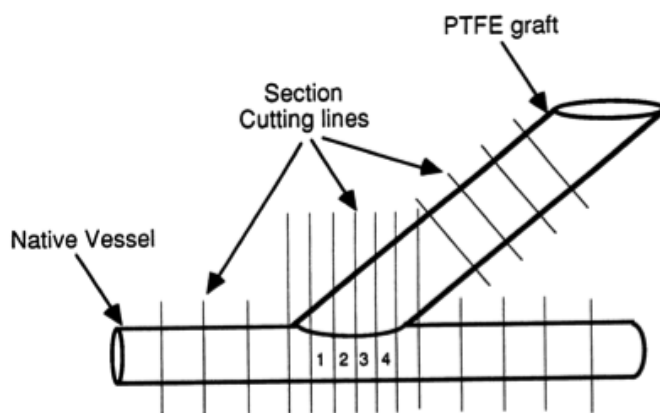


Figure 5.3. Sectioning diagram for *in vivo* anastomosis evaluation. Sections were cut throughout the anastomosis to evaluate tissue ingrowth.

Graft sections were analyzed with respect to total neointimal area. The mean tissue ingrowth area was measured by drawing a 2 mm line along the graft lumen, from each side of the anastomosis, and calculating the area of tissue ingrowth within that region. H&E sections were imaged with a Nikon Optiphot-2 microscope equipped with a Hitachi HV-C 20 U color video camera. Image-Pro Plus software (Media Cybernetics) was used to measure lesion dimensions and composition.

5.4.14 Correlation of in vitro Hemostasis and ex vivo and in vivo Thrombosis

Each *ex vivo* shunt and *in vivo* implant had a paired *in vitro* control graft. The *in vitro control* was treated in an identical manner to the matched *ex vivo* and *in vivo* samples. Each *in vitro* sample was sectioned for imaging, functional response assays, and RNA isolation (Figure 5.4). Functional and gene expression results were compared to platelet deposition and fibrin data in the *ex vivo* shunt model and to tissue ingrowth in the *in vivo* model.

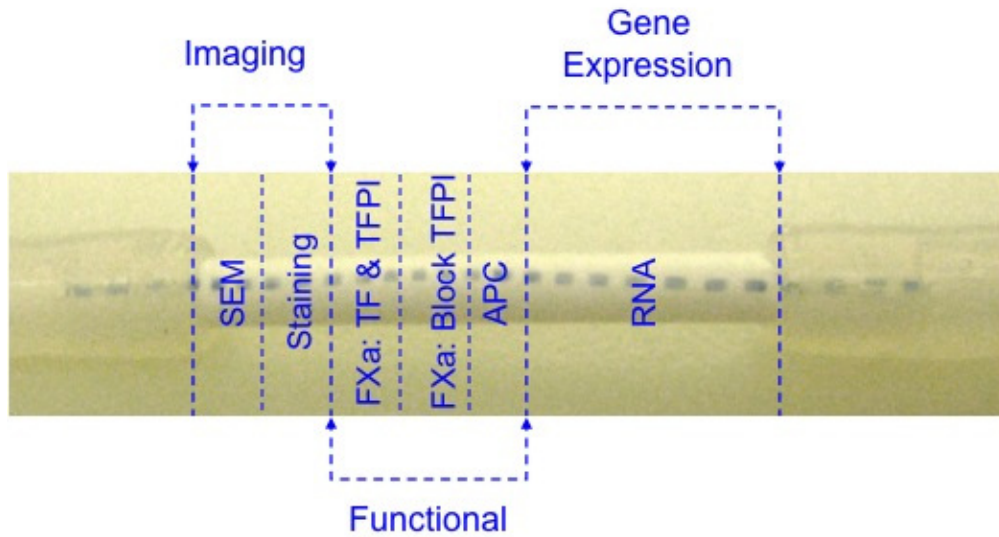


Figure 5.4. Sectioning of the *in vitro* controls for each section of the graft used for RNA isolation, functional assays and imaging.

5.4.15 Statistical analyses

All data are expressed as the mean \pm standard deviation. Student's *t*-test, linear regression, and one-way ANOVA with Tukey post hoc tests were used for hypothesis testing, with $p < 0.05$ as the measure for statistical significance. The number of independent tests is listed for each experiment.

5.5 Results

5.5.1 Endothelial Outgrowth Cell Isolation

EOCs were successfully isolated and expanded from baboon peripheral blood. Plates displayed good outgrowth colonies by 14 days in culture. Cells rapidly expanded in culture and displayed typical endothelial cell cobblestone morphology (Figure 5.5). EC morphology was maintained through multiple passages of cells.

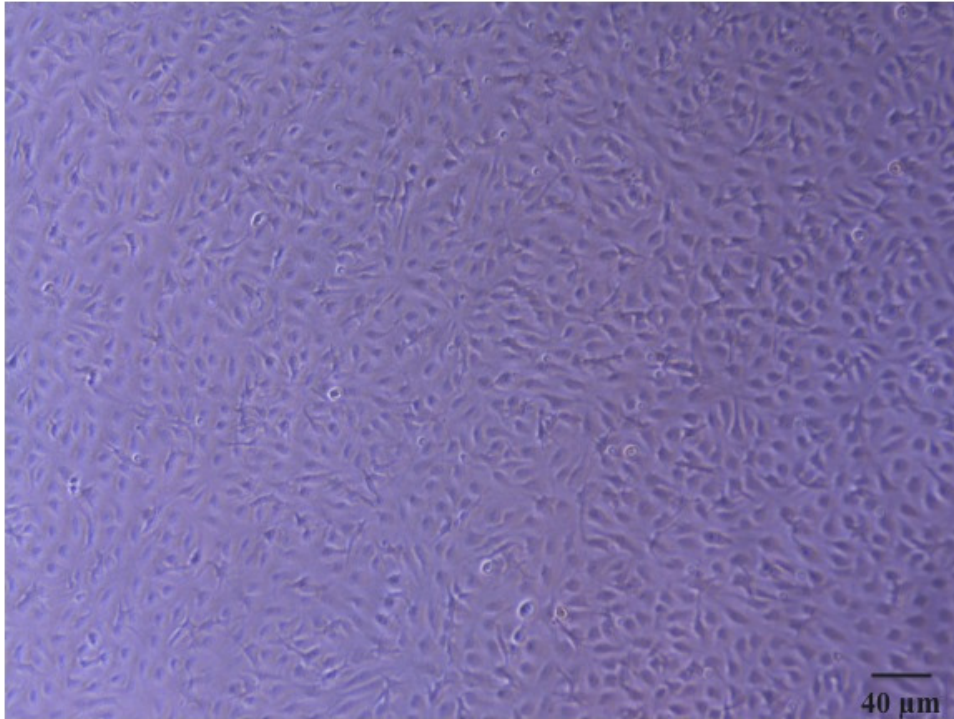


Figure 5.5. EOCs outgrowth cells at passage 0 on fibronectin coated wells. Image shows typical EOC cobblestone morphology. Deirdre Anderson acquired and provided this image.

5.5.2 Flat plate studies

EOCs were cultured on adsorbed type I collagen, type IV collagen, fibronectin and α -elastin coated surfaces. Cells were confluent with typical EC morphology after 48 hours in culture (Figure 5.6). Total DNA determined by the pico green assay indicated significantly greater DNA content (ANOVA, Tukey post hoc, $*p < 0.05$) and thus greater cell numbers on the type I collagen and fibronectin coated surfaces than on the α -elastin and type IV collagen surfaces (Figure 5.7).

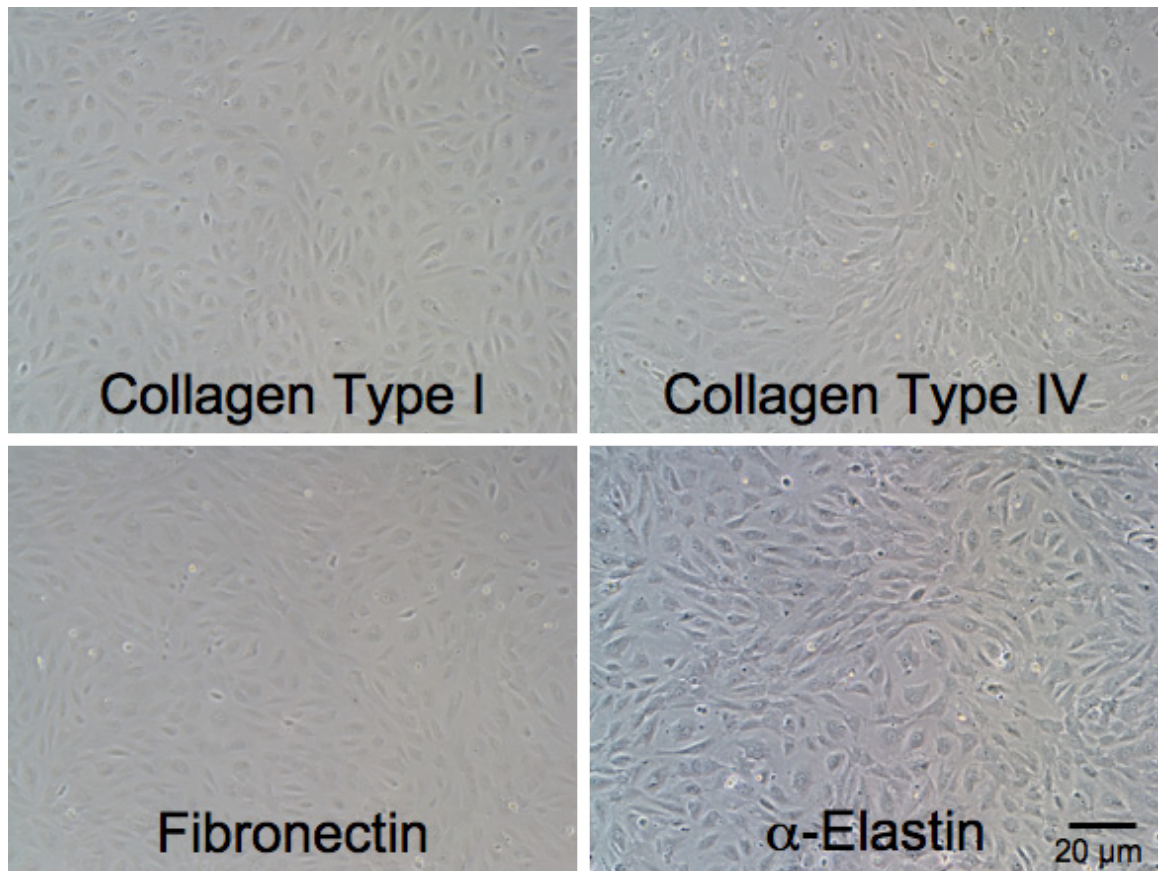


Figure 5.6. EOCs on each ECM surface after 48 hrs in culture. Dishes were coated with 5 $\mu\text{g}/\text{cm}^2$ for 1 hour at room temperature. Cells (3×10^5) were plated on each surface, and maintained in 10% EGM-2 media for 24 hours and Hyskon flow media for 24 hours. Scale bar = 20 μm

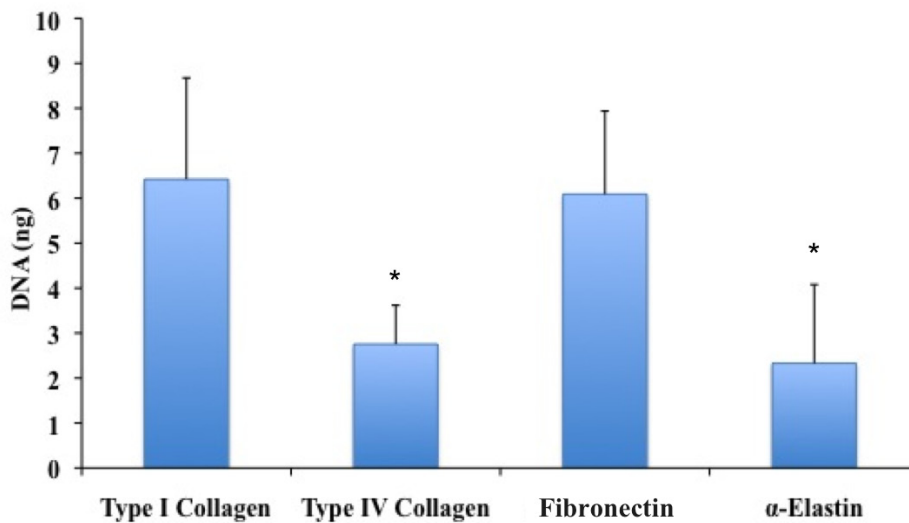


Figure 5.7. DNA/well of EOCs after 48 hrs in culture on each ECM coating. Collagen type I and fibronectin had significantly greater DNA content, and thus more cells, than collagen type IV and α -elastin (ANOVA - Tukey post hoc, * $p < 0.05$). Deirdre Anderson ran the pico green assays.

5.5.3 Gene Expression on Protein Coated Flat Plates

Gene expression and functional responses were quantified on type I collagen, type IV collagen, fibronectin and α -elastin coated surfaces. The gene panel included thrombomodulin (TM), VCAM, endothelial protein C receptor (EPCR), CD39, and tissue factor pathway inhibitor (TFPI). Primers used for these studies (Appendix C) ranged from 90 to 110% efficient and were specific for the genes of interest as confirmed by gel electrophoresis (data not shown). Significant differences in expression was found for EPCR between type I collagen and α -elastin (Figure 5.8). There was a trend for lower CD39 values for type I collagen than α -elastin, as well as lower type IV collagen values than α -elastin (Figure 5.9).

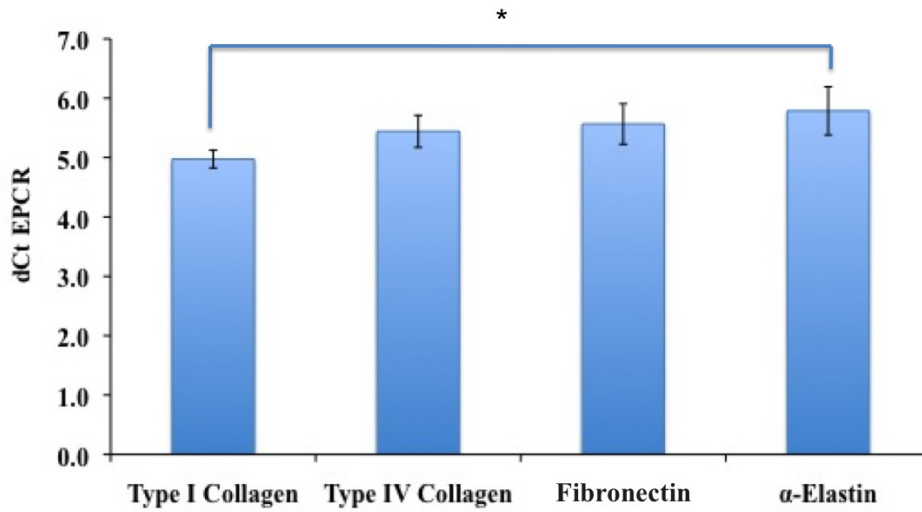


Figure 5.8. EPCR gene expression: There was a significant difference between type I collagen and α -elastin (ANOVA-Tukey post hoc, * $p < 0.05$).

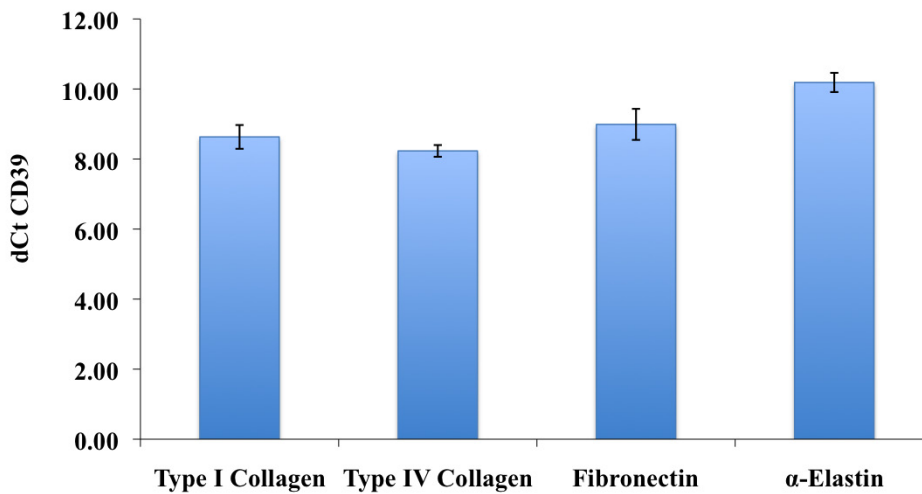
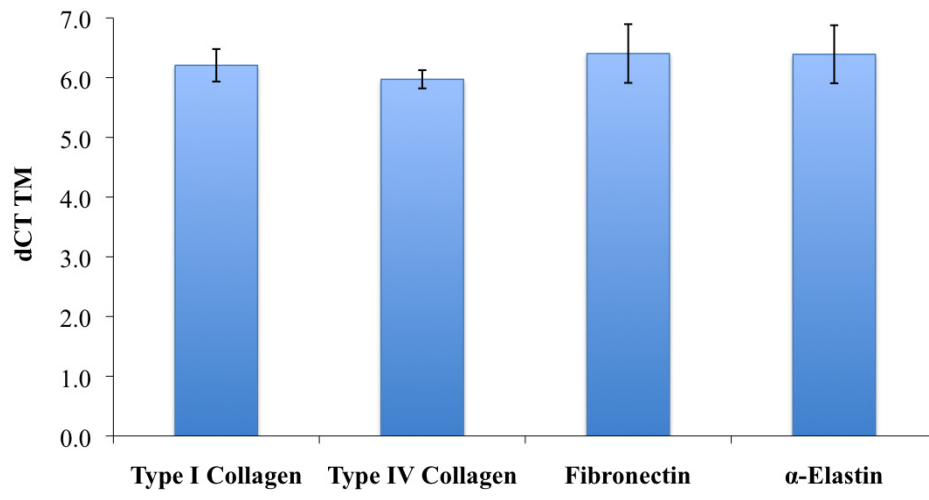


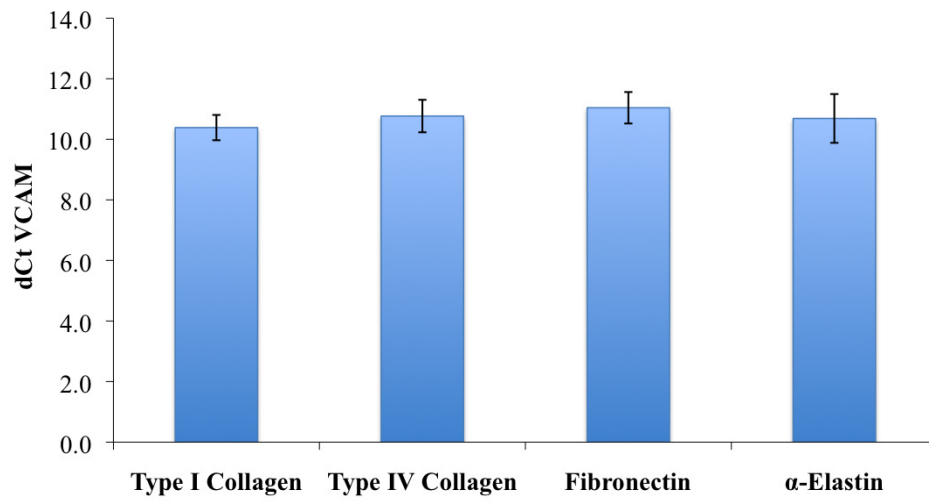
Figure 5.9. CD39 gene expression: There was a trend for lower types I and IV collagens than α -elastin.

There were no significant differences in gene expression on the four protein coated surfaces (Figures 5.10A-C) for TM, VCAM, or TFPI markers (ANOVA).

A.



B.



C.

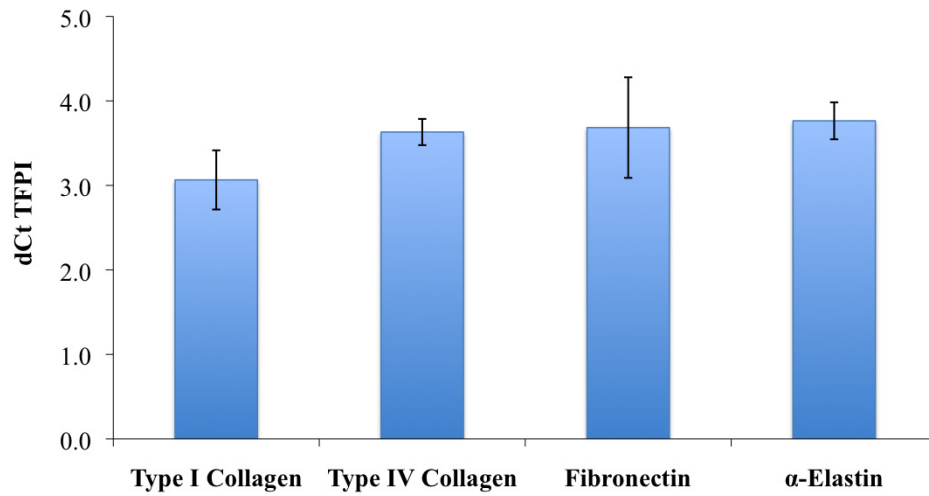


Figure 5.10. (A) TM gene expression (B) VCAM gene expression (C) TFPI gene expression. There were no significant differences between substrates (ANOVA).

5.5.4 Functional Responses on Protein Coated Flat Plates

The activity of APC as measured by ng/mL of factor Xa generated was dependent (ANOVA: Tukey post hoc, $P < 0.05$) on surface coating (Figure 5.11) with type I collagen (164 ± 20 ng/mL) and FN (164 ± 14 ng/mL) displaying a higher activity than both type IV collagen (61 ± 22 ng/mL) and α -elastin (61 ± 15 ng/mL). Factor Xa signals were typically undetectable in samples without the TFPI Ab. Factor Xa activity (Figure 5.12) was independent (ANOVA) of surface coating.

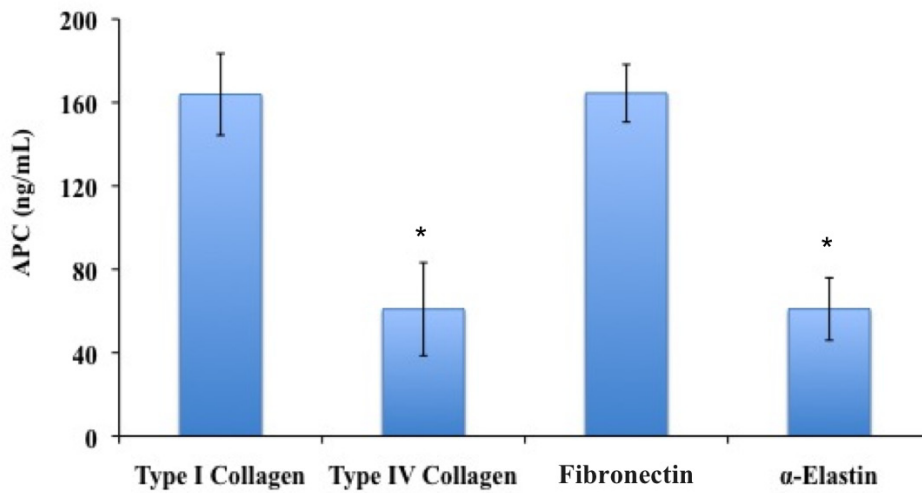


Figure 5.11. APC activity assay: Type 1 collagen and fibronectin had significantly greater activity than type IV collagen and α-elastin (ANOVA-Tukey post hoc, *p < 0.05). Deirdre Anderson assisted with the functional activity assay for this study.

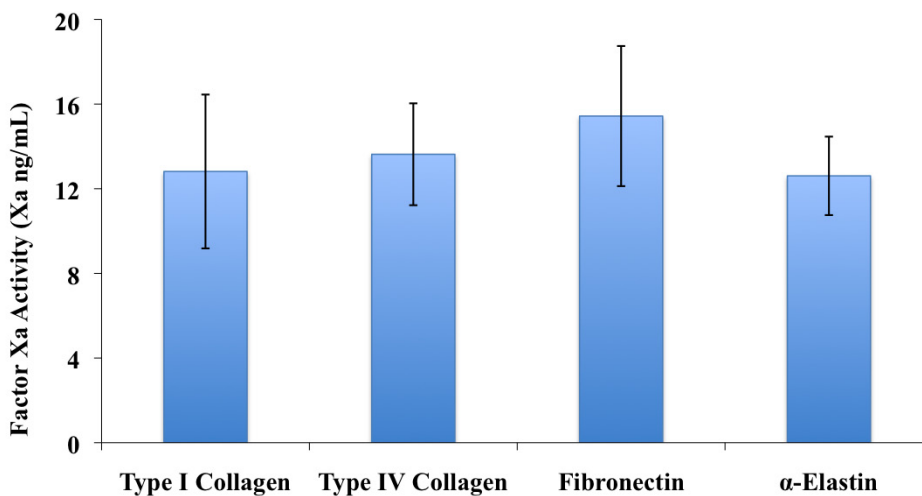


Figure 5.12. TFPI activity assay: The amount of factor Xa (ug/mL) produced in samples with and without blocking TFPI. Samples without TFPI inhibition had no detectable Xa. There were no significant differences between substrates (ANOVA). Deirdre Anderson assisted with the functional activity assay for this study.

5.5.5 Platelet Aggregation

Platelet aggregation varied between protein solutions tested. Fibronectin and α -elastin did not react with the platelets and thus had no response in this test system. Samples of α -elastin were tested up to 800 $\mu\text{g}/\text{mL}$ and fibronectin was tested at 20 and 40 $\mu\text{g}/\text{mL}$ to confirm the lack of a response. Chronolog collagen used as the standard had an average aggregation time of 2.74 ± 0.34 minutes with a percent clearance of $73 \pm 2.9\%$. MP type I collagen (MP Biomedical) demonstrated a more variable response. Our type I collagen solution activated the platelets to a slightly lower response level, but took longer for the reaction to plateau. The response was delayed for the 20 $\mu\text{g}/\text{mL}$ samples so 40 and 80 $\mu\text{g}/\text{mL}$ were tested. The average aggregation time for 40 $\mu\text{g}/\text{mL}$ was 7.13 ± 3.20 minutes with a percent clearance of $67.2 \pm 2.9\%$ and 80 $\mu\text{g}/\text{mL}$ had an average aggregation time of 4.6 ± 0.82 minutes with a percent clearance of $67.8 \pm 6.0\%$. MP type I collagen at 40 $\mu\text{g}/\text{mL}$ had a significantly longer clearance time than Chronolog collagen at 20 $\mu\text{g}/\text{mL}$ (ANOVA-Tukey post hoc, $p < 0.05$). It took 4 times as much type I collagen (80 $\mu\text{g}/\text{mL}$) to attain no significant difference in aggregation times as compared to Chronolog collagen. The % clearance or magnitude of the response was not significantly different between collagens (Figure 5.13).

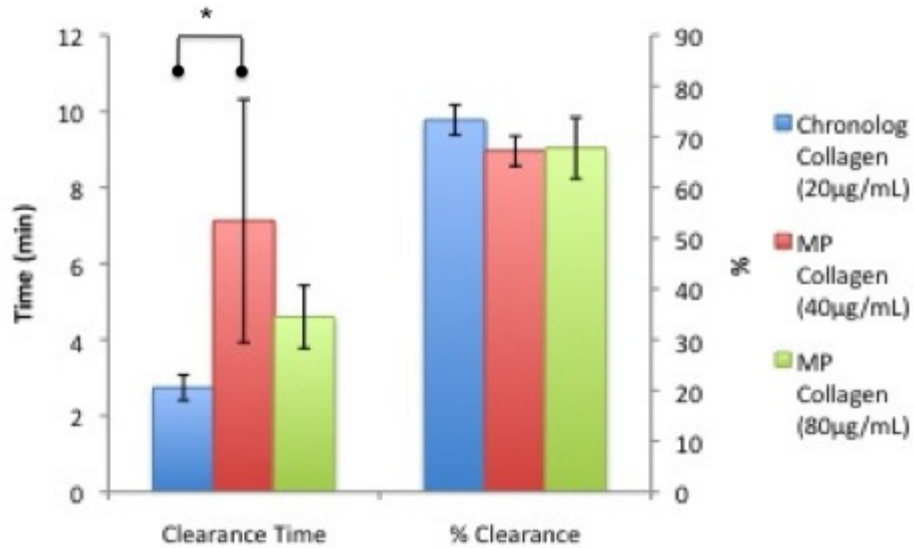


Figure 5.13. Platelet aggregation time and percent clearance for Chronolog type I fibrillar collagen and MP type I collagen. MP collagen at 40 µg/mL had a more variable response and significantly longer clearance time than Chronolog collagen at 20 µg/mL. The % clearance or magnitude of the response was not significantly different between collagens. (ANOVA-Tukey post hoc, *p < 0.05). Ulla Marzec assisted with the platelet aggregation studies.

5.5.6 *Ex vivo shunt Graft Studies*

EOCs were successfully seeded onto the lumen of type I collagen and fibronectin impregnated ePTFE grafts. Cells formed confluent monolayers and spread on the surfaces of the grafts after 48 hours of growth and hyskon flow media conditioning (Figure 5.14).

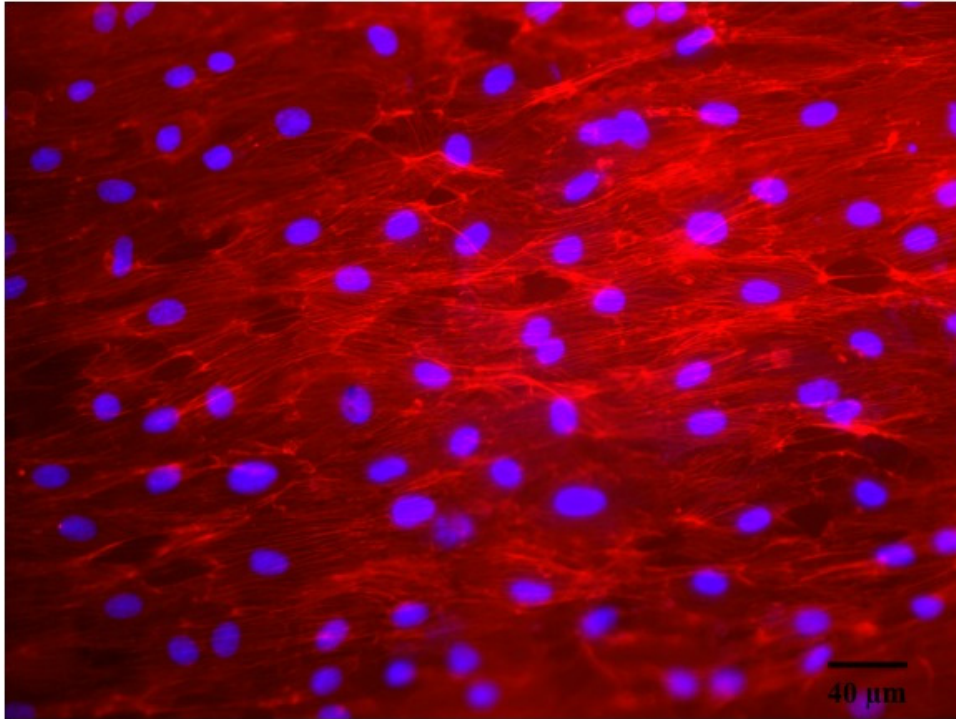


Figure 5.14. EOCs on type I collagen coated ePTFE graft surface after 48 hours. Nuclei stained with DAPI are shown in blue and the cytoskeleton (f-actin) is stained with rhodamine phalloidin shown in red. EOCs attached and spread on the ePTFE modified surface.

5.5.7 Cell Retention on EOC-seeded ePTFE grafts

The durability of cell retention was tested under *ex vivo* shunt flow conditions (100 mL/min) on both type I collagen and fibronectin. Cell numbers initially dropped from the no flow starting condition but remained stable for one hour throughout the duration of a standard shunt study period (Figure 5.15). There was no difference in cell number between the type I collagen and fibronectin grafts with and average cell number of $27,308 \pm 638$ on collagen and $24,940 \pm 1049$ on fibronectin between 5 and 60 minutes of flow. The durability of the cell attachment was also tested under *in vivo* flow conditions by ramping the flow rate to 250 mL/min (Figure 5.16). Cells remained stably adhered

with no significant cell loss throughout the high flow test with average cell numbers between 60 and 90 minutes of flow of $26,241 \pm 521$ for type I collagen and $24,906 \pm 786$ for fibronectin. These numbers represent the number of initially seeded cells not ones that proliferated on the surface during the 48 hour media conditioning phase.

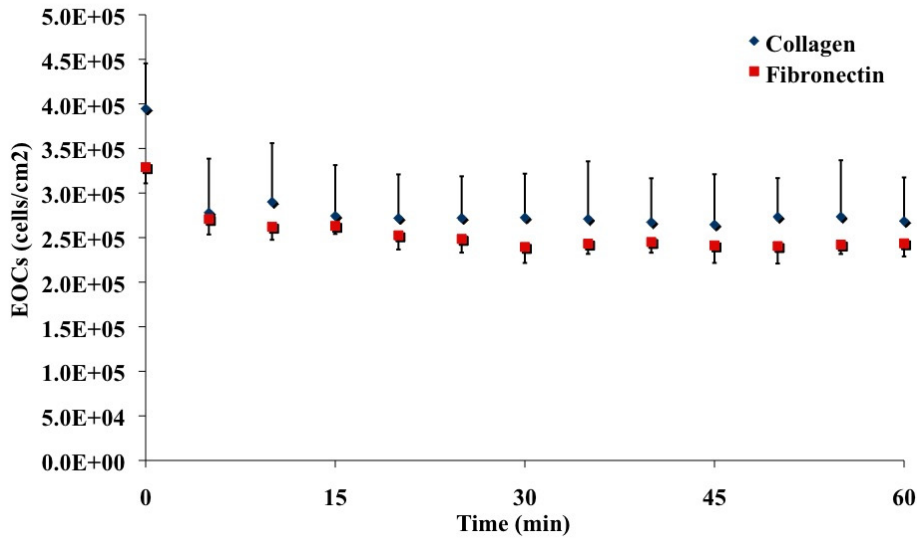


Figure 5.15. Durability of ¹¹¹Indium labeled EOCs on protein coated ePTFE at 100 mL/min flow rate tested in the baboon shunt system. There was an initial drop (from static to first 5 min frame) in cell numbers with the initiation of flow, but cells remained stable on the graft through 60 min at standard flow rates used in the *ex vivo* shunt studies. Ulla Marzec and Jennifer Greisel assisted with the *ex vivo* shunt studies.

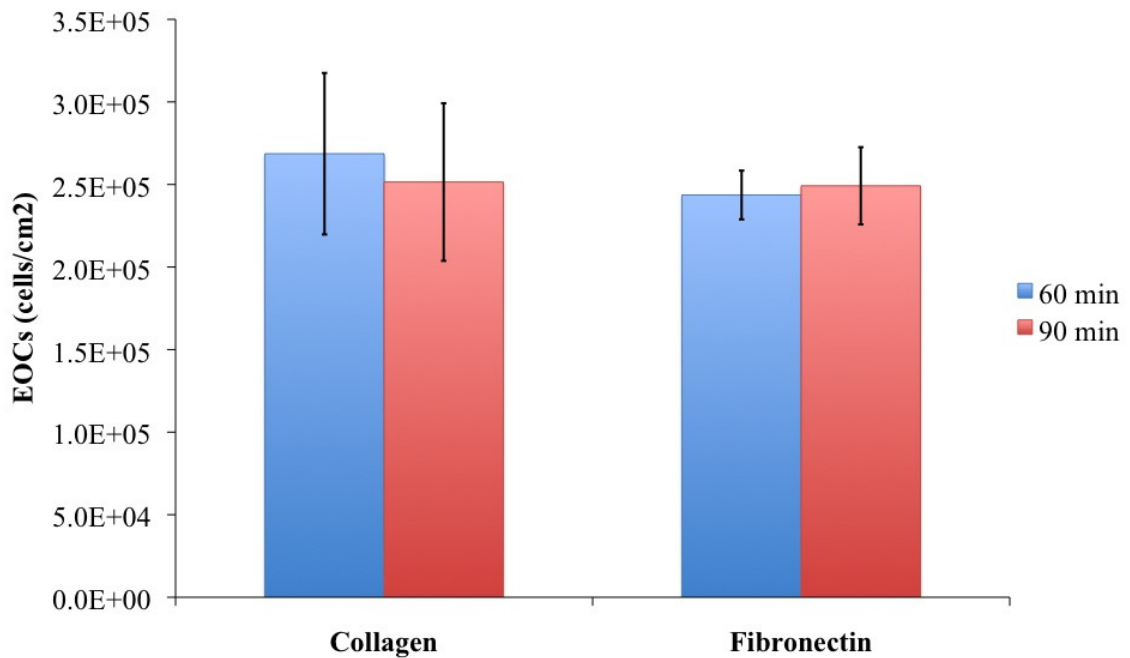


Figure 5.16. Durability of ¹¹¹Indium labeled EOCs on protein coated ePTFE with a flow rate increase from 100 mL/min to 250 mL/min tested in the baboon shunt model system between 60 and 90 min after the initiation of flow. There is no significant difference in cell coverage (ttest). Ulla Marzec and Jennifer Greisel assisted with the ex vivo shunt studies.

5.5.8 Platelet Response on EOC-seeded ePTFE grafts

All study grafts remained patent throughout the *ex vivo* studies. There was a variable platelet response in the *ex vivo* model with a range of 0.11 to 2.03 x 10⁹ platelets adhering to a 2 cm region at 40 minutes (Figure 5.17). There were no significant differences (ttest) in platelet numbers between the fibronectin and type I collagen ePTFE grafts with an average platelet count of 0.68 ± 0.66 x 10⁹ for type I collagen and 1.38 ± 0.57 x 10⁹ for fibronectin. A post hoc power analysis determined that 14 samples for each group is required to achieve significance with an α of 0.05 and 80% power.

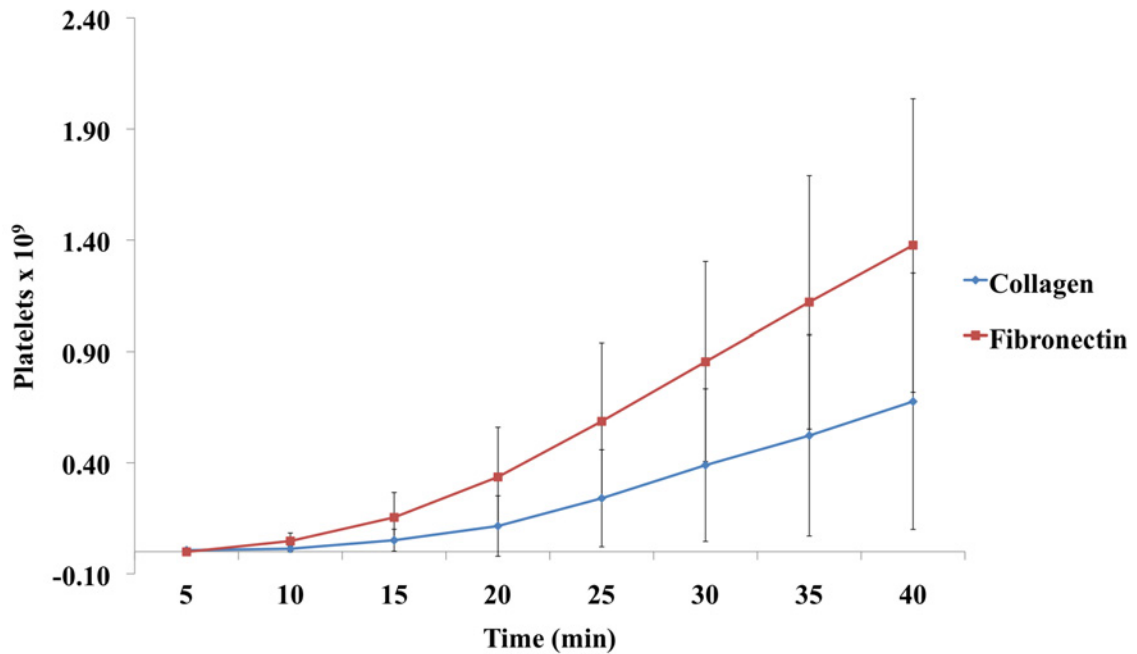


Figure 5.17. Cumulative platelet deposition on the EOC ePTFE graft surface over the first 40 min of the flow period. Fibronectin modified samples are shown in red, and type I collagen impregnated samples are shown in blue. Ulla Marzec and Jennifer Greisel assisted with the ex vivo shunt studies.

5.5.9 Gene Expression for EOC-seeded ePTFE grafts

Each *ex vivo* shunt graft was paired to an identical *in vitro* control. RT PCR was used to measure the gene responses of EOCs to each protein modified ePTFE graft. There were no significant differences in gene expression for most of the coagulation and inflammatory gene panels between type I collagen and fibronectin, with the exception of TFPI and VCAM, which showed differences when paired by study day (Figures 5.18 and 5.19). TFPI had average dCt values of 3.42 ± 0.55 and 3.83 ± 0.54 and VCAM had average dCt values of 10.12 ± 1.36 and 10.35 ± 1.30 for type I collagen and fibronectin respectively.

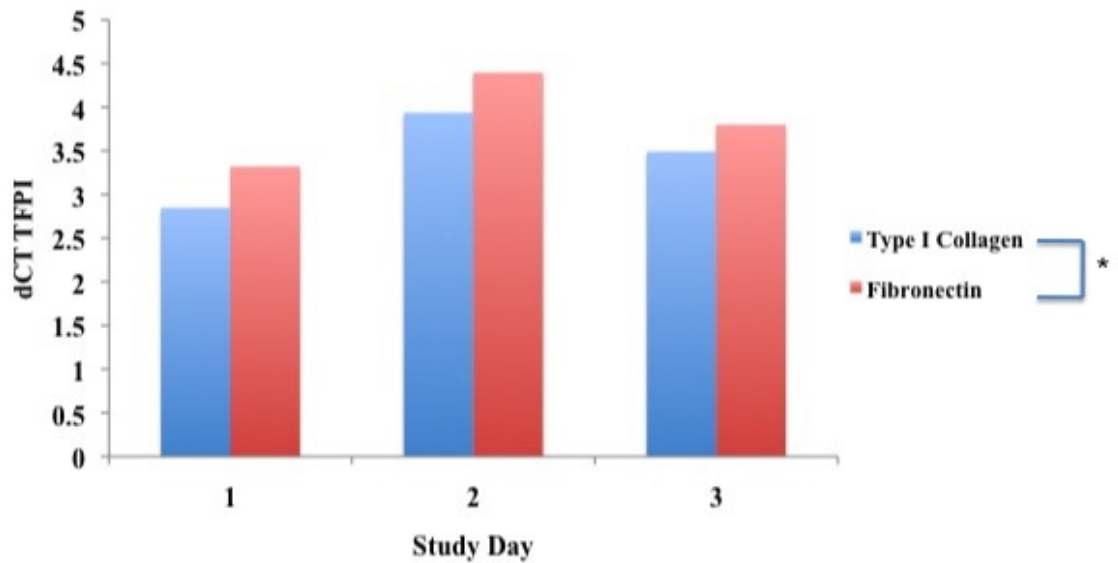


Figure 5.18. TFPI gene expression for *in vitro* controls for the shunt studies. There was a significant difference in expression between type I collagen and fibronectin when paired to the study day (paired ttest, * $p < 0.05$).

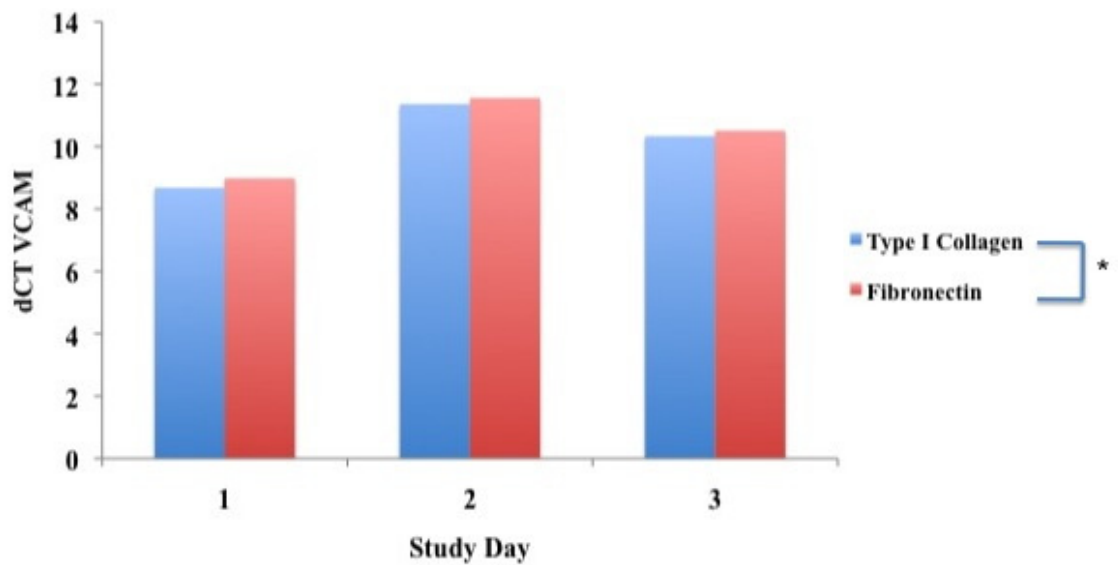


Figure 5.19. VCAM gene expression for *in vitro* controls for the shunt studies. There was a significant difference in expression between type I collagen and fibronectin when paired to the study day (paired ttest, * $p < 0.05$).

5.5.10 Functional Activity Assays for EOC-seeded ePTFE grafts

The functional studies for the *in vitro* controls showed no differences (paired ttest) between fibronectin and type I collagen grafts in the APC and factor Xa generated. These values were normalized to the graft surface area to correct for size differences in test samples (Figures 5.20 and 5.21).

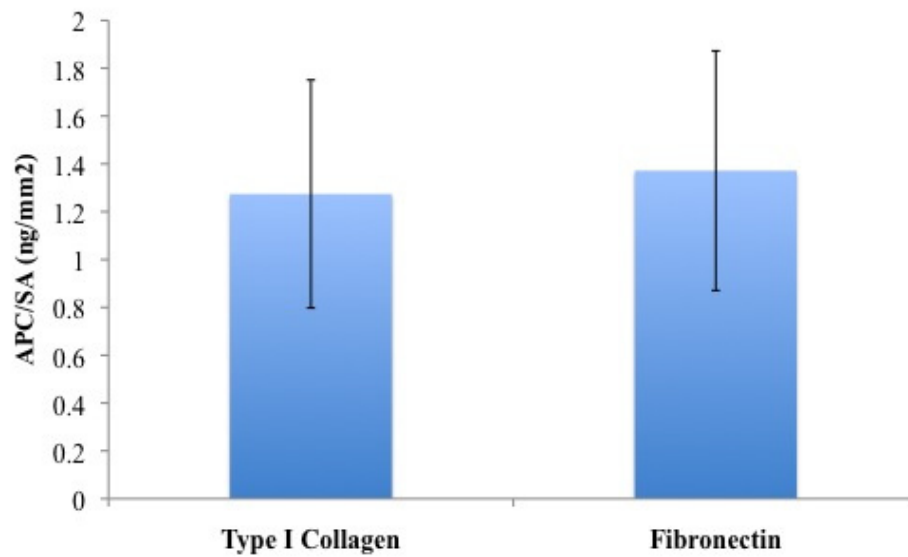


Figure 5.20. APC activity assay on the *in vitro* controls for type I collagen and fibronectin modified shunts. There were no significant differences in activity between protein coatings. APC data were paired for the study day (paired ttest). Deirdre Anderson assisted with the functional activity assay for this study.

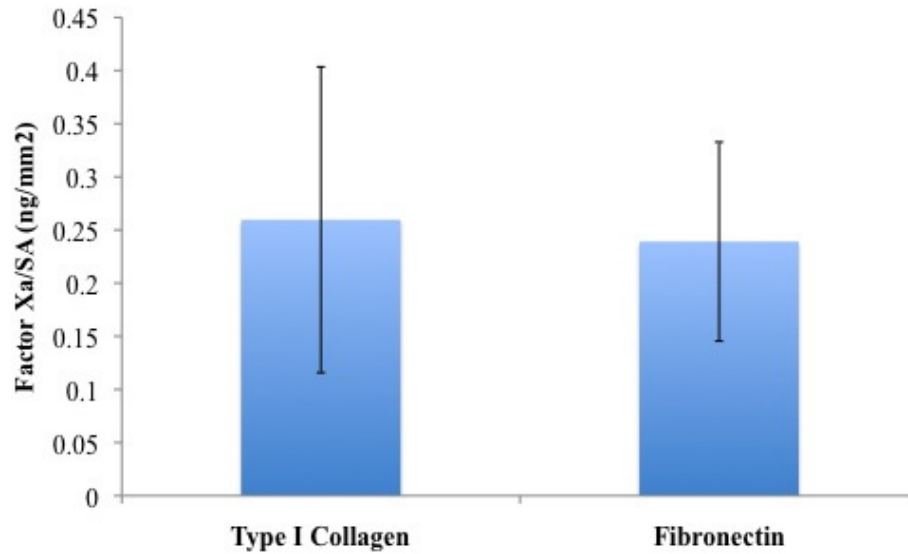


Figure 5.21. Factor Xa activity assay on the *in vitro* controls for type I collagen and fibronectin modified shunts. There were no significant differences in activity between protein coatings. Factor Xa data were paired for the study day (paired ttest). Deirdre Anderson assisted with the functional activity assay for this study.

Platelet numbers were found to correlate to factor Xa activity in the presence of TFPI blocking antibody (Figure 5.22). A linear relationship was established predicting the number of platelets adhering based on the ng of factor Xa per ng of DNA with an equation of $y = 0.16x + 0.42$ with an R^2 value of 0.85.

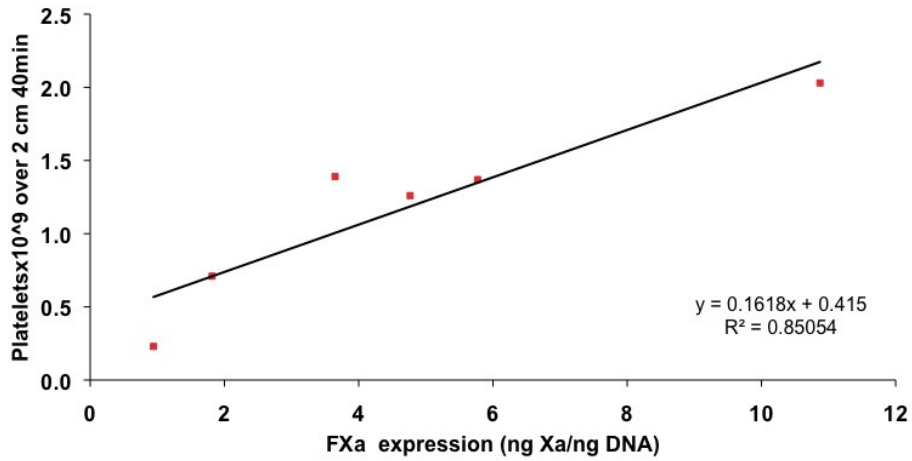


Figure 5.22. Correlation of platelet accumulation on the graft surface and FXa production in the presence of TFPI blocking antibody on both type I collagen and fibronectin coated ePTFE grafts. Deirdre Anderson assisted with the functional activity assay for this study.

The amount of fibrin deposited on the graft surface during the *ex vivo* shunt studies was measured. There were no significant differences (paired ttest) between the type I collagen and fibronectin modified ePTFE grafts. The amount was measured for a 2 cm region in the distal portion of the graft (Figure 5.23).

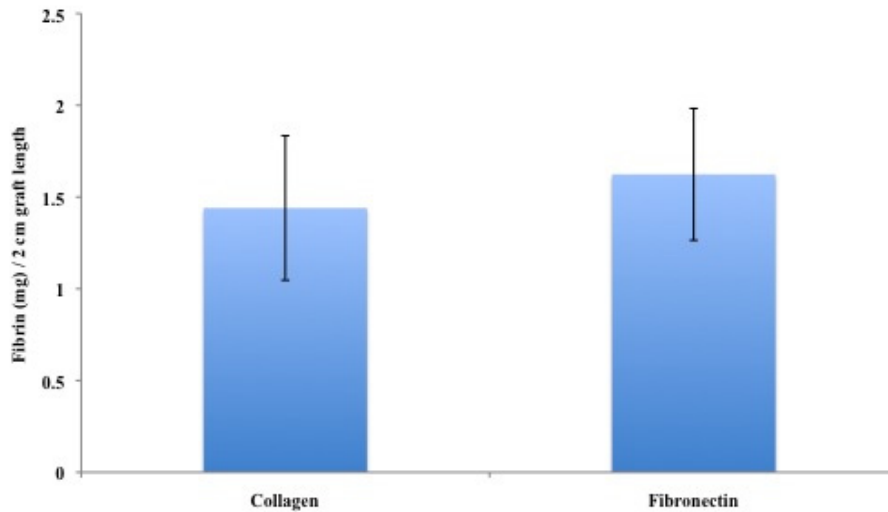


Figure 5.23. Fibrin accumulation on 2cm length of the type I collagen and fibronectin modified ePTFE shunt grafts. There were no significant difference in the amount of fibrin deposited on the surface of the graft between protein coatings (paired ttest) data were paired to the study day. Ulla Marzec and Jennifer Greisel assisted with the fibrin quantification for the ex vivo shunt studies.

5.5.11 In vivo shunt Graft Studies

Implants of type I collagen impregnated and untreated ePTFE grafts were tested in a baboon aorto-iliac bypass model. The grafts were implanted successfully with end to side anastomoses (Figure 5.24). Flow was reestablished and confirmed for both sides of the grafts. Iliac arteries were tied off to direct all flow through the bypass grafts. All grafts both controls and type I collagen modified EOC-seeded were patent upon explant at 1 month (Figure 5.25).

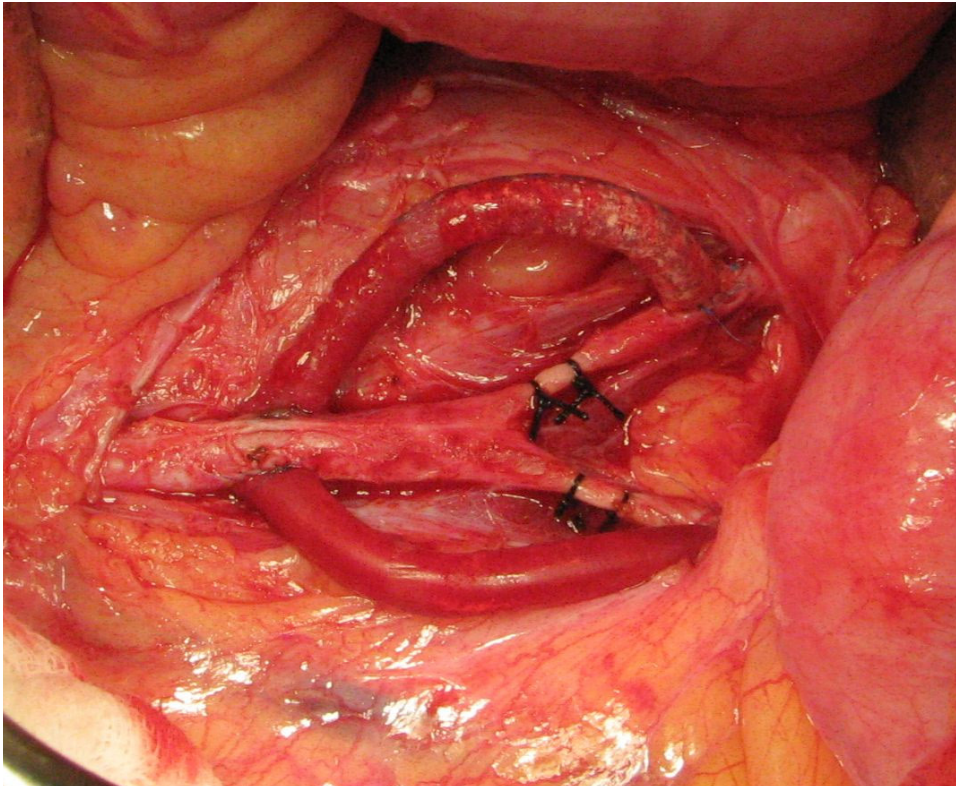


Figure 5.24. Implant of type I collagen coated EOC-seeded ePTFE graft in a baboon aorto-iliac bypass model. Dr. Howard Song implanted grafts with the assistance of the ONPRC surgical staff.

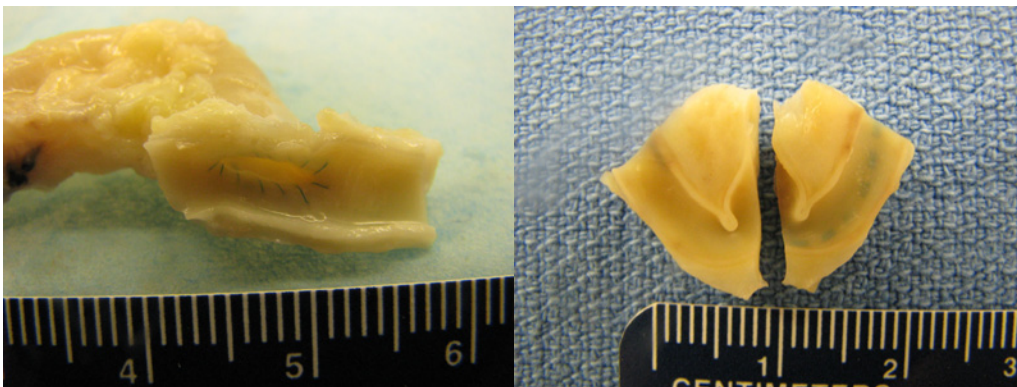


Figure 5.25. Explant after 1 month of a type I collagen coated EOC-seeded ePTFE graft in a baboon aorto-iliac bypass model. All grafts were patent at 1 month.

5.5.12 Tissue Ingrowth

There were two control animals and two cell seeded animals evaluated for tissue ingrowth at 1 month. Sectioned cell seeded grafts showed more tissue ingrowth on the second EOC-seeded grafts than on the first test animal (Figure 5.26). The TF expression was higher for the *in vitro* control for the animal with greater tissue ingrowth.

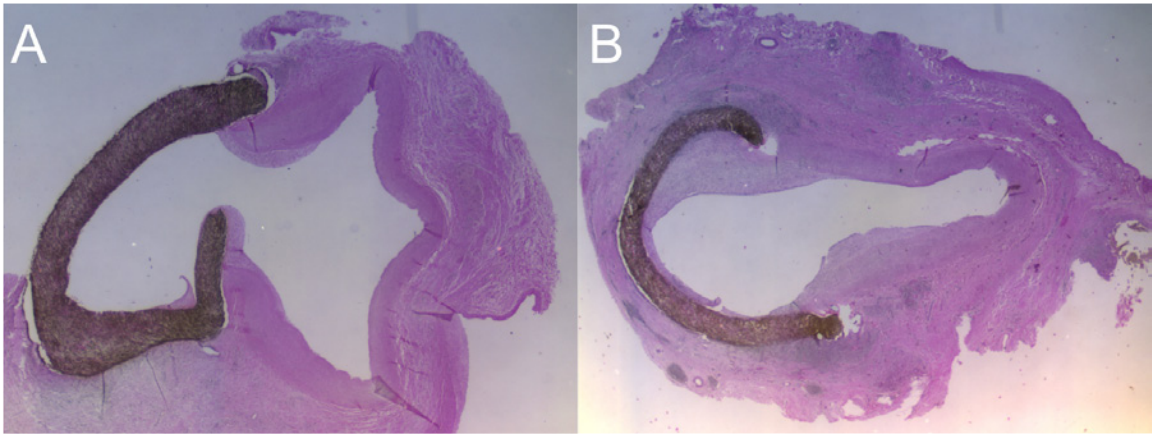


Figure 5.26. Representative histology sections of 1 month explants of type I collagen coated EOC-seeded ePTFE grafts in a baboon aorto-iliac bypass model. All implant grafts were patent at 1 month, but there was variable pannus ingrowth between samples with (A) showing little ingrowth and (B) showing significantly more tissue ingrowth. The TF expression for the matched *in vitro* control was higher in the B sample than the A. Deirdre Anderson assisted with the tissue ingrowth evaluations for this study.

Tissue ingrowth for the untreated controls and EOC seeded ePTFE grafts are shown for the distal and proximal locations for two implant animals. Further implants will be performed to determine significant differences between the treatment and control groups (Figure 5.27). A post hoc power analysis determined that 28 samples for each group is required to achieve significance with an α of 0.05 and 80% power.

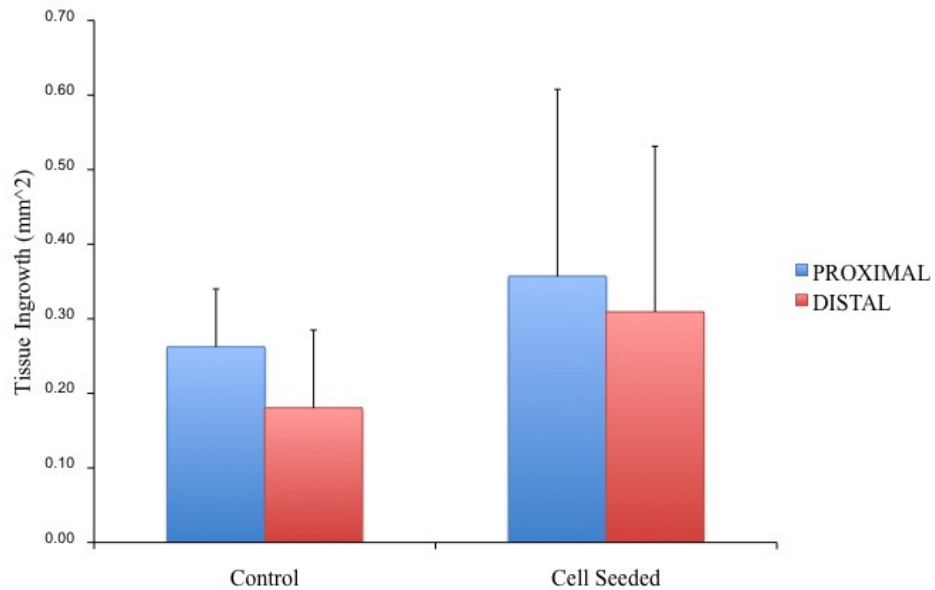


Figure 5.27. Tissue ingrowth for untreated ePTFE controls and collagen coated EOC-seeded ePTFE grafts one month after implant. Further implants will be conducted to determine significant differences between the control and the EOC-seeded grafts. These are average values for proximal and distal anastomoses for two grafts per animal and two animals per group for a total of four grafts per treatment group. Deirdre Anderson assisted with the tissue ingrowth evaluations for this study.

Tissue ingrowth was broken out by graft position, anastomosis site, and animal (Figure 5.28). This demonstrates the differences between test subjects. It was not a single anastomosis location that caused the variation between animals, but a difference between either test days or animal responses.

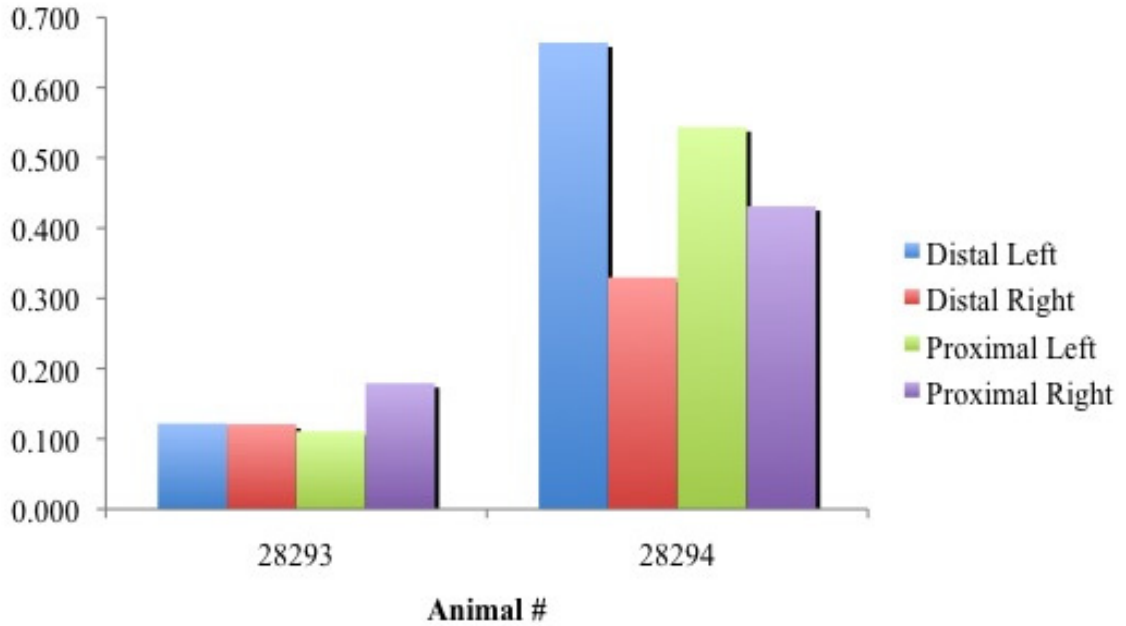


Figure 5.28. Tissue ingrowth for untreated ePTFE controls and collagen coated EOC-seeded ePTFE grafts one month after implant. There were no significant differences between the control and the EOC-seeded grafts. These are averaged numbers for proximal and distal anastomoses averaged between two grafts per animal and two animals per group for a total of four grafts per treatment group. Deirdre Anderson assisted with the tissue ingrowth evaluations for this study.

Values for tissue ingrowth were combined for each section and location. This gave average ingrowth value for each animal, with an average ingrowth of 0.136 ± 0.077 for 28293 and $0.521 \pm 0.110 \text{ mm}^2$ for 28294 (Figure 5.29).

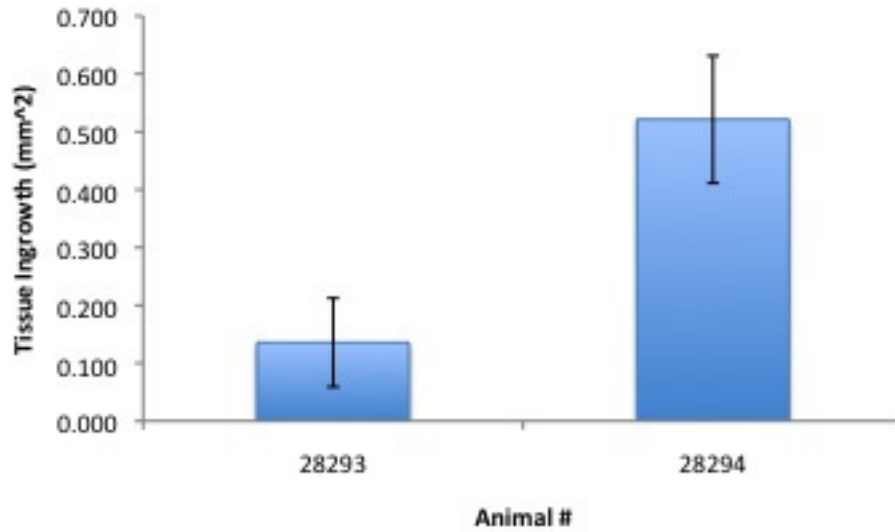


Figure 5.29. Tissue ingrowth for collagen coated EOC-seeded ePTFE grafts one month after implant. There were differences between animals. These are averaged numbers combining the proximal and distal anastomoses with two grafts per animal for a total of 4 anastomoses per animal analyzed. Deirdre Anderson assisted with the tissue ingrowth evaluations for this study.

Tissue sections were evaluated for EC cell coverage (Figure 5.30). Both the controls and the EOC-seeded grafts showed cell coverage on the luminal surface. The control grafts demonstrated EC ingrowth from the native tissue at the anastomosis site. The origin of the EC layer on the EOC-seeded grafts is unknown they could be originally seeded cell or infiltrating cells from the anastomosis site.

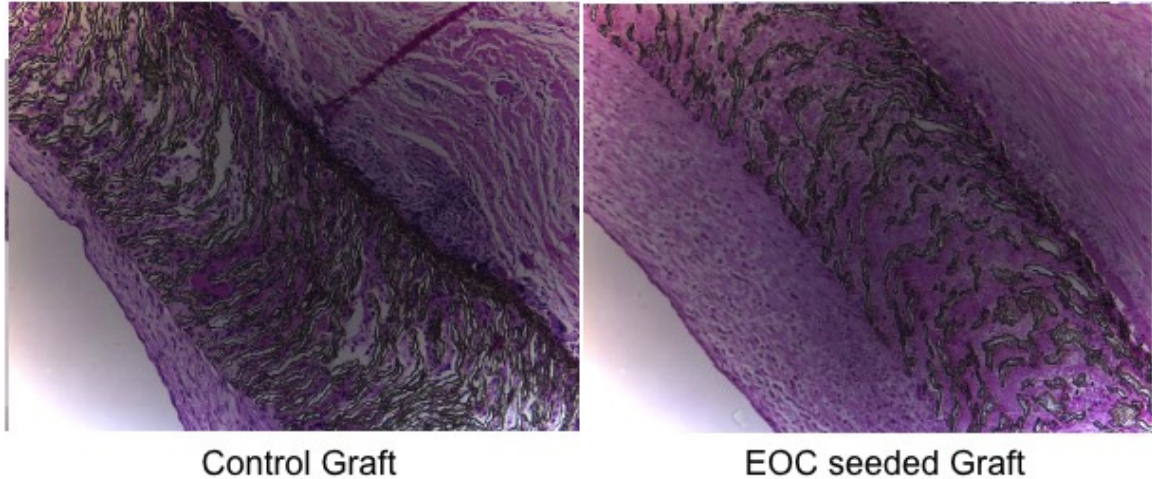


Figure 5.30. Endothelial cell layer on ePTFE control grafts (left) and EOC-seeded type I collagen modified grafts (right). A distinct cell layer can be seen on both luminal surfaces. Deirdre Anderson assisted with the tissue ingrowth evaluations for this study.

5.6 Discussion

Difficulties in harvesting autologous cells has limited the usefulness of graft endothelialization strategies. EOCs are an attractive autologous cell source for vascular tissue engineering, because they are readily isolated from blood, expanded *in vitro*, and shown to grow and proliferate on ECM coated surfaces [91]. Wang et al. showed that ECM has an immediate affect on EOCs upon separation form blood. Isolation of the cells expanded on fibronectin coatings resulted in over twice the number of derived cells than cells isolated on type IV collagen, type I collagen and laminin [218]. The role of ECM coatings in regulating the hemostatic functions of EOCs remains largely unknown. Lund et al. demonstrated EOCs ability to respond to shear stress with a decrease in thrombotic and inflammatory gene markers when stimulated with $TNF\alpha$ [214]. Cuccini et al. demonstrated an EC like response to $TNF\alpha$ stimulation with increased TF and thrombin generation without affecting the cells migration, proliferation, or tube formation properties [215]. Ensley et al. also demonstrated EOCs ability to adopt a

thromboresistant phenotype with the application of shear stress under non-stimulated more physiologically relevant conditions [216]. This is the first study to investigate thrombotic and inflammatory responses of EOCs on different ECM-modified ePTFE vascular grafts.

Endothelial outgrowth cells (EOCs) were isolated from baboon circulating blood, and are derived from the endothelial progenitor cells (EPCs) pool found in circulating blood. EPCs and EOCs have both been used to describe populations of cells derived from peripheral blood and bone marrow. Timmermans et al. gives a detailed summary of the subtle difference in multiple cells populations that have been defined as endothelial progenitors [219]. EOCs was determined to be a better description for the cell population used in this study, since we selected for the late (5-22 days) outgrowth population of cells with mature endothelial cell markers [91]. EPCs have angiogenic potential and are thought to play a significant role in vascular injury repair [220].

The ECM is known to play a ubiquitous role in the regulation of mature endothelial cell phenotype, proliferation, apoptosis, cellular contractility, protein synthesis, and production of nitric oxide [9]. ECM composition modulates mature endothelial functions, and would therefore be expected to modulate the functions of EOCs. The ECM is key in sensing and responding to mechanical stimuli and acts as a mechanosensor via integrins to transmit signals to the ECs [10]. The effect of ECM substrate on EOC hemostatic phenotype was evaluated by changes in gene expression at 48 hours of coagulation and inflammatory gene panels. EOC functional responses were also measured through

activated protein C and factor Xa activity assays. The coagulation cascade is honed to respond to vascular injury or stress to protect the vasculature.

Flat plate *in vitro* assays were conducted to isolate the effect of protein surface alone on EOC functional responses. These studies were used to determine which proteins to use in three-dimensional graft construct *ex vivo* shunt and *in vivo* implant studies. There were significantly more cells on the type I collagen and fibronectin coated surfaces than on α -elastin and type IV collagen as evaluated by the pico green assay. It is not known why EOCs adhered and proliferated more readily on these surfaces, but it may be due to the adhesion mechanisms and proliferative cues of the protein matrix. The majority of the coagulation gene panel showed no differences in expression with the exception of EPCR and CD39 in which there were differences between both collagens as compared to α -elastin. The APC activity assay showed significantly higher activity, or greater protection on the type I collagen and fibronectin coated surfaces than on type IV collagen or α -elastin. There were no differences in factor Xa production in the tissue factor activity assay. Type I collagen and fibronectin were chosen for the three-dimensional ePTFE graft studies because of the more consistent growth properties and higher activity of APC.

Baboons with chronic femoral AV shunts were used to assess the effects of EPC functional responses on thrombus formation. This model was chosen because it is well established and permits excellent control of relevant variables including blood flow rate (arterial vs. venous), blood flow geometry (e.g., laminar vs. recirculating flow), the

nature of the thrombogenic surface, and the coagulability of the blood (e.g., no use of anticoagulants) [221-224]. As a result, outcomes have proven to be highly reproducible and the model has become a recognized means for evaluating mechanisms of thrombosis and the effects of therapeutic interventions [221-226].

EOCs seeded on type I collagen and fibronectin impregnated ePTFE confluent attached and spread on the lumen of our modified ePTFE grafts. Cell seeding and protein coating strategies were optimized for these studies. Protein coating procedures were tested with a range of concentrations from 0.5 mg/mL to 4 mg/mL. Protein quantification assays using the BCA protein assay (Thermo Scientific) were performed to confirm the deposition of protein on the graft surface. Graft surfaces were also stained with Oregon Green to confirm the consistency and completeness of protein distribution. The cell seeding protocol was tested with a range of cell concentrations and seeding methodologies. Cells were seeded between 5×10^4 to 3×10^5 cells/mL. Alternative rotation strategies were also evaluated. Strategies ranged from a single cell inoculation with 4 rotations of 90° over 2 hours to a single inoculation with no rotation to pinpoint the cell coverage of each seeding inoculation. About 1/3 of the lumen surface or a spread of 120° was obtained from the single inoculation testing. This result was expanded to achieve full overlapping cell coverage on the graft surface using three rotations of 120° and separate seeding inoculates spaced 40 minutes apart. Confluence was confirmed using this seeding protocol.

Ranjan et al. investigated the effect of ECM coatings on ECs derived from adult

saphenous vein and mammary arteries that when maintained in subconfluent densities expressed CD133 an EC precursor marker. These progenitor like cells had differential adhesion to ECM coatings when seeded on fibronectin, type I collagen, type IV collagen, and a mix of these proteins and showed resistance to shear detachment when seeded on ECM coated ePTFE [207]. These are not EOCs and are not a viable autologous cell source for vascular grafts, but are expected to respond similarly on ECM coatings of ePTFE. Durability studies were conducted on both type I collagen and fibronectin modified ePTFE tubular grafts to challenge EOC adhesion and resistance to shear detachment under *ex vivo* shunt conditions. Cell numbers initially dropped from the no flow starting condition but remained stable for one hour throughout the duration of a standard shunt study period. The initial slight drop in cell number was most likely due to loosely adherent cells washing off of the surface of the graft upon the initiation of flow. The durability of the cell attachment was also tested under *in vivo* flow conditions by ramping the flow rate to 250 mL/min. Cells remained stably adhered with no significant cell loss throughout the high flow test.

All study grafts remained patent throughout the *ex vivo* and *in vivo* studies. There was a variable platelet response in the *ex vivo* model with 0.11 to 2.03×10^9 platelets adhering to a 2 cm region at 40 minutes. There were no significant differences in platelet numbers between the fibronectin and type I collagen ePTFE grafts. This range seems to be due to a natural variability in the animal response to the EOCs. The protein used does not appear to influence the function of the cells enough to produce significant differences in platelet numbers.

There were no significant differences in gene expression for the coagulation and inflammatory gene panels for the *in vitro* ePTFE graft controls, with the exception of TFPI and VCAM between type I collagen and fibronectin. Interestingly, the factor Xa activity measured in the *in vitro* control for each of the *ex vivo* shunts, correlated to the number of platelets adhered to the graft surface, suggesting that the TF pathway is critical in determining initial success or failure due to thrombosis. Factor Xa generation in our EOC population is undetectable unless TFPI activity is blocked. Others have simulated the TF activity with TNF α to understand EOCs regulation of thrombosis [214, 215]. We used a TFPI antibody to isolate the response of TF under normal/nonstimulated physiological stress conditions. The APC activity assay did not result in similar correlations. This suggests that the TF pathway is the more critical or determinative pathway for initial graft response over the APC protective pathway. Thrombosis is a dynamic phenomenon with multiple factors combining to elicit a response. We believe that multiple factors should be evaluated when evaluating a vascular graft material, but factor Xa generation by TF may be a significant driving factor in predicting graft outcomes.

There is a significant need for predictive *in vitro* models that can predict *in vivo* outcomes. There are many research studies that characterize vascular cell responses to external stimuli such as, response to fluid flow, biochemical factors, and surface modifications. While these help in understanding biochemical signaling of vascular cells, it is not known what combination of factors will lead to a successful *in vivo* vascular graft

once tested in animal models. This need is amplified by the number of vascular graft materials currently in development and the relatively few that have succeeded and become clinical treatments for vascular disease.

5.7 Conclusions

ECM-modified two-dimensional flat plate and three-dimensional ePTFE graft surfaces were evaluated for thrombogenic and inflammatory responses of EOCs in *in vitro*, *ex vivo* shunt, and *in vivo* implant models. EOCs are a viable and readily isolated autologous cell source, which can be used to endothelialize tissue-engineered vascular biomaterials. This study suggests that the protein used to modify the surface did not have a significant influence on the EOCs gene, functional, platelet adhesion, or tissue ingrowth responses. The ECM two-dimensional coating studies showed significantly higher EOC cell density on type I collagen and fibronectin compared to type IV collagen and α -elastin. EOCs on type I collagen and fibronectin demonstrated less thrombogenic potential with significantly higher APC activity and EPCR gene expression, and along with their superior growth characteristics, were chosen for three-dimensional ePTFE studies. Three-dimensional ePTFE platelet accumulation studies showed no differences between protein substrates. There was a distinct correlation between the number of adhered platelets and factor Xa generation when TFPI activity was blocked. Tissue factor, controlling factor Xa generation, is a significant indicator of initial graft thrombosis and should be evaluated when predicting *in vivo* outcomes.

Chapter 6: Conclusions and Future Directions

6.1 Characterization of Protein Structure

Studies in Chapter 3 described the macroscopic structural characteristics of electrospun human recombinant tropoelastin biomaterials. It was shown that an increase in protein concentration leads to an increase in fiber diameter. Electrospinning parameters such as accelerating voltage gap distance and target dimensions can be used to design biomimetic scaffolds. This work characterized the macroscopic structure of the bulk electrospun materials, but did not evaluate protein microstructure and monomer organization.

Coacervation is a process by which tropoelastin monomers self-organize to assemble into elastin fibers prior to cross-linking and is exploitable *in vitro*. Preliminary TEM imaging was conducted on uncross-linked rTE coacervates (Figure 6.1). The self assembly of fibrils and banding of the protein was demonstrated.

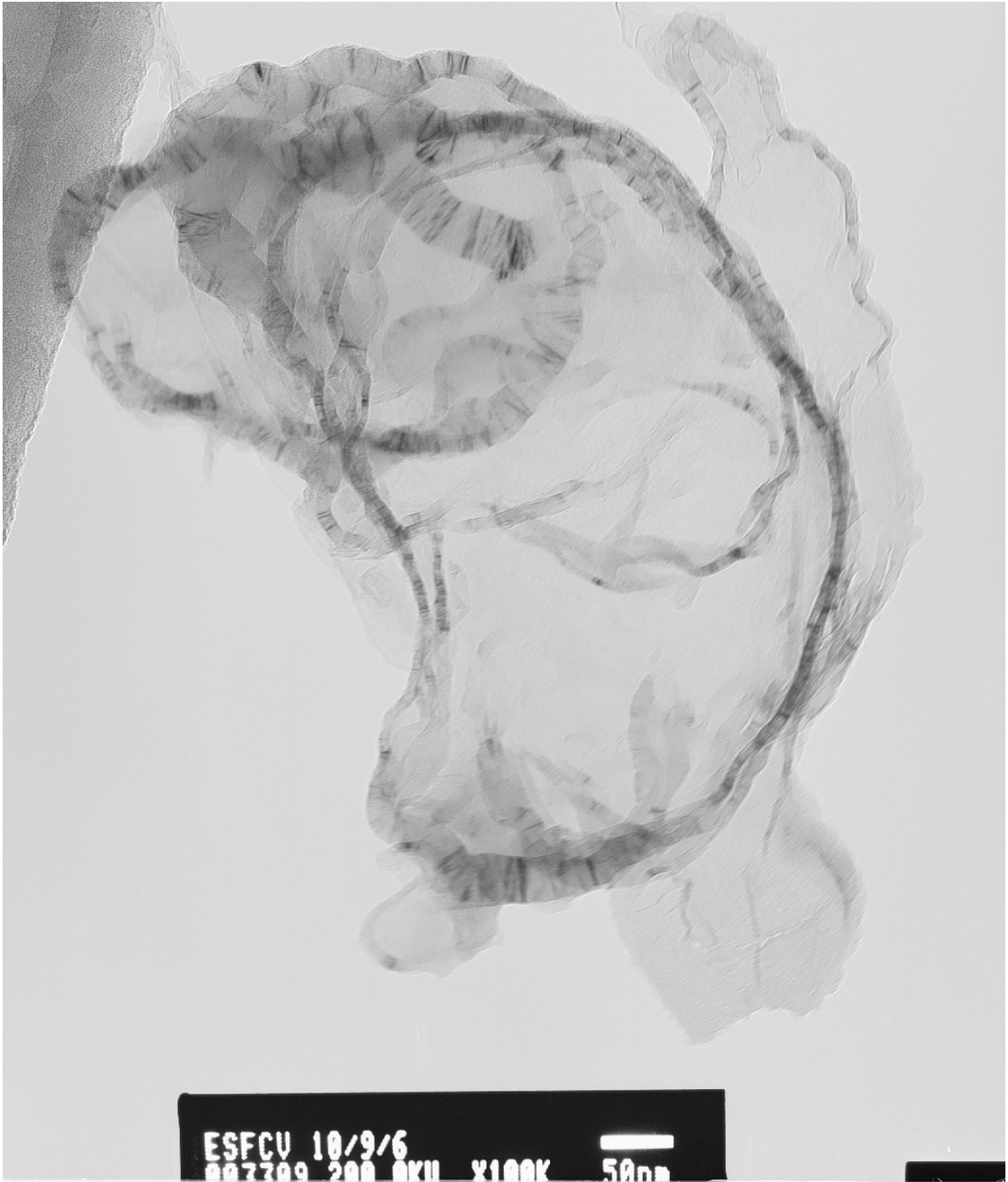


Figure 6.1. TEM of a tropoelastin coacervate. Banding can be seen along self assembled fibrils. TEM imaging was done with the assistance of Dr. Jack McCarthy.

Fibers with properties similar to native elastin could potentially be generated either by electrospinning from a tropoelastin coacervate or by inducing coacervation following electrospinning.

The first method requires electrospinning from an aqueous environment with controlled environmental conditions. The rTE solution will be suspended in PBS with a pH of 7.4 and heated to 37°C. Once the reaction is observed the separated aqueous phase will be removed from the syringe leaving behind an organized viscous rTE coacervate. While maintaining the temperature at 37°C, e.g. in an environmental chamber, the syringe will be loaded into the syringe pump and electrospun using a much lower delivery rate (0.2 mL/hr) and smaller gap distances, and has been validated for electrospinning other aqueous solutions. Once the parameters are optimized and shown to produce fibers, the protein structure will be evaluated for banding with TEM and circular dichroism for determining protein conformation.

The second method produces the initial biomaterial as described in Chapters 3 and 4, but alters the post processing. Prior to cross-linking, the electrospun mat will be loaded into an environmental chamber with temperature and humidity control. The humidity provides the water required for the reaction. The level of humidity will be set high enough to induce a conformational change in the protein, but not so high as to disassociate the macro-fiber structure. The temperature will be set to 37°C once the humidity is achieved. A balance of these parameters should be attainable such that the tropoelastin monomers within electrospun fibers organize into a native coacervate

organized assembly. Once organized, the biomaterial will be cross-linked, as before, to lock the structure in place. These biomaterials will also be evaluated for banding with TEM and circular dichroism to determine protein conformation.

6.2 Strengthening the Electrospun Tropoelastin Biomaterial

The biomaterials developed in Chapter 3 were evaluated for their mechanical properties in Chapter 4. These materials were shown to have similar mechanical characteristics to native elastin within the working physiologic loading range. To function effectively as a vascular graft biomaterial, a higher tensile failure stress and burst pressure will be required. This can be achieved by adding electrospun collagen to the matrix to create a true composite material. These composites can be designed to utilize the unique mechanical properties of each contributing material. Coelectrospinning has been developed and tested with tropoelastin and collagen. Flat plate studies have shown that cospinning affects the distribution and spread of the fibers (Figure 6.2). Tropoelastin spun at 15 wt% had a larger spread of fibers than 8.3 wt% collagen when coelectrospun onto a flat copper foil covered plate.

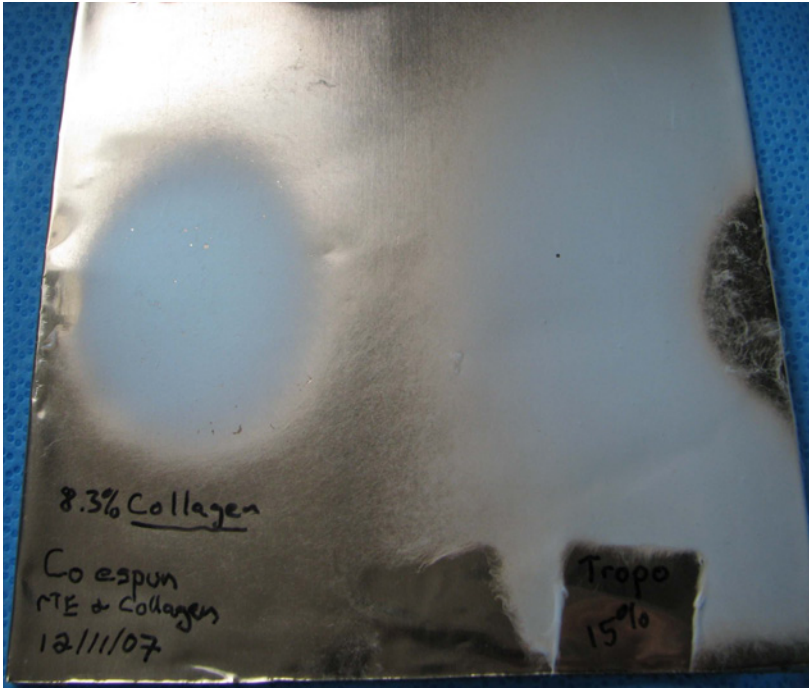


Figure 6.2. Distribution of fiber for co-electrospinning of collagen and tropoelastin. There was a larger spread of protein for tropoelastin than collagen. Collagen is shown on the left hand side and tropoelastin is shown on the right hand side.

Coelectrospinning uses two parallel sources, e.g. separate syringes, to interweave individual distinct fibers of collagen and tropoelastin (Figure 6.3). The resulting composite determines the mechanical properties of the matrix.

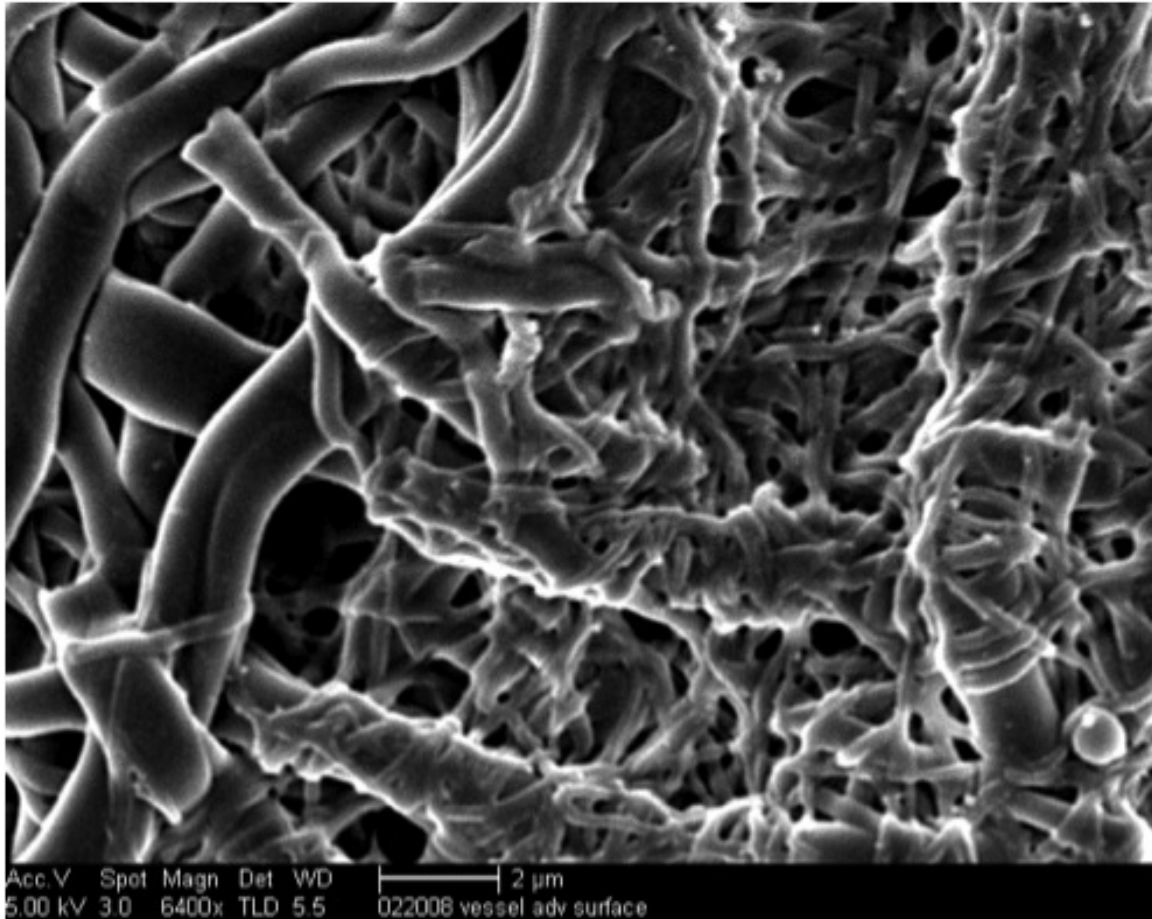


Figure 6.3. Coelectrospun tropoelastin and collagen fibers. Distinct fiber morphologies are seen within the biomaterial.

These studies have been initiated and materials of coelectrospun proteins produced. Mechanics of the material tend to be dominated by the collagen (data not shown). A careful design of a true composite material will be completed to maintain the elasticity provided by the tropoelastin and the higher tensile strength of electrospun collagen.

6.3 Strain energy density function of electrospun tropoelastin

Chapter 5 describes the derivation and application of a strain energy density function to extracted elastin. This was accomplished using a modified burst pressure biaxial testing

system. Longitudinal and circumferential displacements and force/pressure relationships were recorded dynamically. A model was defined for extracted elastin tubular constructs.

This method could be applied to the biomaterials developed in Chapters 3 and 4. Chapter 4 described the uniaxial mechanical properties of this biomaterial. It would be useful to test electrospun polytropoelastin spun onto 4mm diameter mandrels under biaxial loading conditions, as this is how the materials will be loaded *in vivo*. The same curve fit or function, polynomial, can be used for tropoelastin and extracted elastin as they showed similar uniaxial mechanical properties. Their mechanical properties can then be compared to uniaxial mechanical properties detailed in Chapter 4.

6.4 *In vivo* implant with paired controls

Chapter 6 evaluated individual ECM components' effect on thrombosis and inflammation using clinically relevant ePTFE synthetic graft models. Grafts were modified with ECM proteins and evaluated in *in vitro*, acute *ex vivo* shunt, and chronic *in vivo* test systems. This study demonstrates the importance of tissue factor, evaluated with a factor Xa activity assay, in the acute *ex vivo* thrombotic response.

Further work needs to be done to characterize the *in vivo* response of collagen modified ePTFE grafts seeded with EOCs. A power analysis indicated that 28 animals in each test group would be required to achieve significance. A change in the model will be implemented to reduce the number of animal required for this study. In Chapter 6 the same treatment group was implanted on both left and right sides with a single *in vitro*

control graft. Statistical power and efficiency will be added to the study by implementing a change in the implant model. A power analysis determined that 7 implant animals will be required to achieve significance with an α of 0.05 and 80% power. A control and a treatment graft will be implanted in each animal, along with corresponding *in vitro* controls; paired results will decrease the effect of variability between animals and will double the effective sample number. The results will be compared to *in vitro* gene expression as well as functional activity assays to determine predictive outcomes for the chronic studies.

6.5 Flow Conditioning of EOC-seeded Collagen Modified ePTFE Grafts

Studies in Chapter 6 were conducted using media conditioning alone under static conditions. Flow conditioning will be applied to the grafts to induce prothrombotic and antithrombotic conditions. Laminar shear stress is known to be atheroprotective and induce antithrombotic cellular responses. Oscillatory flow induces the prothrombotic condition. These flow profiles will be applied to tubular ePTFE grafts to change the gene expression and functional assay profile. The study model was designed such that the addition of flow variables will be easily implemented. Grafts will be tested in parallel in *ex vivo* shunts and *in vivo* implants, and will be compared to the *in vitro* results to determine *in vitro* predictors of success.

6.6 Scientific Impact

This work highlights the importance of elastin in vascular graft design and the practical development of elastin biomaterials using human recombinant tropoelastin. Collagen and

elastin are the two major structural proteins of the arterial wall. End stage aneurysm disease and supraaortic stenosis have been associated with the pathologic loss of elastin or deficiency in elastin expression [19-26]. Elastin has unique properties making it a natural choice as a component in tissue-engineered constructs that require long term durability, antithrombogenic properties, and elasticity. Elastin demonstrates these properties: it is highly insoluble with a half life greater than 70 years; modulates cell function reducing the thrombogenic potential of the surface; and it is highly elastic, adding needed compliance to the structure of the material [180]. The amount of scientific research conducted with each protein is highly skewed toward collagen due to its availability and relatively low cost. A PubMed search for 2010 through May 2011, yielded 1566 references with collagen in their titles, but only 103 references to elastin, and just 18 for tropoelastin. Tropoelastin can be produced with standard recombinant protein production and purification techniques in quantities sufficient to enable meaningful research projects. As the importance of elastin and its precursor tropoelastin become recognized, an increase in demand will lower its cost. This work will help promote awareness within the scientific community of the importance of elastin in the development of clinically relevant biomaterials.

While electrospun tropoelastin vascular biomaterials were under further development to add structural tensile support prior to *in vivo* evaluation, the effect of various ECM coatings were evaluated in a clinically relevant ePTFE graft model. The EOC-seeded ECM-modified ePTFE work not only gives insight into the effect of protein surfaces on vascular functional response, it also provides a means by which tissue engineering

researchers will be able to more accurately predict the success or failure of vascular biomaterials using *in vitro* models. This work also highlights the utility of EOCs in tissue engineering. EOCs are a unique and promising autologous cell source for tissue-engineered constructs and should be considered in construct design.

The strain energy density function model and testing system provides a means to attain valuable mechanical properties congruent with burst testing. This is particularly important for biomaterial constructs that are scarce or timely to produce. Burst pressure testing is an important mechanical property, but often only yields information regarding the weakest point of a material. Additional mechanical data inferred from each test will help researchers understand the failure modes of their constructs, thus promoting their development.

The ultimate goal of this work is to understand how the ECM effects vascular functional responses in order to develop clinical vascular graft technologies equivalent to the current gold standards, saphenous veins and mammary arteries, and globally to enable the transition of biomaterials from the benchtop to viable clinical treatments.

References

- [1] AHA. Heart Disease and Stroke Statistics – 2010 Update Dallas, Texas: American Heart Association; 2010.
- [2] Frangos SG, Gahtan V, Sumpio B. Localization of atherosclerosis: role of hemodynamics. *Archives of Surgery* 1999;134:1142-9.
- [3] Kolessov V. Mammary artery-coronary artery anastomosis as method of treatment for angina pectoris. *J Thorac Cardiovasc Surg* 1967;54:535-44.
- [4] L'Heureux N, Dusserre N, Marini A, Garrido S, de la Fuente L, McAllister T. Technology insight: the evolution of tissue-engineered vascular grafts--from research to clinical practice. *Nature clinical practice* 2007;4:389-95.
- [5] Klinkert P, Post PN, Breslau PJ, van Bockel JH. Saphenous vein versus PTFE for above-knee femoropopliteal bypass. A review of the literature. *Eur J Vasc Endovasc Surg* 2004;27:357-62.
- [6] Florian A, Cohn LH, Dammin GJ, Collins JJ, Jr. Small vessel replacement with gore-tex (expanded polytetrafluoroethylene). *Arch Surg* 1976;111:267-70.
- [7] Abbott WM, Rehring TF. Biologic and synthetic prosthetic materials for vascular conduits. In: Hobson RW, Wilson S, Veith FJ, editors. *Vascular Surgery: Principles and Practice* (3rd Edition). New York: Marcel Dekker; 2004. p. 611 – 20.
- [8] Kusumoto FM, M.D. *Cardiovascular Pathophysiology*. First Edition ed. Madison: Fence Creek Publishing; 1999.
- [9] Davis GE, Senger DR. Endothelial extracellular matrix: biosynthesis, remodeling, and functions during vascular morphogenesis and neovessel stabilization. *Circ Res* 2005;97:1093-107.
- [10] Schwartz MA. Integrins and extracellular matrix in mechanotransduction. *Cold Spring Harb Perspect Biol* 2010;2:a005066.
- [11] Weber M. Basement membrane proteins. *Kidney Int* 1992;41:620-8.
- [12] Giro MG, Davidson JM. Elastin. *Methods in enzymology* 1988;163:656-73.
- [13] Uitto J. Biochemistry of the elastic fibers in normal connective tissues and its alterations in diseases. *The Journal of investigative dermatology* 1979;72:1-10.

- [14] Vrhovski B, Weiss AS. Biochemistry of tropoelastin. *European journal of biochemistry / FEBS* 1998;258:1-18.
- [15] Bressan GM, Argos P, Stanley KK. Repeating structure of chick tropoelastin revealed by complementary DNA cloning. *Biochemistry* 1987;26:1497-503.
- [16] Indik Z, Yeh H, Ornstein-Goldstein N, Sheppard P, Anderson N, Rosenbloom JC, et al. Alternative splicing of human elastin mRNA indicated by sequence analysis of cloned genomic and complementary DNA. *Proc Natl Acad Sci U S A* 1987;84:5680-4.
- [17] Pierce RA, Deak SB, Stolle CA, Boyd CD. Heterogeneity of rat tropoelastin mRNA revealed by cDNA cloning. *Biochemistry* 1990;29:9677-83.
- [18] Raju K, Anwar RA. Primary structures of bovine elastin a, b, and c deduced from the sequences of cDNA clones. *J Biol Chem* 1987;262:5755-62.
- [19] Baxter BT, McGee GS, Shively VP, Drummond IA, Dixit SN, Yamauchi M, et al. Elastin content, cross-links, and mRNA in normal and aneurysmal human aorta. *J Vasc Surg* 1992;16:192-200.
- [20] Curran ME, Atkinson DL, Ewart AK, Morris CA, Leppert MF, Keating MT. The elastin gene is disrupted by a translocation associated with supravalvular aortic stenosis. *Cell* 1993;73:159-68.
- [21] Ewart AK, Jin W, Atkinson D, Morris CA, Keating MT. Supravalvular aortic stenosis associated with a deletion disrupting the elastin gene. *The Journal of clinical investigation* 1994;93:1071-7.
- [22] Gandhi RH, Irizarry E, Cantor JO, Keller S, Nackman GB, Halpern VJ, et al. Analysis of elastin cross-linking and the connective tissue matrix of abdominal aortic aneurysms. *Surgery* 1994;115:617-20.
- [23] Hunter GC, Dubick MA, Keen CL, Eskelson CD. Effects of hypertension on aortic antioxidant status in human abdominal aneurysmal and occlusive disease. *Proceedings of the Society for Experimental Biology and Medicine Society for Experimental Biology and Medicine (New York, NY)* 1991;196:273-9.
- [24] Li DY, Toland AE, Boak BB, Atkinson DL, Ensing GJ, Morris CA, et al. Elastin point mutations cause an obstructive vascular disease, supravalvular aortic stenosis. *Hum Mol Genet* 1997;6:1021-8.

- [25] Rizzo RJ, McCarthy WJ, Dixit SN, Lilly MP, Shively VP, Flinn WR, et al. Collagen types and matrix protein content in human abdominal aortic aneurysms. *J Vasc Surg* 1989;10:365-73.
- [26] Urban Z, Michels VV, Thibodeau SN, Donis-Keller H, Csiszar K, Boyd CD. Supravalvular aortic stenosis: a splice site mutation within the elastin gene results in reduced expression of two aberrantly spliced transcripts. *Hum Genet* 1999;104:135-42.
- [27] Alberts BJ, Alexander; Lewis, Julian; Raff, Martin; Roberts, Keith; Walter, Peter. *Molecular Biology of the Cell*. 4th ed. ed. New York and London: Garland Science; 2002.
- [28] Muiznieks LD, Weiss AS, Keeley FW. Structural disorder and dynamics of elastin. *Biochem Cell Biol* 2010;88:239-50.
- [29] Baldock C, Oberhauser AF, Ma L, Lammie D, Siegler V, Mithieux SM, et al. Shape of tropoelastin, the highly extensible protein that controls human tissue elasticity. *Proceedings of the National Academy of Sciences of the United States of America* 2011;108:4322-7.
- [30] Wise SG, Weiss AS. Tropoelastin. *Int J Biochem Cell Biol* 2009;41:494-7.
- [31] Hinek A, Braun KR, Liu K, Wang Y, Wight TN. Retrovirally mediated overexpression of versican v3 reverses impaired elastogenesis and heightened proliferation exhibited by fibroblasts from Costello syndrome and Hurler disease patients. *Am J Pathol* 2004;164:119-31.
- [32] Toonkool P, Regan DG, Kuchel PW, Morris MB, Weiss AS. Thermodynamic and hydrodynamic properties of human tropoelastin. Analytical ultracentrifuge and pulsed field-gradient spin-echo NMR studies. *J Biol Chem* 2001;276:28042-50.
- [33] Vrhovski B, Jensen S, Weiss AS. Coacervation characteristics of recombinant human tropoelastin. *European journal of biochemistry / FEBS* 1997;250:92-8.
- [34] Fischer GM, Llauro JG. Collagen and elastin content in canine arteries selected from functionally different vascular beds. *Circulation research* 1966;19:394-9.
- [35] Gelse K, Poschl E, Aigner T. Collagens--structure, function, and biosynthesis. *Adv Drug Deliv Rev* 2003;55:1531-46.
- [36] Malfait F, Wenstrup RJ, De Paepe A. Clinical and genetic aspects of Ehlers-Danlos syndrome, classic type. *Genet Med* 2010;12:597-605.

- [37] Marini JC, Forlino A, Cabral WA, Barnes AM, San Antonio JD, Milgrom S, et al. Consortium for osteogenesis imperfecta mutations in the helical domain of type I collagen: regions rich in lethal mutations align with collagen binding sites for integrins and proteoglycans. *Hum Mutat* 2007;28:209-21.
- [38] Stanley JR, Woodley DT, Katz SI, Martin GR. Structure and function of basement membrane. *The Journal of investigative dermatology* 1982;79 Suppl 1:69s-72s.
- [39] Pankov R, Yamada KM. Fibronectin at a glance. *J Cell Sci* 2002;115:3861-3.
- [40] Hay ED. *Cell biology of Extracellular Matrix*. 2nd ed. New York, NY: Plenum Press; 1991.
- [41] Sawyer PN, Fitzgerald J, Kaplitt MJ, Sanders RJ, Williams GM, Leather RP, et al. Ten year experience with the negatively charged glutaraldehyde-tanned vascular graft in peripheral vascular surgery. Initial multicenter trial. *Am J Surg* 1987;154:533-7.
- [42] Dardik H, Wengerter K, Qin F, Pangilinan A, Silvestri F, Wolodiger F, et al. Comparative decades of experience with glutaraldehyde-tanned human umbilical cord vein graft for lower limb revascularization: an analysis of 1275 cases. *J Vasc Surg* 2002;35:64-71.
- [43] Strobel R, Boontje AH, Van Den Dungen JJ. Aneurysm formation in modified human umbilical vein grafts. *Eur J Vasc Endovasc Surg* 1996;11:417-20.
- [44] Gui L, Muto A, Chan SA, Breuer CK, Niklason LE. Development of decellularized human umbilical arteries as small-diameter vascular grafts. *Tissue Eng Part A* 2009;15:2665-76.
- [45] McAllister TN, Maruszewski M, Garrido SA, Wystrychowski W, Dusserre N, Marini A, et al. Effectiveness of haemodialysis access with an autologous tissue-engineered vascular graft: a multicentre cohort study. *Lancet* 2009;373:1440-6.
- [46] Bhattarai SR, Bhattarai N, Yi HK, Hwang PH, Cha DI, Kim HY. Novel biodegradable electrospun membrane: scaffold for tissue engineering. *Biomaterials* 2004;25:2595-602.
- [47] Katti DS, Robinson KW, Ko FK, Laurencin CT. Bioresorbable nanofiber-based systems for wound healing and drug delivery: optimization of fabrication parameters. *J Biomed Mater Res B Appl Biomater* 2004;70:286-96.

- [48] Kim K, Yu M, Zong X, Chiu J, Fang D, Seo YS, et al. Control of degradation rate and hydrophilicity in electrospun non-woven poly(D,L-lactide) nanofiber scaffolds for biomedical applications. *Biomaterials* 2003;24:4977-85.
- [49] Li WJ, Laurencin CT, Caterson EJ, Tuan RS, Ko FK. Electrospun nanofibrous structure: a novel scaffold for tissue engineering. *Journal of biomedical materials research* 2002;60:613-21.
- [50] Khil MS, Cha DI, Kim HY, Kim IS, Bhattarai N. Electrospun nanofibrous polyurethane membrane as wound dressing. *J Biomed Mater Res B Appl Biomater* 2003;67:675-9.
- [51] Li WJ, Danielson KG, Alexander PG, Tuan RS. Biological response of chondrocytes cultured in three-dimensional nanofibrous poly(epsilon-caprolactone) scaffolds. *J Biomed Mater Res A* 2003;67:1105-14.
- [52] Mo XM, Xu CY, Kotaki M, Ramakrishna S. Electrospun P(LLA-CL) nanofiber: a biomimetic extracellular matrix for smooth muscle cell and endothelial cell proliferation. *Biomaterials* 2004;25:1883-90.
- [53] Shin M, Ishii O, Sueda T, Vacanti JP. Contractile cardiac grafts using a novel nanofibrous mesh. *Biomaterials* 2004;25:3717-23.
- [54] Shin M, Yoshimoto H, Vacanti JP. In vivo bone tissue engineering using mesenchymal stem cells on a novel electrospun nanofibrous scaffold. *Tissue engineering* 2004;10:33-41.
- [55] Xu CY, Inai R, Kotaki M, Ramakrishna S. Aligned biodegradable nanofibrous structure: a potential scaffold for blood vessel engineering. *Biomaterials* 2004;25:877-86.
- [56] Yoshimoto H, Shin YM, Terai H, Vacanti JP. A biodegradable nanofiber scaffold by electrospinning and its potential for bone tissue engineering. *Biomaterials* 2003;24:2077-82.
- [57] Boland ED, Matthews JA, Pawlowski KJ, Simpson DG, Wnek GE, Bowlin GL. Electrospinning collagen and elastin: preliminary vascular tissue engineering. *Front Biosci* 2004;9:1422-32.
- [58] Matthews JA, Wnek GE, Simpson DG, Bowlin GL. Electrospinning of collagen nanofibers. *Biomacromolecules* 2002;3:232-8.

- [59] Huang L, Apkarian RP, Chaikof EL. High-resolution analysis of engineered type I collagen nanofibers by electron microscopy. *Scanning* 2001;23:372-5.
- [60] Huang L, Nagapudi K, Apkarian RP, Chaikof EL. Engineered collagen-PEO nanofibers and fabrics. *J Biomater Sci Polym Ed* 2001;12:979-93.
- [61] Li M, Mondrinos MJ, Gandhi MR, Ko FK, Weiss AS, Lelkes PI. Electrospun protein fibers as matrices for tissue engineering. *Biomaterials* 2005;26:5999-6008.
- [62] Zilla P, Bezuidenhout D, Human P. Prosthetic vascular grafts: wrong models, wrong questions and no healing. *Biomaterials* 2007;28:5009-27.
- [63] Sarkar S, Sales KM, Hamilton G, Seifalian AM. Addressing thrombogenicity in vascular graft construction. *J Biomed Mater Res B Appl Biomater* 2007;82:100-8.
- [64] Guidoin R, Marois Y, Deng X, Chakfe N, Marois M, Roy R, et al. Can collagen impregnated polyester arterial prostheses be recommended as small diameter blood conduits? *ASAIO J* 1996;42:974-83.
- [65] Olsson P, Sanchez J, Mollnes TE, Riesenfeld J. On the blood compatibility of end-point immobilized heparin. *J Biomater Sci Polym Ed* 2000;11:1261-73.
- [66] Tanzi MC. Bioactive technologies for hemocompatibility. *Expert Rev Med Devices* 2005;2:473-92.
- [67] Lin PH, Chen C, Bush RL, Yao Q, Lumsden AB, Hanson SR. Small-caliber heparin-coated ePTFE grafts reduce platelet deposition and neointimal hyperplasia in a baboon model. *J Vasc Surg* 2004;39:1322-8.
- [68] Lin PH, Bush RL, Yao Q, Lumsden AB, Chen C. Evaluation of platelet deposition and neointimal hyperplasia of heparin-coated small-caliber ePTFE grafts in a canine femoral artery bypass model. *J Surg Res* 2004;118:45-52.
- [69] Aldenhoff YB, van Der Veen FH, ter Woorst J, Habets J, Poole-Warren LA, Koole LH. Performance of a polyurethane vascular prosthesis carrying a dipyridamole (Persantin) coating on its luminal surface. *J Biomed Mater Res* 2001;54:224-33.
- [70] van der Lei B, Bartels HL, Robinson PH, Bakker WW. Reduced thrombogenicity of vascular prostheses by coating with ADP-ase. *Int Angiol* 1992;11:268-71.
- [71] Costa AF, Gamermann PW, Picon PX, Mosmann MP, Kettlun AM, Valenzuela MA, et al. Intravenous apyrase administration reduces arterial thrombosis in a rabbit model of endothelial denudation in vivo. *Blood Coagul Fibrinolysis* 2004;15:545-51.

- [72] Rubin BG, Toursarkissian B, Petrincec D, Yang LY, Eisenberg PR, Abendschein DR. Preincubation of Dacron grafts with recombinant tissue factor pathway inhibitor decreases their thrombogenicity in vivo. *J Vasc Surg* 1996;24:865-70.
- [73] Sun LB, Utoh J, Moriyama S, Tagami H, Okamoto K, Kitamura N. Pretreatment of a Dacron graft with tissue factor pathway inhibitor decreases thrombogenicity and neointimal thickness: a preliminary animal study. *ASAIO J* 2001;47:325-8.
- [74] Kowalewski R, Zimnoch L, Wojtukiewicz MZ, Glowinski S, Glowinski J. Coagulation activators and inhibitors in the neointima of polyester vascular grafts. *Blood Coagul Fibrinolysis* 2003;14:433-9.
- [75] Mureebe L, Turnquist SE, Silver D. Inhibition of intimal hyperplasia by direct thrombin inhibitors in an animal vein bypass model. *Ann Vasc Surg* 2004;18:147-50.
- [76] McGuigan AP, Sefton MV. The influence of biomaterials on endothelial cell thrombogenicity. *Biomaterials* 2007;28:2547-71.
- [77] Graham LM, Vinter DW, Ford JW, Kahn RH, Burkel WE, Stanley JC. Endothelial cell seeding of prosthetic vascular grafts: early experimental studies with cultured autologous canine endothelium. *Arch Surg* 1980;115:929-33.
- [78] Zhang Z, Wang Z, Liu S, Kodama M. Pore size, tissue ingrowth, and endothelialization of small-diameter microporous polyurethane vascular prostheses. *Biomaterials* 2004;25:177-87.
- [79] Bordenave L, Remy-Zolghadri M, Fernandez P, Bareille R, Midy D. Clinical performance of vascular grafts lined with endothelial cells. *Endothelium* 1999;6:267-75.
- [80] Davies P, F. Flow-mediated endothelial mechanotransduction. *Physiological Reviews* 1995;75:519-60.
- [81] Traub O, Berk BC. Laminar shear stress: mechanisms by which endothelial cells transduce an atheroprotective force. *Arteriosclerosis, Thrombosis, and Vascular Biology* 1998;18:677-85.
- [82] Barakat A, I. Responsiveness of vascular endothelium to shear stress: Potential role of ion channels and cellular cytoskeleton (Review). *International Journal of Molecular Medicine* 1999;4:323-32.

- [83] Kaushal S, Amiel GE, Guleserian KJ, Shapira OM, Perry T, Sutherland FW, et al. Functional small-diameter neovessels created using endothelial progenitor cells expanded ex vivo. *Nat Med* 2001;7:1035-40.
- [84] Griese DP, Ehsan A, Melo LG, Kong D, Zhang L, Mann MJ, et al. Isolation and transplantation of autologous circulating endothelial cells into denuded vessels and prosthetic grafts: implications for cell-based vascular therapy. *Circulation* 2003;108:2710-5.
- [85] Asahara T, Murohara T, Sullivan A, Silver M, van der Zee R, Li T, et al. Isolation of putative progenitor endothelial cells for angiogenesis. *Science* 1997;275:964-7.
- [86] Lin Y, Weisdorf DJ, Solovey A, Hebbel RP. Origins of circulating endothelial cells and endothelial outgrowth from blood. *The Journal of clinical investigation* 2000;105:71-7.
- [87] Salacinski HJ, Tiwari A, Hamilton G, Seifalian AM. Cellular engineering of vascular bypass grafts: role of chemical coatings for enhancing endothelial cell attachment. *Med Biol Eng Comput* 2001;39:609-18.
- [88] Assmus B, Schachinger V, Teupe C, Britten M, Lehmann R, Dobert N, et al. Transplantation of Progenitor Cells and Regeneration Enhancement in Acute Myocardial Infarction (TOPCARE-AMI). *Circulation* 2002;106:3009-17.
- [89] Beranek JT. Vascular endothelial cell is a stem cell for neointimal formation after injury. *J Thorac Cardiovasc Surg* 2001;121:820-1.
- [90] Rafii S, Lyden D. Therapeutic stem and progenitor cell transplantation for organ vascularization and regeneration. *Nat Med* 2003;9:702-12.
- [91] Hinds MT, Ma M, Tran N, Ensley AE, Kladakis SM, Vartanian KB, et al. Potential of baboon endothelial progenitor cells for tissue engineered vascular grafts. *J Biomed Mater Res A* 2008;86:804-12.
- [92] Broekelmann TJ, Kozel BA, Ishibashi H, Werneck CC, Keeley FW, Zhang L, et al. Tropoelastin interacts with cell-surface glycosaminoglycans via its COOH-terminal domain. *J Biol Chem* 2005;280:40939-47.
- [93] Mecham RP, Hinek A, Entwistle R, Wrenn DS, Griffin GL, Senior RM. Elastin binds to a multifunctional 67-kilodalton peripheral membrane protein. *Biochemistry* 1989;28:3716-22.

- [94] Mochizuki S, Brassart B, Hinek A. Signaling pathways transduced through the elastin receptor facilitate proliferation of arterial smooth muscle cells. *J Biol Chem* 2002;277:44854-63.
- [95] Akiyama SK. Integrins in cell adhesion and signaling. *Hum Cell* 1996;9:181-6.
- [96] Rodgers UR, Weiss AS. Integrin alpha v beta 3 binds a unique non-RGD site near the C-terminus of human tropoelastin. *Biochimie* 2004;86:173-8.
- [97] Karnik SK, Brooke BS, Bayes-Genis A, Sorensen L, Wythe JD, Schwartz RS, et al. A critical role for elastin signaling in vascular morphogenesis and disease. *Development* 2003;130:411-23.
- [98] Hinek A, Rabinovitch M. The ductus arteriosus migratory smooth muscle cell phenotype processes tropoelastin to a 52-kDa product associated with impaired assembly of elastic laminae. *J Biol Chem* 1993;268:1405-13.
- [99] Hinek A, Wrenn DS, Mecham RP, Barondes SH. The elastin receptor: a galactoside-binding protein. *Science* 1988;239:1539-41.
- [100] Robert L, Jacob MP, Fulop T, Timar J, Hornebeck W. Elastonection and the elastin receptor. *Pathol Biol (Paris)* 1989;37:736-41.
- [101] Mecham RP, Hinek A, Griffin GL, Senior RM, Liotta LA. The elastin receptor shows structural and functional similarities to the 67-kDa tumor cell laminin receptor. *J Biol Chem* 1989;264:16652-7.
- [102] Blood CH, Sasse J, Brodt P, Zetter BR. Identification of a tumor cell receptor for VGVAPG, an elastin-derived chemotactic peptide. *J Cell Biol* 1988;107:1987-93.
- [103] Hornebeck W, Tixier JM, Robert L. Inducible adhesion of mesenchymal cells to elastic fibers: elastonection. *Proc Natl Acad Sci U S A* 1986;83:5517-20.
- [104] Grosso LE, Scott M. PGAIPG, a repeated hexapeptide of bovine and human tropoelastin, is chemotactic for neutrophils and Lewis lung carcinoma cells. *Archives of biochemistry and biophysics* 1993;305:401-4.
- [105] Long MM, King VJ, Prasad KU, Freeman BA, Urry DW. Elastin repeat peptides as chemoattractants for bovine aortic endothelial cells. *J Cell Physiol* 1989;140:512-8.
- [106] Davies PF. Hemodynamic shear stress and the endothelium in cardiovascular pathophysiology. *Nature clinical practice* 2009;6:16-26.

- [107] Bertina RM. The role of procoagulants and anticoagulants in the development of venous thromboembolism. *Thromb Res* 2009;123 Suppl 4:S41-5.
- [108] Lloyd-Jones D, Adams RJ, Brown TM, Carnethon M, Dai S, De Simone G, et al. Heart disease and stroke statistics--2010 update: a report from the American Heart Association. *Circulation*;121:e46-e215.
- [109] Brewster DC. Prosthetic grafts (4th ed). In: Rutherford RB, editor. *Vascular Surgery*. Philadelphia: W. B. Saunders; 1995. p. 492–521.
- [110] Megelski S, Stephens JS, Chase DB, Rabolt JF. Micro- and Nanostructured Surface Morphology on Electrospun Polymer Fibers. *Macromolecules* 2002;35:8456-66.
- [111] Murugan R, Ramakrishna S. Nano-featured scaffolds for tissue engineering: a review of spinning methodologies. *Tissue engineering* 2006;12:435-47.
- [112] Roach MR, Burton AC. The reason for the shape of the distensibility curves of arteries. *Canadian journal of biochemistry and physiology* 1957;35:681-90.
- [113] Daamen WF, Veerkamp JH, van Hest JC, van Kuppevelt TH. Elastin as a biomaterial for tissue engineering. *Biomaterials* 2007;28:4378-98.
- [114] Patel A, Fine B, Sandig M, Mequanint K. Elastin biosynthesis: The missing link in tissue-engineered blood vessels. *Cardiovasc Res* 2006;71:40-9.
- [115] Buttafoco L, Kolkman NG, Poot AA, Dijkstra PJ, Vermes I, Feijen J. Electrospinning collagen and elastin for tissue engineering small diameter blood vessels. *J Control Release* 2005;101:322-4.
- [116] Buttafoco L, Kolkman NG, Engbers-Buijtenhuijs P, Poot AA, Dijkstra PJ, Vermes I, et al. Electrospinning of collagen and elastin for tissue engineering applications. *Biomaterials* 2006;27:724-34.
- [117] Lee SJ, Yoo JJ, Lim GJ, Atala A, Stitzel J. In vitro evaluation of electrospun nanofiber scaffolds for vascular graft application. *J Biomed Mater Res A* 2007;83:999-1008.
- [118] Li M, Mondrinos MJ, Chen X, Gandhi MR, Ko FK, Lelkes PI. Co-electrospun poly(lactide-co-glycolide), gelatin, and elastin blends for tissue engineering scaffolds. *J Biomed Mater Res A* 2006;79:963-73.
- [119] Stitzel J, Liu J, Lee SJ, Komura M, Berry J, Soker S, et al. Controlled fabrication of a biological vascular substitute. *Biomaterials* 2006;27:1088-94.

- [120] Rnjak J, Li Z, Maitz PK, Wise SG, Weiss AS. Primary human dermal fibroblast interactions with open weave three-dimensional scaffolds prepared from synthetic human elastin. *Biomaterials* 2009;30:6469-77.
- [121] Lowry O, Gilligan D, Katersky E. The determination of collagen and elastin in tissues, with results obtained in various normal tissues from different species. *J Biol Chem* 1941;139:795-804.
- [122] Lansing A, Rosenthal T, Alex M, Dempsey E. The structure and chemical characterization of elastic fibers as revealed by elastase and by electron microscopy. *Anat Rec* 1952;114:555-75.
- [123] Vartanian KB, Kirkpatrick SJ, Hanson SR, Hinds MT. Endothelial cell cytoskeletal alignment independent of fluid shear stress on micropatterned surfaces. *Biochem Biophys Res Commun* 2008;371:787-92.
- [124] Stegemann JP, Nerem RM. Phenotype modulation in vascular tissue engineering using biochemical and mechanical stimulation. *Ann Biomed Eng* 2003;31:391-402.
- [125] Heydarkhan-Hagvall S, Schenke-Layland K, Dhanasopon AP, Rofail F, Smith H, Wu BM, et al. Three-dimensional electrospun ECM-based hybrid scaffolds for cardiovascular tissue engineering. *Biomaterials* 2008;29:2907-14.
- [126] Smith MJ, McClure MJ, Sell SA, Barnes CP, Walpoth BH, Simpson DG, et al. Suture-reinforced electrospun polydioxanone-elastin small-diameter tubes for use in vascular tissue engineering: a feasibility study. *Acta Biomater* 2008;4:58-66.
- [127] Smith MJ, White KL, Jr., Smith DC, Bowlin GL. In vitro evaluations of innate and acquired immune responses to electrospun polydioxanone-elastin blends. *Biomaterials* 2009;30:149-59.
- [128] Thomas V, Zhang X, Catledge SA, Vohra YK. Functionally graded electrospun scaffolds with tunable mechanical properties for vascular tissue regeneration. *Biomed Mater* 2007;2:224-32.
- [129] Zhang X, Thomas V, Xu Y, Bellis SL, Vohra YK. An in vitro regenerated functional human endothelium on a nanofibrous electrospun scaffold. *Biomaterials*;31:4376-81.
- [130] Koombhongse S, Liu W, Reneker DH. Flat polymer ribbons and other shapes by electrospinning. *Journal of Polymer Science Part B: Polymer Physics* 2001;39:2598-606.

- [131] Zeugolis DI, Paul GR, Attenburrow G. Cross-linking of extruded collagen fibers--a biomimetic three-dimensional scaffold for tissue engineering applications. *J Biomed Mater Res A* 2009;89:895-908.
- [132] Mithieux SM, Rasko JE, Weiss AS. Synthetic elastin hydrogels derived from massive elastic assemblies of self-organized human protein monomers. *Biomaterials* 2004;25:4921-7.
- [133] Mithieux SM, Wise SG, Raftery MJ, Starcher B, Weiss AS. A model two-component system for studying the architecture of elastin assembly in vitro. *J Struct Biol* 2005;149:282-9.
- [134] Wise SG, Mithieux SM, Raftery MJ, Weiss AS. Specificity in the coacervation of tropoelastin: solvent exposed lysines. *J Struct Biol* 2005;149:273-81.
- [135] Nivison-Smith L, Rnjak J, Weiss AS. Synthetic human elastin microfibers: stable cross-linked tropoelastin and cell interactive constructs for tissue engineering applications. *Acta Biomater*;6:354-9.
- [136] Dyksterhuis LB, Baldock C, Lammie D, Wess TJ, Weiss AS. Domains 17-27 of tropoelastin contain key regions of contact for coacervation and contain an unusual turn-containing crosslinking domain. *Matrix Biol* 2007;26:125-35.
- [137] Karnik SK, Wythe JD, Sorensen L, Brooke BS, Urness LD, Li DY. Elastin induces myofibrillogenesis via a specific domain, VGVAPG. *Matrix Biol* 2003;22:409-25.
- [138] Hinek A, Rabinovitch M, Keeley F, Okamura-Oho Y, Callahan J. The 67-kD elastin/laminin-binding protein is related to an enzymatically inactive, alternatively spliced form of beta-galactosidase. *J Clin Invest* 1993;91:1198-205.
- [139] Bax DV, Rodgers UR, Bilek MM, Weiss AS. Cell adhesion to tropoelastin is mediated via the C-terminal GRKRRK motif and integrin alphaVbeta3. *J Biol Chem* 2009;284:28616-23.
- [140] Lloyd-Jones D, Adams RJ, Brown TM, Carnethon M, Dai S, De Simone G, et al. Heart disease and stroke statistics--2010 update: a report from the American Heart Association. *Circulation* 2010;121:e46-e215.
- [141] Brewster D. Prosthetic Grafts. In Rutherford Rd (ed) 1995; *Vascular Surgery*:492-508.

- [142] Kakisis JD, Liapis CD, Breuer C, Sumpio BE. Artificial blood vessel: the Holy Grail of peripheral vascular surgery. *J Vasc Surg* 2005;41:349-54.
- [143] McGregor CG, Carpentier A, Lila N, Logan JS, Byrne GW. Cardiac xenotransplantation technology provides materials for improved bioprosthetic heart valves. *J Thorac Cardiovasc Surg* 2011;141:269-75.
- [144] Okuhn SP, Connelly DP, Calakos N, Ferrell L, Pan MX, Goldstone J. Does compliance mismatch alone cause neointimal hyperplasia? *J Vasc Surg* 1989;9:35-45.
- [145] Uchida N, Kambic H, Emoto H, Chen JF, Hsu S, Murabayshi S, et al. Compliance effects on small diameter polyurethane graft patency. *Journal of biomedical materials research* 1993;27:1269-79.
- [146] Wu MH, Shi Q, Sauvage LR, Kaplan S, Hayashida N, Patel MD, et al. The direct effect of graft compliance mismatch per se on development of host arterial intimal hyperplasia at the anastomotic interface. *Ann Vasc Surg* 1993;7:156-68.
- [147] Kidson IG, Abbott WM. Low compliance and arterial graft occlusion. *Circulation* 1978;58:11-4.
- [148] Hunter GC, Carson SN, Wong HN, French S. Experimental small-diameter graft patency: effect of compliance, porosity and graft healing potential. *Curr Surg* 1980;37:439-41.
- [149] Kidson IG. The effect of wall mechanical properties on patency of arterial grafts. *Ann R Coll Surg Engl* 1983;65:24-9.
- [150] Clark RE, Apostolou S, Kardos JL. Mismatch of mechanical properties as a cause of arterial prostheses thrombosis. *Surg Forum* 1976;27:208-10.
- [151] Kinley CE, Marble AE. Compliance: a continuing problem with vascular grafts. *J Cardiovasc Surg (Torino)* 1980;21:163-70.
- [152] Baird RN, Abbott WM. Pulsatile blood-flow in arterial grafts. *Lancet* 1976;2:948-50.
- [153] Abbott WM, Megerman J, Hasson JE, L'Italien G, Warnock DF. Effect of compliance mismatch on vascular graft patency. *J Vasc Surg* 1987;5:376-82.
- [154] Campbell JH, Efendy JL, Campbell GR. Novel vascular graft grown within recipient's own peritoneal cavity. *Circulation research* 1999;85:1173-8.

- [155] Cao Y, Zhang B, Croll T, Rolfe BE, Campbell JH, Campbell GR, et al. Engineering tissue tubes using novel multilayered scaffolds in the rat peritoneal cavity. *J Biomed Mater Res A* 2008;87:719-27.
- [156] Stickler P, De Visscher G, Mesure L, Famaey N, Martin D, Campbell JH, et al. Cyclically stretching developing tissue in vivo enhances mechanical strength and organization of vascular grafts. *Acta Biomater* 2010;6:2448-56.
- [157] Brennan MP, Dardik A, Hibino N, Roh JD, Nelson GN, Papademitris X, et al. Tissue-engineered vascular grafts demonstrate evidence of growth and development when implanted in a juvenile animal model. *Ann Surg* 2008;248:370-7.
- [158] Roh JD, Sawh-Martinez R, Brennan MP, Jay SM, Devine L, Rao DA, et al. Tissue-engineered vascular grafts transform into mature blood vessels via an inflammation-mediated process of vascular remodeling. *Proc Natl Acad Sci U S A* 2010;107:4669-74.
- [159] Shin'oka T, Matsumura G, Hibino N, Naito Y, Watanabe M, Konuma T, et al. Midterm clinical result of tissue-engineered vascular autografts seeded with autologous bone marrow cells. *J Thorac Cardiovasc Surg* 2005;129:1330-8.
- [160] Zhang X, Thomas V, Xu Y, Bellis SL, Vohra YK. An in vitro regenerated functional human endothelium on a nanofibrous electrospun scaffold. *Biomaterials* 2010;31:4376-81.
- [161] Zhang X, Thomas V, Vohra YK. Two ply tubular scaffolds comprised of proteins/poliglecaprone/polycaprolactone fibers. *J Mater Sci Mater Med* 2010;21:541-9.
- [162] McClure MJ, Sell SA, Simpson DG, Walpoth BH, Bowlin GL. A three-layered electrospun matrix to mimic native arterial architecture using polycaprolactone, elastin, and collagen: A preliminary study. *Acta Biomater* 2010.
- [163] Pham QP, Sharma U, Mikos AG. Electrospinning of polymeric nanofibers for tissue engineering applications: a review. *Tissue Eng* 2006;12:1197-211.
- [164] El-Kurdi MS, Hong Y, Stankus JJ, Soletti L, Wagner WR, Vorp DA. Transient elastic support for vein grafts using a constricting microfibrillar polymer wrap. *Biomaterials* 2008;29:3213-20.
- [165] Abbott WM, Rehring TF. Biologic and Synthetic Prosthetic Materials for Vascular Conduits. In: Hobson RW, Wilson SE, Veith FJ, editors. *Vascular Surgery: Principles and Practice*. 3rd ed. New York: Marcel Dekker; 2004. p. 611-20.

- [166] Annabi N, Mithieux SM, Boughton EA, Ruys AJ, Weiss AS, Dehghani F. Synthesis of highly porous crosslinked elastin hydrogels and their interaction with fibroblasts in vitro. *Biomaterials* 2009;30:4550-7.
- [167] Hinds MT, Rowe RC, Ren Z, Teach J, Wu PC, Kirkpatrick SJ, et al. Development of a reinforced porcine elastin composite vascular scaffold. *J Biomed Mater Res A* 2006;77:458-69.
- [168] Faury G, Pezet M, Knutsen RH, Boyle WA, Heximer SP, McLean SE, et al. Developmental adaptation of the mouse cardiovascular system to elastin haploinsufficiency. *J Clin Invest* 2003;112:1419-28.
- [169] Li DY, Brooke B, Davis EC, Mecham RP, Sorensen LK, Boak BB, et al. Elastin is an essential determinant of arterial morphogenesis. *Nature* 1998;393:276-80.
- [170] Li DY, Faury G, Taylor DG, Davis EC, Boyle WA, Mecham RP, et al. Novel arterial pathology in mice and humans hemizygous for elastin. *J Clin Invest* 1998;102:1783-7.
- [171] Sallach RE, Cui W, Wen J, Martinez A, Conticello VP, Chaikof EL. Elastin-mimetic protein polymers capable of physical and chemical crosslinking. *Biomaterials* 2009;30:409-22.
- [172] Caves JM, Cui W, Wen J, Kumar VA, Haller CA, Chaikof EL. Elastin-like protein matrix reinforced with collagen microfibers for soft tissue repair. *Biomaterials* 2011;32:5371-9.
- [173] Caves JM, Kumar VA, Martinez AW, Kim J, Ripberger CM, Haller CA, et al. The use of microfiber composites of elastin-like protein matrix reinforced with synthetic collagen in the design of vascular grafts. *Biomaterials* 2010;31:7175-82.
- [174] ANSI/AAMI/ISO. Cardiovascular implants—Tubular vascular prostheses. 7198:1998/2001 2001.
- [175] Rutten M, Janes MA, Laraway B, Gregory C, Gregory K. Comparison of quantum dots and CM-DiI for labeling porcine autologous bone marrow mononuclear cells. *The Open Stem Cell Journal* 2010;2:25-36.
- [176] Sell SA, McClure MJ, Barnes CP, Knapp DC, Walpoth BH, Simpson DG, et al. Electrospun polydioxanone-elastin blends: potential for bioresorbable vascular grafts. *Biomed Mater* 2006;1:72-80.

- [177] Huang C, Chen R, Ke Q, Morsi Y, Zhang K, Mo X. Electrospun collagen-chitosan-TPU nanofibrous scaffolds for tissue engineered tubular grafts. *Colloids Surf B Biointerfaces* 2011;82:307-15.
- [178] Wise SG, Byrom MJ, Waterhouse A, Bannon PG, Weiss AS, Ng MK. A multilayered synthetic human elastin/polycaprolactone hybrid vascular graft with tailored mechanical properties. *Acta Biomater* 2011;7:295-303.
- [179] Bonani W, Maniglio D, Motta A, Tan W, Migliaresi C. Biohybrid nanofiber constructs with anisotropic biomechanical properties. *J Biomed Mater Res B Appl Biomater* 2011;96:276-86.
- [180] Wise SG, Mithieux SM, Weiss AS. Engineered tropoelastin and elastin-based biomaterials. *Adv Protein Chem Struct Biol* 2009;78:1-24.
- [181] Waterhouse A, Yin Y, Wise SG, Bax DV, McKenzie DR, Bilek MM, et al. The immobilization of recombinant human tropoelastin on metals using a plasma-activated coating to improve the biocompatibility of coronary stents. *Biomaterials* 2010;31:8332-40.
- [182] Zeugolis DI, Paul GR, Attenburrow G. Cross-linking of extruded collagen fibers-A biomimetic three-dimensional scaffold for tissue engineering applications. *J Biomed Mater Res A* 2008.
- [183] Cohen J, Litwin SB, Aaron A, Fine S. The rupture force and tensile strength of canine aortic tissue. *The Journal of surgical research* 1972;13:321-33.
- [184] Coulson WF. The effect of proteolytic enzymes on the tensile strength of whole aorta and isolated aortic elastin. *Biochimica et biophysica acta* 1971;237:378-86.
- [185] Haut RC, Garg BD, Metke M, Josa M, Kaye MP. Mechanical properties of the canine aorta following hypercholesterolemia. *Journal of biomechanical engineering* 1980;102:98-102.
- [186] Hayashi K. Fundamental and applied studies of mechanical properties of cardiovascular tissues. *Biorheology* 1982;19:425-36.
- [187] Litwin SB, Cohen J, Fine S. Effects of sterilization and preservation on the rupture force and tensile strength of canine aortic tissue. *The Journal of surgical research* 1973;15:198-206.

- [188] Purslow PP. Positional variations in fracture toughness, stiffness and strength of descending thoracic pig aorta. *Journal of biomechanics* 1983;16:947-53.
- [189] Farand P, Garon A, Plante GE. Structure of large arteries: Orientation of elastin in rabbit aortic internal elastic lamina and in the elastic lamellae of aortic media. *Microvascular Research* 2007;73:95-9.
- [190] Carta L, Wagenseil JE, Knutsen RH, Mariko B, Faury G, Davis EC, et al. Discrete contributions of elastic fiber components to arterial development and mechanical compliance. *Arterioscler Thromb Vasc Biol* 2009;29:2083-9.
- [191] McKenna KA, Gregory KW, Sarao RC, Maslen CL, Glanville RW, Hinds MT. Structural and cellular characterization of electrospun recombinant human tropoelastin biomaterials. *J Biomater Appl* 2011.
- [192] Nowatzki PJ, Tirrell DA. Physical properties of artificial extracellular matrix protein films prepared by isocyanate crosslinking. *Biomaterials* 2004;25:1261-7.
- [193] Di Zio K, Tirrell DA. Mechanical Properties of Artificial Protein Matrices Engineered for Control of Cell and Tissue Behavior. *Macromolecules* 2003;36:1553-8.
- [194] Konig G, McAllister TN, Dusserre N, Garrido SA, Iyican C, Marini A, et al. Mechanical properties of completely autologous human tissue engineered blood vessels compared to human saphenous vein and mammary artery. *Biomaterials* 2009;30:1542-50.
- [195] Zeugolis DI, Khew ST, Yew ES, Ekaputra AK, Tong YW, Yung LY, et al. Electro-spinning of pure collagen nano-fibres - just an expensive way to make gelatin? *Biomaterials* 2008;29:2293-305.
- [196] Nam J, Huang Y, Agarwal S, Lannutti J. Materials selection and residual solvent retention in biodegradable electrospun fibers. *Journal of Applied Polymer Science* 2008;107:1547-54.
- [197] Niklason LE, Gao J, Abbott WM, Hirschi KK, Houser S, Marini R, et al. Functional arteries grown in vitro. *Science* 1999;284:489-93.
- [198] Thomas V, Zhang X, Vohra YK. A biomimetic tubular scaffold with spatially designed nanofibers of protein/PDS bio-blends. *Biotechnol Bioeng* 2009;104:1025-33.
- [199] Berglund JD, Mohseni MM, Nerem RM, Sambanis A. A biological hybrid model for collagen-based tissue engineered vascular constructs. *Biomaterials* 2003;24:1241-54.

- [200] Greisler HP, Gosselin C, Ren D, Kang SS, Kim DU. Biointeractive polymers and tissue engineered blood vessels. *Biomaterials* 1996;17:329-36.
- [201] L'Heureux N, Paquet S, Labbe R, Germain L, Auger FA. A completely biological tissue-engineered human blood vessel. *FASEB J* 1998;12:47-56.
- [202] Masuda S, Doi K, Satoh S, Oka T, Matsuda T. Vascular endothelial growth factor enhances vascularization in microporous small caliber polyurethane grafts. *ASAIO J* 1997;43:M530-4.
- [203] Niklason LE, Langer RS. Advances in tissue engineering of blood vessels and other tissues. *Transpl Immunol* 1997;5:303-6.
- [204] Zilla P, Deutsch M, Meinhart J, Puschmann R, Eberl T, Minar E, et al. Clinical in vitro endothelialization of femoropopliteal bypass grafts: an actuarial follow-up over three years. *J Vasc Surg* 1994;19:540-8.
- [205] McKenna KA, Gregory, K.W., Sarao, R.C., Maslen, C.L., Glanville, R.W., and Hinds, M.T. . Structural and cellular characterization of electrospun recombinant human tropoelastin biomaterials. *Journal of Biomaterials Applications* 2011;in press.
- [206] Meinhart JG, Deutsch M, Fischlein T, Howanietz N, Froschl A, Zilla P. Clinical autologous in vitro endothelialization of 153 infrainguinal ePTFE grafts. *The Annals of thoracic surgery* 2001;71:S327-31.
- [207] Ranjan AK, Kumar U, Hardikar AA, Poddar P, Nair PD. Human blood vessel-derived endothelial progenitors for endothelialization of small diameter vascular prosthesis. *PLoS One* 2009;4:e7718.
- [208] Sacks MS, Sun W. Multiaxial mechanical behavior of biological materials. *Annu Rev Biomed Eng* 2003;5:251-84.
- [209] Vito RP, Dixon SA. Blood vessel constitutive models-1995-2002. *Annu Rev Biomed Eng* 2003;5:413-39.
- [210] Lyman DJ, Albo D, Jr., Jackson R, Knutson K. Development of small diameter vascular prostheses. *Trans Am Soc Artif Intern Organs* 1977;23:253-61.
- [211] Fung YC. *Biomechanics: Mechanical Properties of Living Tissues* Second ed. New York, NY: Springer-Verlag; 1993.
- [212] Fung YC. Inversion of a Class of Nonlinear Stress-Strain Relationships of Biological Soft Tissues. *Journal of biomechanical engineering* 1979;101:23-7.

- [213] Girton TS, Oegema TR, Grassl ED, Isenberg BC, Tranquillo RT. Mechanisms of stiffening and strengthening in media-equivalents fabricated using glycation. *Journal of biomechanical engineering* 2000;122:216-23.
- [214] Lund T, Hermansen SE, Andreasen TV, Olsen JO, Osterud B, Myrmel T, et al. Shear stress regulates inflammatory and thrombogenic gene transcripts in cultured human endothelial progenitor cells. *Thromb Haemost* 2010;104:582-91.
- [215] Cucuini W, Poitevin S, Poitevin G, Dignat-George F, Cornillet-Lefebvre P, Sabatier F, et al. Tissue factor up-regulation in proinflammatory conditions confers thrombin generation capacity to endothelial colony-forming cells without influencing non-coagulant properties in vitro. *J Thromb Haemost* 2010;8:2042-52.
- [216] Ensley A, Nerem RM, Anderson D, Hanson SR, Hinds MT. Fluid shear stress alters the hemostatic properties of endothelial outgrowth cells. *Tissue engineering* 2011;Submitted.
- [217] Zilla P, von Oppell U, Deutsch M. The endothelium: a key to the future. *J Card Surg* 1993;8:32-60.
- [218] Wang C, Jiao C, Hanlon HD, Zheng W, Tomanek RJ, Schatteman GC. Mechanical, cellular, and molecular factors interact to modulate circulating endothelial cell progenitors. *Am J Physiol Heart Circ Physiol* 2004;286:H1985-93.
- [219] Timmermans F, Plum J, Yoder MC, Ingram DA, Vandekerckhove B, Case J. Endothelial progenitor cells: identity defined? *J Cell Mol Med* 2009;13:87-102.
- [220] Zampetaki A, Kirton JP, Xu Q. Vascular repair by endothelial progenitor cells. *Cardiovasc Res* 2008;78:413-21.
- [221] Hanson SR, Kotze HF, Savage B, Harker LA. Platelet interactions with Dacron vascular grafts. A model of acute thrombosis in baboons. *Arteriosclerosis* 1985;5:595-603.
- [222] Torem S, Schneider PA, Hanson SR. Monoclonal antibody-induced inhibition of platelet function: effects on hemostasis and vascular graft thrombosis in baboons. *J Vasc Surg* 1988;7:172-80.
- [223] Schneider PA, Kotze HF, Heyns AD, Hanson SR. Thromboembolic potential of synthetic vascular grafts in baboons. *J Vasc Surg* 1989;10:75-82.

- [224] Krupski WC, Bass A, Kelly AB, Ruggeri ZM, Harker LA, Hanson SR. Interruption of vascular thrombosis by bolus anti-platelet glycoprotein IIb/IIIa monoclonal antibodies in baboons. *J Vasc Surg* 1993;17:294-304.
- [225] Cadroy Y, Horbett TA, Hanson SR. Discrimination between platelet-mediated and coagulation-mediated mechanisms in a model of complex thrombus formation in vivo. *J Lab Clin Med* 1989;113:436-48.
- [226] Cadroy Y, Hanson SR. Effects of red blood cell concentration on hemostasis and thrombus formation in a primate model. *Blood* 1990;75:2185-93.

Appendix A

MATLAB code for image analysis program used to quantify orientation of electrospun fibers.

```
% Locate fiber orientation in images
% Image must be square
% Algorithm: Begin with edge detection based on approximation to
% the derivative. Perform Radon transform on the segmented image.
% Calculate maximum projection angles. Relate to image orientation.
% Calculate probability distribution function of fiber orientation.
%
%10/30/02 S J Kirkpatrick
%
close all
clear all
I=imread('C:\Documents and
Settings\lagerquk\Desktop\images\actin\Fig6_BaCaEC_actin_24hr.jpg');
%I=im2bw(I);
I=rgb2gray(I);
%I=imrotate(I,60);
%Var=.75;%add noise to image
%I=imnoise(I,'gaussian',0,Var);
figure(1);imshow(I);colorbar

I=imcrop;
%kernal =[1;0;-1]/2;%first order discrete difference
kernal=[-1;8;0;-8;1]/12;%second order first derivative operator. Detects curvature in the
gradient
%kernal=[1;-9;45;0;-45;9;-1]/60;%third order first derivative operator
%kernal2=[-3 32 -168 672 0 -672 168 -32 3]%/fourth order first derivative operator
%Antisymmetric derivative filters with recursive U correction filter
%kernal=[-0.575841;0.416642;0.0478413;-0.00435846];%third order
%Another class of antisymmetric derivative filters -weighted least square optimized
%kernal=[0.74038;-0.12019];%
%kernal=[-1;27;-27;1]/24%second order with even number of coefficients%(first
derivative)
%BW=filter2(kernal,I,'valid');%
%%%%%%%%%%%%%%
%Second derivative operators
%kernal=[-2.20914;1.10457];%r=1
%kernal=[-2.71081;1.48229;-0.126882];%r=2
%kernal=[-2.92373;1.65895;-0.224751;0.0276655];%r=3
%kernal=[-3.03578;1.75838;-0.291985;0.0597665;-0.00827];%r=4
%kernal=[-3.10308;1.81996;-0.338852;0.088077;-0.0206659;0.00301915];%r=5
```

```

%
I=double(I);
BW=filter(kernal,1,I,[],2);%filter in x-direction
BW2=filter(kernal,1,I);%filter in y-direction
BW3=BW+BW2;% If using a second derivative, this is the Laplacian
%BW3=filter2(kernal,I);
mag=sqrt((BW.^2)+(BW2.^2));
unit=BW3./mag;
%BW=edge(I,'canny');

figure(2);imagesc(I);colormap(gray);axis square
figure(3);imshow(BW);%colormap(gray)% Horizontal derivative image
figure(4);imshow(BW2);%colormap(gray)% Vertical derivative image
figure(5);image(mag);colormap(gray(20))% Magnitude of the gradient image
figure(6);imshow(BW3);%colormap(gray)%colorbar% Gradient image
BW3=imcrop;

%%
%At this point, the gradient image (BW3) can be divided by the magnitude of
%the gradient image(mag) to create a unit vector image. Then perform a
%Radon transform on the unit vector image. Seems to be not as good,
%though.
%mag=sqrt(BW3.^2);
%unit=BW3./mag;
theta=0:179;
[R, xp]=radon(BW3,theta);
figure(7);imagesc(theta, xp,R);colorbar;xlabel('\theta (degrees)');ylabel
('xp');colormap(hot)
set(gca,'XTick',0:20:360);
Beta=max(abs(R));
figure(8);plot(theta,Beta,'linewidth',2);title('Maximum Projection Angle');xlabel('\theta
(degrees)');ylabel('Maximum Value of R')
figure(9);plot((theta-90),Beta,'linewidth',2);title('Fiber Angle Spectrum Relative to
Horizontal');xlabel('\theta (degrees)');
%ylabel('Maximum Value of R')
figure(10);plot((90-(theta-90)),Beta,'linewidth',2);title('Fiber Angle Spectrum Relative to
Vertical');xlabel('\theta (degrees)');
%ylabel('Maximum Value of R');
%
%Probability Distribution Function
Area=trapz((theta-90),Beta);
Prob=(Beta./Area);
Prob=Prob/max(Prob);
figure(11);plot((theta-90),Prob,'r','linewidth',2);title('Normalized Probability Distribution
of Fiber Orientation Relative to Horizontal'); xlabel('\theta (degrees)');ylabel('P(\theta)');
%

```

```
angle=find((Prob)==1);
littleD = [Prob(angle-20:angle+20)];
bigD = [Prob(1:angle-21) Prob(angle+21:end)];
sumlittleD = sum(littleD);
sumbigD = sum(bigD);
alignindex = (sumlittleD/(sumbigD+sumlittleD))/0.22;
angle
alignindex
% spect=fftshift(fft2(BW3));
% spect=spect.*conj(spect);
% figure(12);imagesc(log(abs(spect)))
% %SNR = 10*log10((mean(I(:))/sqrt(Var)))
% %end
```

Appendix B

MATLAB code for analysis of biaxial testing device for defining the strain energy density function.

```
clear all
close all
%code for stress strain analysis of data
%Kathy Lagerquist
%02/23/2004
load presinc.txt;

%assign variables to datafile columns
t = presinc(:,1);
p = presinc(:,2);
cd = presinc(:,3); %cd is circ disp
af = presinc(:,4);

%input measured parameters
gauge = 50e-3; %measure length in m
th = 2.75e-3; %thicknes in m
width = 6.5e-3; %width in m
Loz = gauge; %mm gage length in mm
Lo = ((cd(1,1)*1e-3)) % initial diameter
xsec=th*width;

ns = length(t); %calculate the number of samples in data file

for i = 1:ns; % input the number of samples measured
    Ld(i)=Lo + (cd(i)*1e-3);
    Lz(i)=Loz + (cd(i)/cd(i));
end

for i = 1:ns;
    lambdad(i) = (Ld(i)/Lo);
    lambdaz(i) = (Lz(i)/Loz);
end

%plots axial force axial disp and time

figure (1);
plot (t,cd);
title('Circumferential Displacement vs Time');
xlabel('Time (s)');
ylabel ('Circumferential Displacement (mm)');
```



```

figure (2);
plot (t,p);
title('Pressure vs Time');
xlabel('Time (s)');
ylabel ('Pressure (mmHg)');

figure (3);
plot (cd,p);
title('Pressure vs Displacement');
xlabel('Displacement (mm)');
ylabel ('Pressure (mmHg)');

%define strains
for i = 1:ns; % input the number of samples measured
    % GreenE(i) = ((L2(i)*L2(i))-Lo^2)/(2*Lo^2);
    Ezz(i) = 0.5*((lambdaz(i)^2)-1);
    Edd(i) = 0.5*((lambdad(i)^2)-1);
end

%plots for strain defs
figure (4);
hold on
plot (t,Edd);
xlabel('Time (s)');
ylabel('Circumferential Strain');
plot (t,Ezz);
xlabel('Time (s)');
ylabel('Longitudinal Strain');
hold off

%define stresses
for i = 1:ns;
Sigmadd(i) = ((p(i)*cd(i))/th);
Sigmazz(i) = ((p(i)*cd(i))/(2*th));
end

%CircS = CircS';
%LongS=LongS';
%CircS = filtfilt(ones(1,3),3,CircS);
%LongS = filtfilt(ones(1,3),3,LongS);
%for i = 1:ns;
%   KirchS(i)=1/lambda1(i)*GreenS(i);
% end

% KirchS = filtfilt(ones(1,3),3,KirchS);

```

```

% for i = 1:ns;
%   EulerS(i) = (af(i))/(L2(i)*th); %note this is not using changing thickness
% end

```

```

figure (5);
hold on
plot (t,Sigmadd,'b -');
plot (t,Sigmazz,'r :');
xlabel('Time (s)');
ylabel('Stress (Pa)');
legend('Circumferential Stress','Longitudinal Stress');
hold off

```

```

figure (6);
plot (Edd,Sigmadd);
title ('Stress vs Strain Plot')
xlabel ('Circumferential Strain');
ylabel ('Circumferential Stress');

```

```

figure(8);
plot (Ezz,Sigmazz);
title ('Stress vs Strain Plot')
xlabel ('Longitudinal Strain');
ylabel ('Longitudinal Stress');

```

```

%work under curve
work= cumtrapz(Edd,Sigmadd);

```

```

figure(10);
plot(Edd,work);
xlabel ('Circumferential Strain');
ylabel ('Work');
worksum = sum(work)

```

```

%rhow
rhow=work*1.33;
s11=diff(rhow)./diff(Edd);
% s11=s11/mass;
Edd = Edd(1:129);
rhow = rhow(1:129);
% KirchS = KirchS(1:129);

```

```

% figure(11);
% hold on
% plot(GreenE,s11,'r');

```

```

% plot(GreenE,KirchS);

% xlabel ('Green Strain');
% ylabel ('Kirchoff Stress & mass*s11');
% legend('mass*s11','Kirchoff Stress')
% hold off
Ezz = Ezz(1:129);
t1 = t(1:129)';
t(1,1:129)=[t1];
t(2,1:129)=[t1];
y(1,1:129)=[Edd];
y(2,1:129)=[Ezz];

%polynomial fit
options = OPTIMSET('maxfuneval',1e6,'maxiter',1e4);
x = [1e6 1e6 1e6];
[x,resnorm,residual] = lsqcurvefit('mypoly',x,t,y);%,[],[],options);
break
stress= (x(1)*Edd.^2)+(x(2)*Ezz.^2)+(2*x(3)*Edd*Ezz);

figure(12);
hold on
plot(Edd,stress,'r');
plot(Edd,rhow);
text(0.11,1e6,'y = x(1)*GreenE + x(2)*GreenE^2 + x(3)*GreenE^3 + x(4)*GreenE^4');
x
n=length (residual);
RMS=sqrt(resnorm/n);
plot(Edd,residual,'co');
xlabel ('Strain');
ylabel ('Stress');
legend ('Curvefit','rhow','residuals');
hold off

```

MATLAB code for the ‘mypoly’ function used in themain program.

```
function F = mypoly(x,y)
```

$$F = (x(1)*y(1,:).^2)+(x(2)*y(2,:).^2)+(2*x(3)*y(1,:)*y(2,:).);$$

Appendix C

Primers used for RT-PCR Studies

Gene	Forward	Reverse
GAPDH	CCTCAACGACCACTTTGTCA	TTACTCCTTGGAGGCCATGT
TF	CACCGACGAGATTGTGAAGGAT	TTCCCTGCCGGGTAGGAG
TFPI	GACTCCGCAATCAACCAAGGT	TGCTGGAGTGAGACACCATGA
TM (5)	GGTGGACGGCGAGTGTGTGG	GGTGTGGGGTTCGCAGTCGG
EPCR	CACCCTGCAGCAGCTCAATGC	ACATCGCCGTCCACCTGTGC
CD39	AGTGATTCCAAGGTCCCAGCACC	TCCTGAGCAACCGCATGCCT
ICAM	GCAGTCAACAGCTAAAACCTTCCT	GCAGCGTAGGGTAAGGTTCTTG
VCAM-1C	GGGAAGATGGTCGTGATCCTT	TGAGACGGAGTCACCAATCTG
PECAM_A	CCCAGTTTGAGGTCATAAAAGGA	AGGCAAAGTTCCACTGATCGA
eNOSD	TGGTACATGAGCACTGAGATCG	CCACGTTGATTTCCACTGCTG

Biographical Sketch

Kathryn Alyce McKenna was born in Salt Lake City, Utah on May 22, 1974 to Lynn and Ellen Lagerquist. She attended the University of Utah for two years between 1991 and 1993, while finishing her high school degree at Olympus in 1992. She transferred to Claremont McKenna College in 1993 and completed a Bachelor of Arts degree in Biology in 1995. She stayed at Claremont for another year while working on a research project with McDonnell Douglas Aerospace company associated with their development of the Delta Clipper. She then moved back to Utah to work with Dr. Richard Bland studying acute respiratory distress syndrome in preterm lambs. She then attended graduate school at the University of California, Davis working for Dr. Abdul Barakat investigating multi-directional flow effects on endothelial cells. Following her graduation in 2001 with a Masters of Science degree in Biomedical Engineering, she moved to Oregon to work at the Oregon Medical Laser Center. She has worked at OMLC for 10 years, concurrent with her PhD work, primarily developing and testing bioreactor systems to condition vascular cells to mechanical stimuli, both pressure, shear forces, and cyclic stress and strains, prior to implant. She is a member of the Sigma Xi honorary scientific research fraternity, the Golden Key National Honor Society and received a departmental commendation from the department of Psychology at Claremont McKenna College. During this time she has presented her work at numerous conferences and contributed to several publications. Her presented and published works include:

Peer-reviewed publications (in chronological order)

1. Bland, Richard D., Carlton, David P., Day, Ron W., Macritchie, Amy N., Albertine, Kurt H., **Lagerquist, K.** (Annual Meeting of the American Pediatric Society and the Society for Pediatric Research New Orleans, Louisiana, USA May 1-5, 1998). Continuous inhalation of nitric oxide from birth preserves the pulmonary vasoconstrictor response to hypoxia in chronically ventilated preterm lambs. In: *Pediatric Research* April, 1998. 43 (4 PART 2) 276A.
2. Bland, Richard D., Albertine, Kurt H., Carlton, David P., Day, Ron W., Stolworthy, Lloyd D., Jones, Greg P., **Lagerquist, K.** (Annual Meeting of the American Pediatric Society and the Society for Pediatric Research New Orleans, Louisiana, USA May 1-5, 1998). Continuous inhalation of nitric oxide from birth decreases airway resistance and bronchiolar smooth muscle in chronically ventilated preterm lambs. In: *Pediatric Research* April, 1998. 43 (4 PART 2) 275A.
3. Bland, R., Carlton, D., Albertine, K., Kullama, L., Day, R., Macritchie, A., **Lagerquist, K.** (Annual Meeting of the Professional Research Scientists on Experimental Biology 98, Part II San Francisco, California, USA April 18-22, 1998). Pulmonary vascular effects of nitric oxide and cGMP in preterm lambs with chronic lung injury. In: *FASEB Journal* March 20, 1998. 12(5): A645.
4. Bland, R., Carlton, D., Albertine, K., Kullama, L., Day, R., Macritchie, A., **Lagerquist, K.** (Meeting of the Western Section of the American Federation for Medical Research Carmel, California, USA February 5-7, 1998). Pulmonary vascular effects of inhaled nitric oxide and intravenous 8-bromo-cGMP in preterm lambs with chronic lung injury. In: *Journal of Investigative Medicine* Jan., 1998. 46 (1): 122A.
5. Ren Z, Xie H, **Lagerquist KA**, Burke A, Prahl S, Gregory KW, Furnary AP. Optimal dye concentration and irradiance for laser-assisted vascular anastomosis. *J Clin Laser Med Surg.* 2004 Apr;22(2):81-6.
6. Campbell C, Bazar A, Wu Ping-Cheng, **McKenna K**, Henrie M, Troi K, Gregory K. A simple apparatus and process to produce novel elastin biomaterials. *Trends in Biomaterials and Artificial Organs.* A biannual journal published by the Society for Biomaterials and Artificial Organs India. July 2005. 19 (1). 1-6.
7. **McKenna KA**, Gregory KW, Sarao RC, Maslen CL, Glanville RW, Hinds MT. Structural and cellular characterization of electrospun recombinant human tropoelastin biomaterials. *J Biomater Appl.* 2011 May 17.

8. **McKenna KA**, Hinds MT, Sarao RC, Wu PC, Maslen CL, Glanville RW, Babcock D, Gregory KW. Mechanical property characterization of electrospun recombinant human tropoelastin for vascular graft biomaterials. *Acta Biomaterialia*. Accepted August 1, 2011.

Conferences (in chronological order): presenting author underlined

1. **Lagerquist, K.A.**, Suvatne, J, Barakat A.I., “Multi-directional Flow Chamber: Analysis of Endothelial Cell Morphology Dependence on Differential Shear Forces.” 2nd Joint Conference of the IEEE Engineering in Medicine and Biology Society and the Biomedical Engineering Society, October 2002
2. **Lagerquist, K.A.**, Janis, A.D., Hinds, M.T. “Directional Permeability in a Porcine Carotid Elastin Biomaterial vascular conduit.” 2nd Joint Conference of the IEEE Engineering in Medicine and Biology Society and the Biomedical Engineering Society, October 2002
3. Lucchesi, L.D., McCarthy, S.J., **Lagerquist, K.A.**, Gregory, K.W., “Development of an *in vitro* assay to study the burst pressure characteristics of Chitosan sponges,” Society for Biomaterials Conference, April 2002.
4. Hinds, M.T., **Lagerquist, K.A.**, Rowe, R.C., Gregory K.W., and Courtman, D.W., “Cell Adhesion to Porcine Elastin Biomaterials,” ASME Summer Bioengineering Conference, 2003.
5. Kwong, M., Xie, H., **Lagerquist, K.A.**, Kim, S., and Hinds, M.T., “Tympanic Membrane Repair with Elastin Biomaterials,” Society for Biomaterials Conference, April 2003.
6. Janis, A.D., Breneman, K.D., Hinds, M.T., **Lagerquist, K.A.**, and Kirkpatrick, S.J., “The Effects of Chemical Removal of Nucleic Acids on the Mechanical Properties of Porcine Small Intestinal Submucosa,” Society for Biomaterials Conference, April 2003.
7. **Lagerquist, K.A.**, Kwong, M., Gregory, K.W., “Failure Stress of Purified Carotid Elastin.”, Society for Biomaterials Conference, April 2003.
8. Courtman, D.W., **Lagerquist, K.A.**, Rowe, R.C., Gregory, K.W., Hinds, M.T., “Phenotypic changes of Porcine Aortic Smooth Muscle cells Due to Their Attachment to Purified Porcine Arterial Elastin Scaffolds.”, AHA 4th Annual Conference on Arteriosclerosis, Thrombosis and Vascular Biology, May, 2003.

9. **Lagerquist, K.A.**, Jensen-Segal, S., Kirkpatrick S., Hinds, M.T., Gregory, K.W., “Constitutive Modeling of Vascular Constructs: A Modified Burst Pressure Method”, American Society of Biomechanics, September 2004.
10. **Lagerquist, K.A.**, Jensen-Segal, S., Florine, E.M., Campbell, C., Bazar, A., Hinds, M.T., Gregory, K.W., “Development of a Pressure Hold Sodding Method for Tissue-Engineered Arterial Replacements”, BMES Annual Fall Meeting, October 2004.
11. **Lagerquist, K.A.**, Hillis, G., Courtman, D.W., Hanson, S.R., Hinds, M.T., “Evaluation of Tissue Factor Activity of Baboon Circulating Endothelial Cells.”, Tissue Engineering Society International Annual Meeting, October 2004.
12. **McKenna, K.A.**, Anderson, D., Marzec, U, Hanson, S.R., and **Hinds, M.T.**, “Functionally Endothelialized ePTFE Vascular Grafts.”, The 15th Annual Hilton Head Workshop, March 2011.
13. **Anderson, D.**, **McKenna, K.A.**, Hanson, S.R., and Hinds, M.T., “Hemostatic functions of endothelial outgrowth cells are independent of extracellular matrix coatings.”, The 15th Annual Hilton Head Workshop, March 2011.